CONVECTIVE HEAT TRANSFER TO NON-NEWTONIAN FLUIDS
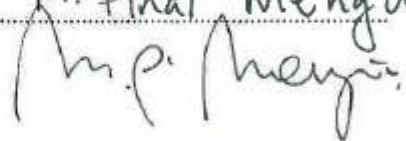
by
MOSTAFA SHOJAEIAN

Submitted to the Graduate School of Engineering and Natural Sciences
in partial fulfillment of
the requirements for the degree of
Master of Science

Sabancı University
July 2015

i

CONVECTIVE HEAT TRANSFER TO NON-NEWTONIAN FLUIDS

APPROVED BY:

Asst. Prof. Dr. / Assoc. Prof. Dr. / Prof. Dr. .... Ali Koşar
        (Thesis Supervisor)

Asst. Prof. Dr. / Assoc. Prof. Dr. / Prof. Dr. ...... M. Pinar Mengüç

Asst. Prof. Dr. / Assoc. Prof. Dr. / Prof. Dr. .... & Mehmet Yıldız

Asst. Prof. Dr. / Assoc. Prof. Dr. / Prof. Dr. ....

Asst. Prof. Dr. / Assoc. Prof. Dr. / Prof. Dr. ....

DATE OF APPROVAL: 21/07/2015

ABSTRACT

CONVECTIVE HEAT TRANSFER TO NON-NEWTONIAN FLUIDS

MOSTAFA SHOJAEIAN

MSc. Thesis, July 2015

Supervisor: Assoc. Prof. Ali Ko ar

In this thesis, the perturbation method was implemented to analytically solve the governing equations relevant to both hydrodynamically and thermally fully developed power-law fluid and plug flows through parallel-plates and circular microchannels under constant isoflux thermal and slip boundary condition. The temperature-dependent properties, being viscosity and thermal conductivity, were considered along with non-linear slip condition in the analysis in addition to viscous dissipation. The velocity, temperature and constant property Nusselt number closed form expressions were derived and then the Nusselt number corresponding to temperature-dependent thermophysical properties was numerically obtained due to their complexity nature. Numerical simulations were also performed for verifying the analytical results. The results indicated that the property variations and slip condition significantly affected thermo-fluid characteristics. The second law analysis was further performed for both constant and variable properties.

Furthermore, an experimental study was performed on nucleate pool boiling of polymeric solutions (aqueous Xanthan gum solutions) by the dissolution of Xanthan gum powder in different amounts into deionized water. Their advantage over new generation fluids such as nanofluids is that they have no side effects such as agglomeration and sedimentation of particles, which is common for nanofluids. The results revealed that heat transfer coefficients of prepared polymeric solutions were lower than those of pure water, while concentration played a significant role in the performance of the heat transfer. In visualization studies, different pool boiling patterns were recorded particularly for high concentrations, which bolsters the heat transfer results.

ÖZET

NEWTONYEN OLMAYAN AKIŞ KANLARIN TAŞINIMLI ISI TRANSFER

MOSTAFA SHOJAEIAN

Yüksek Lisans Tezi, July 2015

Danışman: Assoc. Prof. Ali Koşar

Keywords: Isı Transferi, Newtonyen olmayan akışkanlar,
Kaymalı akış, Mikrokanal, Havuz kaynaması

Bu tezde, hidrodinamik ve termal açıdan tam gelişmiş Newtonyen olmayan akışkanların, piston akışı şeklinde (plug flow), paralel iki düzlem plaka arasından ve dairesel mikrokanallardan geçirilmesinin pertürbasyon metoduyla analitik olarak çözümü icra edilmiştir. Sınır koşulları olarak sabit ısı akısı ve kayma sınır koşulu kullanılmıştır. Viskoz yayılmaya ek olarak, viskozite ve termal iletkenlik gibi sıcaklığa bağlı olan özellikler göz önünde bulundurulmasının yanı sıra lineer olmayan kayma koşulu dikkate alınmıştır. Hız, sıcaklık ve sabit özellikli Nusselt sayısı kapalı form ifadeleri elde edilmiştir. Daha sonra, nümerik olarak Nusselt sayısı, sıcaklığa bağlı termofiziksel özellikler ile ilişkili şekliyle bulunmuştur. Analitik sonuçları doğrulamak için nümerik simülasyonlar da yapılmıştır. Sonuçlar, özellik değişimlerinin ve kayma koşulunun önemli ölçüde termo-akışkan özelliklerini etkilemiş olduğunu göstermektedir. İkinci termodinamik yasa analizi, sabit ve değişken özellikler için de ayrı ayrı incelenmiştir.
Buna ek olarak, polimerik solüsyonların (Su bazlı Xanthan Gum solüsyonları) çekirdekli havuz kaynaması deneysel olarak incelenmiştir. Deneyler, Xantham gum tozunun farklı miktarlarda de-iyonize su içerisinde çözünmesiyle gerçekleştirilmiştir. Nanoakışkanlar gibi yeni jenerasyon akışkanlara göre bu solüsyonların avantajı, nanoakışkanlarda sıkça karşılaşılan partiküllerin topaklanması ve sedimantasyonu gibi problemleriyle karşılaşılmamasıdır. Sonuçlar, polimerik solüsyonların ısı transferi katsayılarının saf sudan daha düşük olduğunu ve konsantrasyonun ısı transferi üzerinde önemli bir etkisi olduğunu göstermiştir. Görüntüleme çalışmalarında, özellikle yüksek konsantrasyonlarda, ısı transferi sonuçlarını destekleyen orijinal havuz kaynama görüntüleri elde edilmiştir.

This M.Sc. thesis is dedicated to my family and to all teachers
who have devoted themselves to improve science and
have enlightened the way of human beings
to knowledge and justice

ACKNOWLEDGMENT

TABLE OF CONTENTS

LIST OF FIGURES

LIST OF TABLES

LIST OF SYMBOLS AND ABBREVIATIONS

A   Constant defined by Eqs. (3.15), (4.23) and (5.27)

A   Constant defined by Eq. Eq. (4.25) and (5.29)

a   Defined by Eq. (3.32)

b   Defined by Eq. (3.32)

b   A coefficient in Eqs. (4.4) and (5.4)

Be   Bejan number

Br   Brinkman number

$C_{31},\ldots, C_{34}$ Constant defined in Eq. (3.22)

$C_{41},\ldots, C_{46}$ Constant defined in Eq. (4.34)

$C_{51},\ldots, C_{55}$ Constant defined in Eq. (5.39)

CC   Circular channel

c_p Specific heat at constant pressure

CP   Constant property

D   Hydraulic diameter

f   Friction factor

f Slip-friction coefficient

F   Dimensionless slip-friction coefficient

G   Power-law exponent

H   Height of channel

k   Thermal conductivity of fluid

l   Slip length

m   0 for parallel-plates channel and 1 for circular channel

$\overset{\bullet}{m}$ Mass flow rate

n   Power-law index

N_s Dimensionless entropy generation number

$<N_s>$ Global entropy generation rate

Nu   Nusselt Number

Po   Poiseuille number

P   Pressure

Pe   Peclet number

PP   Parallel-plates

q''	Heat flux
Re	Reynolds number
R	Dimensional radial position in coordinate system
r	Dimensionless radial position in coordinate system
r_0	Radius of circular channel
S	Cross-section area
$\dot{S}$	Entropy generation
T	Temperature
U, V	Dimensional velocity component in the x, y directions
u, v	Dimensionless velocity component in the x, y directions
VP	Variable property
U_m	Mean velocity
X, Y	Dimensional position in coordinate system
x, y	Dimensionless position in coordinate system

Greek Symbols

	Slip coefficient
ε	Perturbation parameter
	Defined by Eq. (5.22)
	Specific heat ratio of fluid
μ	Dynamic viscosity of fluid
	Defined by Eq. (3.9a)
	Density of fluid
	Dimensionless temperature
	Shear stress
	Consistency factor
	Defined by Eq. (3.22)
	Source term (here, viscous dissipation)
	Defined as $q''D/T_i k$ or $q'' r_0 / T_i k$
	Perimeter 5
	Defined by Eq. (3.45)
δ	Perimeter

Γ Defined by Eq. (5.9)

$_v$ Tangential momentum accommodation coefficient

Subscripts

i Fluid properties at the inlet

m Mean or bulk

s Fluid properties at the surface

w Wall

ws Wall slip

CHAPTER 1

INTRODUCTION

Rapid progress in microfabrication techniques has resulted in micro devices involving heat and fluid flow. Experimental and analytical studies investigating parametric effects on convective heat transfer and entropy generation rate are of cardinal significance to successfully assess heat and fluid flow characteristics in micro- and nano-scale and to identify their differences from conventional scale. One of the most important parameters in micro and nano flows is the slip effect, which strongly influences fluid motion at the fluid-solid interface. Under certain conditions such as very low pressure, hydrophobic surfaces, and small-size channels with characteristic lengths between 1 µm and 1 mm, the continuum assumption may not be accurate, particularly in micro devices, which find applications in medicine, fuel cells, biomedical reaction chambers, Lab-On-a-Chip technology and heat exchangers for electronics cooling. Therefore, it is important to investigate slip flows in order to provide useful prediction tools for convective heat transfer in micro devices.

When the characteristic length (or size of channel) is reduced down to micro-and nano scale, the slip effect becomes apparent, which leads to discontinuities in velocity and temperature (only for gases) profiles at the fluid-solid interface. For flows of polymers, this effect may even occur in macro scale [1,2]. Knudsen number (Kn), the ratio of the mean free path to the characteristic length of the channel, is a benchmark to classify flow regimes of gases. Kn in the range of 0.001<Kn<0.1 is in the slip flow regime, where fluid velocity at wall is non-zero (velocity slip condition), and wall temperature and adjacent fluid temperature are not the same (temperature jump condition). Heat and fluid flow characteristics for gas microflows have been investigated in many

experimental studies [3–6] as well as in numerical and theoretical studies taking temperature-jump and velocity-slip effects into account [7–15].

For liquid flows in macro scale, no-slip boundary condition on solid surface is widely assumed, which may not be always correct in micro and nano fluidic systems. Recent experimental studies of microflows revealed that boundary conditions at the channel wall depend on both flow length scale and surface properties. Hydrophobic smooth surfaces such as in polydimethylsiloxane (PDMS materials) made channels [16–18] or hydrophobic liquids could lead to slip conditions at the channel wall [19] for liquid flows, while slip conditions in liquid flows may also occur when liquid moves over surfaces with microscopic roughnesses [20]. Studies reporting slip lengths for liquid microflows are already present in the literature. Joseph and Tabeling [21] reported slip lengths below 100 nm in water flowing inside 10 µm×100 µm×1 cm microchannels in velocity profiles obtained using the particle image velocimetry (PIV) technique. According to the numerical predictions given by El-Genk and Yang [22], slip lengths in the experiments on water flows through microchannels conducted by Celata et al. [23] and Rands et al. [24] were estimated as 1µm and 0.7 µm, respectively. Tretheway and Meinhart [25] reported that the slip length in water flow in a $30×300$ µm^2 channel coated with a monolayer of hydrophobic octadecyltrichlorosilane was approximately 1 µm. Slip lengths ranging from 6 µm to 8 µm were measured by Chun and Lee [18] in their experimental study on 1 mM KCl electrolyte flow with fluorescent polystyrene latex of radius 1.05 µm and dilute concentration of 0.48 ppm in a slit-like channel of 3 cm length, 90 µm width and 1000 µm depth. For Newtonian fluids, such as air and water, the wall slip happens when the scale of channel reduces to the order of molecular dimensions or fractions of a micrometer. However, there exist some investigations on thermal and fluid characteristics of Newtonian liquid in microchannels, considering both slip [13,26–28] and no-slip [29–31] conditions at the surface interface. It has been also observed that slip conditions existed at the channel walls for non-Newtonian fluids, such as polymer solutions and extrusions of polymer melts in capillary tubes because of instabilities induced at sufficiently high stress levels [1,32]. These instabilities were attributed to chain polymer disentanglement [33] and debonding at the interface of wall and polymer [34] and resulted in wall slips for these types of fluids. Bhagavatula and Castro [35] proposed a mathematical model, which used linear Navier slip boundary condition at wall and Carreau viscosity for explaining the rheological behavior corresponding to the coating material. They employed a micro slit rheometer to measure

2

rheological and slip parameters corresponding to the coating material and found that their predictions of pressure and coating thicknesses agreed well with the experimental results.

Being interdisciplinary and having a wide range of application in industry, non-Newtonian fluid flows require a thorough study in terms of experimental, numerical and analytical aspects to find applications in emerging fields. In contrast to Newtonian fluids, the viscosity of non-Newtonian fluids, which are typically involved in complex material structures such as foams, polymer melts, emulsions, slurries, and solutions, shows a different trend when exposed to variations in shear rate. Therefore, an appropriate viscosity model should be implemented for their analysis. Non-Newtonian fluids offer an attractive subject for scientists and engineers from different disciplines to explore mathematical models for relating stress, deformation and heat transfer behaviors [36–39].

CHAPTER 2

LITERATURE SURVEY

2.1 Single-phase flow in duct

Since there are many practical applications related to non-Newtonian fluids, the assessment of their heat transfer characteristics is vital for accomplishing successful thermal designs. A large number of experimental and numerical studies regarding non-Newtonian fluids have been reported in the literature. However, few experimental studies have been conducted to investigate convective heat transfer characteristics of non-Newtonian fluids [40–45]. On the other hand, many numerical investigations on heat transfer of non-Newtonian fluids have been reported in the literature including a wide range of different cases such as forced convection [46–50], natural convection [51–54] and mixed convection [55–58] in addition to the consideration of fluids exposed to external fields such as magnetic field (known as MHD flow [59–61]) and electric field (electroosmosis [62–64]).

Babaie et al. [62] performed a numerical study on heat transfer characteristics of hybrid electroosmotic and pressure driven power-law fluid flows in a microchannel. Their

findings revealed that the thermal characteristics were strongly affected by governing parameters such as flow behavior index, zeta potential, and viscous dissipation. Hung [65] provided an analytical solution for entropy generation rate of fluid flows through circular microchannels under power law assumption. The author reported that viscous dissipation is significant and should be taken into consideration in the entropy generation analysis.

Chen et al. [66] studied heat transfer characteristics of power-law fluid flow in a microchannel and presented dimensionless temperature distributions and fully developed Nusselt numbers for different parameters such as flow behavior index, ratio of Debye length to half channel height, ratio of Joule heating to surface heat flux, and Brinkman number. Sunarso et al. [67] performed numerical simulations to examine wall slip effects on Newtonian and non-Newtonian fluid flows in microchannels. They found that different vortex growth could be observed in micro scale due to the inclusion of wall slip, which qualitatively matched with experimental results. Barkhordari and Etemad [68] conducted a numerical study on convective heat transfer of non-Newtonian fluid flows in microchannels at both constant temperature and constant heat flux boundary conditions. Their computational results showed that a change in the slip coefficient decreased Poiseuille number while increasing local Nusselt number.

Many researchers concentrated on an analytical approach to examine heat and fluid flow characteristics of non-Newtonian fluids for internal convection, which is important for giving an insight into a better design for devices involving non-Newtonian fluids. As a result of such efforts, many studies are present in the literature. For example, Chiba et al. [69] analytically studied convective heat transfer in a pipe exposed to non-axisymmetric heat loads with constant properties including the viscous heating term. Their analysis of the heat transfer was performed by using an integral transform technique, 'Vodicka's method', at which Brinkman number and rheological properties effects on local Nusselt number were exhibited. Pinho and Coelho [70] presented an analytical solution for thermally and hydrodynamically fully developed viscoelastic fluid flows inside a concentric annulus by simplification of the Phan-Thien-Tanner constitutive equation subject to both constant wall heat fluxes and constant wall temperatures under the consideration of viscous dissipation term. They obtained some expressions for the inner and outer Nusselt number in terms of appropriate dimensionless parameters. Manglik and Ding [71] analytically solved the fully developed laminar power-law fluid flows based on the Galerkin integral method in

double-sine shaped channels for constant temperature and heat flux thermal boundary conditions and obtained results for friction factor and Nusselt number. Thayalan and Hung [72] presented a theoretical solution based on the Brinkman-extended Darcy model for power-law fluid flows in porous media. They derived an expression for the overall Nusselt number based on a proposed parabolic model and did their analysis on convective heat transfer characteristics relevant to porous media. Chen [73] presented an analytical solution for convective heat transfer in electroosmotic power-law fluid flows between two parallel-plates by obtaining some expressions for velocity and temperature distributions, and fully developed Nusselt number. Similar studies for a circular channel, based on the linearized Poisson–Boltzmann distribution equation, and for viscoelastic fluids related to Phan-Thien-Tanner (PTT) and Finitely-Extensible-Nonlinear-Elastic (FENE-P) models were also carried out [74,75]. Tso et al. [76] did a theoretical analysis on heat transfer of hydrodynamically and thermally fully developed laminar non-Newtonian fluids between parallel-plates while considering viscous dissipation effects for asymmetric heating and presented a Nusselt number expression in terms of Brinkman number and power-law index.

Semi-analytical solutions of flows inside parallel-plates was performed by Sheela-Francisca et al. [77] for power-law fluids under asymmetric heating conditions, which had a significant effect on Nusselt number in addition to other parameters. Monteiro et al. [78] used the Generalized Integral Transform Technique to derive a hybrid numerical–analytical solution for hydrodynamically fully developed and thermally developing power-law fluid flows within coaxial channels of arbitrary geometric configuration. Siginer and Letelier [79] used asymptotic series in terms of the Weissenberg number, Wi, to examine heat transfer of a class of non-linear viscoelastic fluids flowing in non-circular channels, where Nusselt number was a function of Wi. Mahmud and Fraser [80,81] presented asymptotic Nusselt number and entropy generation expressions for power-law fluid flows inside circular channels and parallel-plates with the use of first and second laws of thermodynamics, while neglecting viscous dissipation.

Considering thermophysical properties as constant like in above mentioned references is not always appropriate, since these properties are a strong function of temperature. Therefore, taking thermophysical properties as temperature-dependent would certainly lead to more accurate results. There exist only few investigations in the literature

considering convective heat transfer of non-Newtonian fluids with temperature-dependent properties [81–85].

There are some experimental evidences confirming the possibility of slippage in non-Newtonian fluids [86–91]. Only few studies including the slip effect in their analysis to obtain heat transfer characteristics of non-Newtonian fluids exist [67,68,92–95]. Slip effects could also play a significant role in heat transfer.

For this aim, the current study provides analytical solutions to governing equations pertinent to both hydrodynamically and thermally fully developed laminar Newtonian and power-law fluid flows as well as plug flows through parallel-plates and circular microchannels under constant heat flux, while viscous dissipation is included, and effects of slip condition of different types, and properties with temperature-dependency are taken into consideration.

To the authors' best knowledge, few analytical studies on forced convection heat transfer of non-Newtonian fluid in microchannels with slip conditions exist in literature. The first chapter aims at proving an analytical solution for non-Newtonian fluid flows between parallel-plates in micro scale subject to isoflux and isothermal thermal wall boundary conditions, while taking the effects of wall slip and viscous dissipation into consideration. This analytical solution has the potential of serving as a prediction tool in convective heat transfer of non-Newtonian fluid flows in micro scale. In all the above mentioned studies, the constant thermophysical property assumption was used. However, this assumption may not be reasonable if there is a significant variation in thermophysical properties with temperature. To the authors' best knowledge, there are only a few studies in the literature related to convective heat transfer of non-Newtonian fluids, which considers the change in thermophysical properties as a function of temperature [82–84]. Molaei-Dehkordi and Memari [96] also carried out a numerical investigation on the transient, hydrodynamically fully developed, laminar power-law fluids flow in the thermally developing entrance region of circular tube, while taking the viscous dissipation, axial conduction, and temperature-dependent viscosity into account. To address the gap in the literature, the second chapter presents an analytical model for convective heat transfer of power-law fluids in circular channels subjected to isoflux thermal wall boundary conditions, while accounting the effect of viscous dissipation. The presented analysis, based on perturbation method, focuses on Nusselt number and global entropy generation in the case of the presence of thermophysical property variations in both the viscosity and thermal conductivity. In order to get more accurate

results and better modeling non-Newtonian fluid flows in microchannels, in the third chapter, the slip and the variable properties parameters have been simultaneously considered along with a modified slip boundary condition consistent with experimental observations [89], which has nonlinear wall shear stress dependency.

2.2 Pool boiling

Boiling heat transfer has a wide range of applications spanning from traditional to emerging industries such as heat exchangers, cooling and heating systems, microfluidic systems and chemical and bioengineering reactors and attracted the attention of many researchers. Nucleate boiling as a common mode of heat transfer appears in almost all boiling phenomena. Pool boiling as a subcategory of boiling happens in the absence of an external flow, and nucleate boiling is one of its basic mechanisms.

During last decades, a large number of investigations have been carried out for understanding physics of boiling and bubble formation and for proposing engineering design guidelines [97–100]. Kim [101] reviewed the mechanisms in nucleate pool boiling and reported enhanced convection, transient conduction, microlayer evaporation, and contact line heat transfer as fundamental mechanisms. Dhir et al. [102] presented a review on numerical simulations of pool boiling. In these reviews, single bubble dynamics and bubble coalescence were examined, and the effects of various parameters such as wall superheat, liquid subcooling, contact angle, gravity were discussed.

 One method for nucleate pool boiling heat transfer enhancement is to the integration of micro/nano structures to surfaces [103–106]. Instead of changing the surface area, another effective method to alter heat transfer characteristics is tuning liquid properties through the addition of nanoparticles [107]. Among the characterization studies on nanofluids, the majority of the published work reported their Newtonian behaviour [108–111], and some of the studies emphasized on non-Newtonian trends in the viscosity [112–115]. Nevertheless, one of the serious issues in the use of nanofluids is their tendency for instability, which appears as agglomeration and deposition of nanoparticles leading to decreased functionality in thermofluidic applications.

An alternative method to improve the performance is the inclusion of additives such as polymeric additives, reagents and surfactants into a base fluid such as water (aqueous surfactant and polymeric solutions)[116], which offers more stability compared to nanofluids.

Many polymeric additives in a pure base fluid (polymeric solutions) generate a shear dependent viscosity, which deviates from Newtonian fluid characteristics. The presence and amount of the additives (e.g. reagent or surfactants) basically change contact angle and interfacial tension of the solution. Interaction between rheological properties of solution with interfacial behavior determines how effective they are on heat transfer and bubble dynamics in boiling. Potchaphakdee and Williams [117] firstly reported the positive effect of polymer additives dissolved in water on boiling heat transfer. They had a minor effect on surface tension and major effect on viscosity, which also significantly influenced heat transfer. The experimental study of Manglik et al. [118], which presented measurements of dynamic and equilibrium surface tension of aqueous surfactant and polymeric solutions, showed that the surfactant and polymer additives in distilled water gave rise to the reduction in surface tension. As Cheng et al. [119] pointed out in their review, the enhancement of nucleate boiling heat transfer of polymeric solutions is mainly controlled by their viscosity, where an optimum viscosity, which is a function of the concentration and the molecular weight of the polymer, could be obtained [120,121]. In this regard, in work of Zhang and Manglik [122], the reduced dynamic surface tension accompanied with adsorption of macromolecules on a heating surface, which probably formed new nucleation sites, was believed to be the primary reason for heat transfer enhancement for hydroxyethyl cellulose (HEC) (with concentration, c, less than critical polymer concentration, c*). Heat transfer deteriorated with concentration for HEC solutions for c> c*. There was also a decreasing trend for Carbopol 934 solutions compared to pure water because of higher viscosity.

Recently, Zhang et al. [123] conducted experiments on boiling heat transfer of (non)ionic liquid polymers for hydrophilic/hydrophobic Alumina Sponge-like nano-porous surfaces (ASNPS) and realized that there is an optimal concentration, beyond which heat transfer performance decreases because of instantaneous liquid impingement and high density small bubbles, while the opposite is valid for concentrations smaller than this optimal one.

The aim of using polymeric solutions as an alternative of pure liquids, especially in dilute form, is to adjust heat transfer characteristics. The results reported in literature are

in contradiction to each other as stated in the review of Wasekar and Manglik [116]. For example, while the results of Kotchaphakdee and Williams [117] demonstrate enhancements in boiling heat transfer on plate heaters submerged in hydroxyl ethyl cellulose (HEC-H) and PA-30 solutions, the results of Wang and Hartnett [124], Hu [125], and Paul and Abdel-Khalik [121] degradation in heat transfer from platinum wire heaters in very dilute aqueous polymeric solutions compared to water. Few studies [126,127] reported that there was not any change in nucleate boiling heat transfer when polymeric additives were used.

The difference in boiling heat transfer of polymeric solutions from pure liquids can be associated with different bubble characteristics such as bubble size, shape, growth rate and release frequency. When compared to water, the bubbles detach from the surface with larger frequencies while having smaller sizes and more regular shapes [125,128,129]. Therefore, some polymeric solutions offer nucleate pool boiling enhancement.

CHAPTER 3

SINGLE-PHASE SLIP FLOW THROUGH PARALLEL-PLATE MICROCHANNELS

3.1 Analysis:

In this study, hydrodynamically and thermally fully developed, steady state, incompressible and laminar flows of non-Newtonian fluids with constant properties and power law assumption were analyzed for two-dimensional parallel-plates. Both isoflux and isothermal boundary conditions were applied to the parallel-plates configuration (Fig. 3.1).
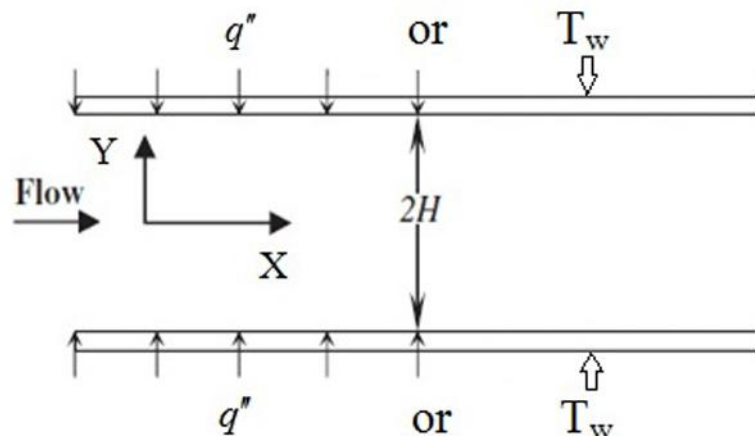
Fig. 3.1 A schematic of the geometry

Axial heat conduction effect in the fluid and wall was neglected, while viscous dissipation and wall slip were taken into account.

For non-Newtonian fluids, the following shear-stress power-law relationship is valid:

$$\tau = w \left| \frac{\partial U}{\partial Y} \right|^{n-1} \left(\frac{\partial U}{\partial Y} \right) \tag{3.1}$$

where   is the consistency factor and n is the power-law index.

The governing equations for fluid flow are continuity, x-momentum, and energy equations and are expressed as:

$$\frac{\partial U}{\partial X} + \frac{\partial V}{\partial Y} = 0 \tag{3.2}$$

$$\frac{\partial}{\partial Y} \left(w \left(\frac{\partial U}{\partial Y} \right)^{n-1} \frac{\partial U}{\partial Y} \right) - \frac{\partial P}{\partial X} = 0 \tag{3.3}$$

$$\cdots c_p U \frac{\partial T}{\partial X} = k \left(\frac{\partial^2 T}{\partial X^2} + \frac{\partial^2 T}{\partial Y^2} \right) + \left(w \left(\frac{\partial U}{\partial Y} \right)^{n-1} \right) \left(\frac{\partial U}{\partial Y} \right)^2 \tag{3.4}$$

where   is the density, P is the pressure, T is the temperature, c_p is the specific heat at constant pressure, k is the thermal conductivity, and U and V are velocity components in X and Y directions.

Linear Navier slip condition is a general boundary condition at the wall introducing the possibility of fluid slip at the interface of solid and fluid in micro scale and is stated as:

$$U_s - U_w = l \left(\frac{\partial U}{\partial Y} \right)_{wall} \tag{3.5}$$

where l is the slip length.

Another slip boundary condition applicable to non-Newtonian fluids is the non-linear Navier slip boundary condition, at which the wall velocity is proportional to the velocity gradient power to the power-law index [130,131].

A general slip boundary condition at wall applicable to every type of slip flow, regardless of Newtonian and non-Newtonian fluid flows, is the consideration of a slip

velocity, U_s, at wall (i.e. $U_{(at\ wall)}=U_s$). This type of slip velocity is taken in this study as the slip boundary condition, which can be then easily transformed into the linear slip boundary condition. It should be also noted that temperature-jump condition occurring in gas flows does not exist for liquid flows.

To facilitate an analytical solution, the governing equations are non-dimensionalized by using the following non-dimensional parameters as:

$$u = \frac{U}{U_m} \qquad v = \frac{V}{U_m} \qquad y = \frac{Y}{D} \qquad x = \frac{X}{D} \qquad p = \frac{P}{...U_m^2}$$

In addition, the following dimensionless numbers are introduced in the analysis:

$$Re = \frac{...U_m^{2-n}D_h^n}{W} \qquad S = \frac{U_s}{U_m} \qquad L = \frac{l}{D}$$

where Re is Reynolds number, L is dimensionless slip length, and   is slip coefficient.

The dimensionless governing equations with slip-boundary condition and no temperature jump condition are analytically solved to obtain the Poiseuille number (Po) and the Nusselt number (Nu), as well as the velocity and temperature distributions. The closed form expressions for Nu and Po corresponding to Newtonian liquid flow characteristics are also presented by letting n=1 while the results for the no-slip boundary condition correspond to the case of   =0, which is mostly valid for macro scale.

The non-dimensionalized x-momentum equation and slip-boundary condition expressions for Non-Newtonian fluid flows between parallel-plates become:

$$\frac{\partial}{\partial y}\left(\left(\frac{\partial u}{\partial y}\right)^{n-1}\frac{\partial u}{\partial y}\right) - Re\frac{\partial p}{\partial x} = 0 \tag{3.6}$$

$$u_w = S \tag{3.7}$$

$$u_s - u_w = L\left(\frac{\partial u}{\partial y}\right)_{y=w} \tag{3.8}$$

Subscripts s and w in all equations stand for the fluid properties at the surface and the wall, respectively.

The momentum equation stated in Eq. (6) can be analytically solved by imposing slip-boundary condition at the wall given in Eq. (7) along with the symmetry condition (via setting the axial velocity gradient at the middle to zero (i.e., $\partial u/\partial y$ (at y=0) =0)).

13

Accordingly, the corresponding dimensionless fully developed axial velocity profile, u, is obtained as:

$$u = \frac{1}{\dfrac{1}{\dfrac{1}{n}+2}-1-\langle(n+1)}\left((4y)^{\frac{1}{n}+1}-1-\langle(n+1)\right)$$ (3.9)

where

$$\langle = \frac{s}{(1-s)(1+2n)}$$ (3.9a)

Poiseuille number, Po = f Re, is defined as:

$$Po = \frac{2\ddagger}{...U^2} = 2m\left|\frac{\partial u}{\partial y}\right|^n$$ (3.10)

By substituting Eq. (9) into Eq. (10), Poiseuille number is derived as:

$$Po = 2w\left(\frac{4(1+2n)(1-s)}{n}\right)^n$$ (3.11)

The next step is solving the energy equation with viscous dissipation term for the two cases, namely, isoflux and isothermal boundary conditions.

For the constant heat flux case, the energy equation containing viscous heating term (viscous dissipation term) should be solved under no temperature-jump condition, while a constant heat flux is applied to the walls. In the energy equation, the longitudinal temperature gradient, T/ X, can be obtained with the application of the first law of thermodynamics to an elemental control volume as:

$$\dot{m}c_p\frac{\partial T}{\partial X} = q''u + \int \sim wdS$$ (3.12)

For a parallel plate channel cross-section, it can be written as:

$$...U_m Hc_p \frac{\partial T}{\partial X} = q^{"}(1+\frac{W}{q^{"}}\int_0^H (\frac{\partial U}{\partial Y})^{n+1}dY) \tag{3.13}$$

The above equation can be solved by introducing Brinkman number, defined as $Br = \dfrac{W U_m^{n+1}}{q^{"}D^n}$, as well as by performing the integral on the right-side as:

$$\frac{\partial T}{\partial X} = \frac{q^{"}A}{...U_m Hc_p} \tag{3.14}$$

where the parameter A is expressed as:

$$A = 1 + \frac{nBr}{4(1+2n)}\left(\frac{4s}{<n}\right)^{n+1} \tag{3.15}$$

Brinkman number, Br, is a dimensionless parameter representing viscous dissipation term. Its positive and negative values refer to wall heating (fluid is being heated) and wall cooling (fluid is being cooled), respectively.

With the introduction of the dimensionless temperature defined as $_" = \dfrac{T - \bar{T}_w}{Dq^{"}/k}$, the energy equation takes the following dimensionless form:

$$4Au = \frac{\partial^2 {}_"}{\partial y^2} + W\left|\frac{\partial u}{\partial y}\right|^{n-1}(\frac{\partial u}{\partial y})^2 \tag{3.16}$$

After the substitution of the velocity expression, Eq. (16) becomes:

$$4Au = \frac{\partial^2 {}_"}{\partial y^2} + Br\left(\frac{4s}{n<}\right)^{n+1}(4y)^{\frac{n+1}{n}} \tag{3.17}$$

The above expression has the following boundary conditions:

15

$$\left.\right|_{(y = 1/4)} = 0, \quad \partial / \partial y \big|_{(y = 0)} = 0 \tag{3.18}$$

Accordingly, an analytical solution for dimensionless temperature distribution can be derived as:

$$\theta = \frac{T - \overline{T}_w}{Dq'' / k} = \frac{\left(\begin{array}{l} A\big[\varsigma(16n + 128n^2 + 368Ln^3 + 448n^4 + 192n^5) + (16n + 112n^2 + 256n^3 + 192n^4)\big]y^2 \\ - A\big[2n^3 + 4n^4\big](4y)^{\frac{1+3n}{n}} + Br\left(\frac{4s}{n\varsigma}\right)^{n+1}\left(\frac{\varsigma}{4}(2n^3 + 6n^4 + 4n^5) + \frac{1}{2}(n^3 + n^4)\right)\big(1 - (4y)^{\frac{1+3n}{n}}\big) \\ - A\big[\varsigma(n + 8n^2 + 23n^3 + 28n^4 + 12n^5) + n + 7n^2 + 14n^3 + 8n^4\big] \end{array} \right)}{8(1+n)(1+2n)(1+3n)(\dfrac{n}{1-s})} \tag{3.19}$$

The dimensionless bulk or mean temperature is given as:

$$\theta_m = \frac{\int u \, \theta_w \, dS}{\int u \, dS} \tag{3.20}$$

After several manipulations, the following expression is obtained:

$$\theta_m = \frac{T_m - \overline{T}_w}{Dq'' / k} = \frac{8\varsigma^2 n^2 + C_{31}n + C_{32}n^2 + C_{33}n^3 + C_{34}n^4 + Br\Phi}{-48(5n + 2)(4n + 1)(\dfrac{n}{1-s})^2} \tag{3.21}$$

where

$$C_{31} = 84\varsigma^2 n^2 + 16\varsigma n$$

$$C_{32} = 320\varsigma^2 n^2 + 152\varsigma n + 8$$

$$C_{33} = 528\varsigma^2 n^2 + 440\varsigma n + 68 \tag{3.22}$$

$$C_{34} = 320\varsigma^2 n^2 + 400\varsigma n + 128$$

$$\Phi = \left(\frac{4s}{\varsigma n}\right)^{n+1}\left(\begin{array}{l} 2n^3 + 7n^4 + \varsigma^2(2n^3 + 11n^4 + 19n^5 + 10n^6) \\ + \varsigma(4n^3 + 18n^4 + 17n^5) \end{array}\right)$$

16

Nusselt number is defined as $Nu = \dfrac{Dq''}{k(\bar{T}_w - T_m)}$ and can also be written in terms of the dimensionless temperature as:

$$Nu = \frac{-1}{''_m} \tag{3.23}$$

Finally, Nusselt number can be expressed in the following form as:

$$Nu = \frac{48(5n+2)(4n+1)(\dfrac{n}{1-s})^2}{8\varsigma^2 n^2 + C_1 n + C_2 n^2 + C_3 n^3 + C_4 n^4 + Br\Phi} \tag{3.24}$$

It can be noted that the above expression is valid for Newtonian flows when n=1 and reduces to 140/(17+108Br), which agrees with the Nusselt number corresponding to the flow between parallel-plates given in the literature [12].

For the case of the linear Navier slip condition, it is sufficient to use the following expression for :

$$s = \frac{4L(1+2n)}{n+4L(1+2n)} \tag{3.25}$$

Second law analysis becomes significant in designing and improving the performance of thermal systems. This analysis in terms of entropy generation and Bejan number, which is based on irrevesibilities in fluid friction and heat transfer, is more significant in thermal systems, where there are high gradients in velocity and temperature, particularly in micro flows. Minimizing entropy generation would help to improve the efficiency of a system [132]. Accordingly, entropy generation rate and Bejan number are presented in this study to provide some insight to the second law analysis.

The volumetric rate of entropy generation can be expressed as [133]:

$$\dot{S} = \frac{k}{T^2}(\nabla T.\nabla T) + \frac{\tilde{\{}}{T} \tag{3.26}$$

where the first and second terms on the right side are (volumetric) Heat Transfer Irreversibility (HTI) and Fluid Friction Irreversibility (FFI), respectively.

For the case of non-Newtonian fluids, entropy generation rate is derived as:

$$\dot{S} = \frac{k}{T_i^2}\left((\frac{\partial T}{\partial X})^2 + (\frac{\partial T}{\partial Y})^2\right) + \frac{w}{T_i}\left|\frac{\partial U}{\partial Y}\right|^{n-1}\left(\frac{\partial U}{\partial Y}\right)^2 \tag{3.27}$$

In non-dimensional form, it can be expressed as:

$$N_s = \dot{S}\frac{D^2}{k\Omega^2} = \left((\frac{4A}{Pe})^2 + (\frac{\partial_n}{\partial y})^2\right) + \frac{Br}{\Omega}\left|\frac{\partial u}{\partial y}\right|^{n+1} \tag{3.28}$$

or

$$N_s = \dot{S}\frac{D^2}{k\Omega^2} = \left((\frac{4A}{Pe})^2 + (\frac{\partial_n}{\partial y})^2\right) + \frac{Br}{\Omega}\left(\frac{4s}{<n}\right)^{n+1}(4y)^{\frac{n+1}{n}} \tag{3.29}$$

where $\quad = q^{''}D/T_i k$ and $\quad / y$ is as follows:

$$\left(\frac{\partial_n}{\partial y}\right) = \frac{\left(\begin{array}{l} -\left[<(4n+28n^2+72n^3+80n^4+32n^5)+4n+24n^2+48n^3+32n^4\right]y+ \\ \left[n^2+4n^3+4n^4\right](4y)^{\frac{1+2n}{n}} + Br\left(\frac{4s}{<n}\right)^{n+1}\left(\begin{array}{l}\frac{<}{4}(n^2+5n^3+8n^4+4n^5)\\ +\frac{1}{4}n^2+n^3+n^4\end{array}\right)\left((4y)^{\frac{1+2n}{n}}-4y\right) \end{array}\right)}{(1+n)(1+2n)^2(\frac{n}{1-s})} \tag{3.30}$$

The main aim of second law analysis is to find parameters minimizing global entropy generation rate, denoted by $<N_s>$, which is related to whole dissipations generated by irreversibilities in the channel, which affect the performance of the system. Therefore, it is required to integrate N_s across the cross-sectional area occupied by the fluid through $<N_s> = \int N_s dS / S$. After performing the integral, one could express $<N_s>$ as follows:

$$< N_s >= (\frac{4A}{Pe})^2 + \left(\frac{a^2}{48} + (1/4)^{\frac{2+4n}{n}} \frac{nb^2}{2+5n} + (1/4)^{\frac{1+4n}{n}} \frac{8abn}{1+4n} \right)$$
$$+ \frac{nBr}{(1+2n)\Omega} \left(\frac{4s}{<n} \right)^{n+1} \tag{3.31}$$

where

$$a = \frac{\left(\begin{array}{l} -<(4n+28n^2+72n^3+80n^4+32n^5)-4n-24n^2-48n^3-32n^4 \\ -4Br\left(\frac{4s}{<n}\right)^{n+1}\left(\frac{<}{4}\left(n^2+5n^3+8n^4+4n^5\right)+\frac{1}{4}n^2+n^3+n^4\right) \end{array} \right)}{(1+n)(1+2n)^2(\frac{n}{1-s})} \tag{3.32}$$

and

$$b = \frac{(4)^{\frac{1+2n}{n}}\left(n^2+4n^3+4n^4+Br\left(\frac{4s}{<n}\right)^{n+1}\left(\frac{<}{4}\left(n^2+5n^3+8n^4+4n^5\right)+\frac{1}{4}n^2+n^3+n^4\right) \right)}{(1+n)(1+2n)^2(\frac{n}{1-s})}$$

The Bejan number, Be, is defined as the ratio of entropy generated due to heat transfer, S_{HTI}, to the total entropy generation rate $S_{(HTI+FFI)}$, and is expressed as:

$$Be = \frac{(\frac{4A}{Pe})^2 + (\frac{\partial_{''}}{\partial y})^2}{\left((\frac{4A}{Pe})^2 + (\frac{\partial_{''}}{\partial y})^2\right) + \frac{Br}{\Omega}\left|\frac{\partial u}{\partial y}\right|^{n+1}} \tag{3.33}$$

or

$$Be = \frac{(\frac{4A}{Pe})^2 + (\frac{\partial_{''}}{\partial y})^2}{\left((\frac{4A}{Pe})^2 + (\frac{\partial_{''}}{\partial y})^2\right) + \frac{Br}{\Omega}\left(\frac{4s}{<n}\right)^{n+1}(4y)^{\frac{n+1}{n}}} \tag{3.34}$$

When the heat transfer irreversibility dominates, the value of Be converges to unity, while the irreversibility is solely caused by to fluid friction when Be goes to 0.

For the isothermal wall boundary condition and fully developed flows, the axial gradient temperature is zero, and Brinkman number does not appear in the energy equation. The dimensionless temperature is then written as:

$$\theta = \frac{T - T_w}{wU^{n+1}/kD^{n-1}} \tag{3.35}$$

Accordingly, the dimensionless energy equation becomes:

$$\frac{\partial^2 \theta}{\partial y^2} = -\left|\frac{\partial u}{\partial y}\right|^{n+1} \tag{3.36}$$

The above equation is also a second-order linear equation, where the convective term is not present. Applying the proper thermal boundary conditions, a solution for temperature distribution is obtained as:

$$\theta = \frac{T - T_w}{wU^{n+1}/kD^{n-1}} = \frac{n^2\left(\dfrac{4s}{\varsigma n}\right)^{n+1}\left(1-(4y)^{\frac{1+3n}{n}}\right)}{16(1+2n)(1+3n)} \tag{3.37}$$

Using the above expression, the mean temperature is deduced as:

$$\theta_m = \frac{T_m - T_w}{wU^{n+1}/kD^{n-1}} = \frac{\left(\dfrac{4s}{\varsigma n}\right)^{n+1}\left(\dfrac{\varsigma}{4}\left(4n^3+18n^4+20n^5\right)+n^3+3n^4\right)}{8(1+2n)(1+4n)(2+5n)\left(\dfrac{n}{1-s}\right)} \tag{3.38}$$

Then, Nu can be obtained from the following expression:

$$Nu = \frac{\left.\dfrac{\partial \theta}{\partial y}\right|_{y=w}}{\theta_m} \tag{3.39}$$

Accordingly, the following expression for Nu can be found:

20

$$Nu = \frac{2(1+4n)(2+5n)(\frac{n}{1-\text{s}})}{n^2 + 3n^3 + \frac{\text{<}}{4}\left(4n^2 + 18n^3 + 20n^4\right)} \qquad (3.40)$$

For Newtonian fluids (n=1), it reduces to:

$$Nu = \frac{140}{8-\text{s}} \qquad (3.41)$$

The results of Eq. (3.41) agree with the results reported in the literature [12].

The entropy generation rate for non-Newtonian fluids and the case of isothermal wall boundary condition is written as:

$$\dot{S} = \frac{k}{T_i^2}\left((\frac{\partial T}{\partial Y})^2\right) + \frac{\text{w}}{T_i}\left|\frac{\partial U}{\partial Y}\right|^{n-1}\left(\frac{\partial U}{\partial Y}\right)^2 \qquad (3.42)$$

Or

$$\dot{S} = \frac{k}{T_i^2}\left((\frac{\partial T}{\partial Y})^2\right) + \frac{\text{w}}{T_i}\left|\frac{\partial U}{\partial Y}\right|^{n+1} \qquad (3.43)$$

Its dimensionless form takes the following form:

$$N_s = \frac{D^2}{k\text{Œ}^2}\dot{S} = (\frac{\partial_{\prime\prime}}{\partial y})^2 + \frac{1}{\text{Œ}}\left(\frac{4\text{s}}{\text{<}n}\right)^{n+1}\left(4y\right)^{\frac{n+1}{n}} \qquad (3.44)$$

where the dimensionless heat flux , , and / y are as follows:

$$\quad = \ U^{n+1}/ T_i \ kD^{n-1} \qquad (3.45)$$

$$\qquad (3.46)$$

$$\frac{\partial_{\prime\prime}}{\partial y} = \frac{-n\left(\frac{4\text{s}}{\text{<}n}\right)^{n+1}\left((4y)^{\frac{1+2n}{n}}\right)}{4(1+2n)}$$

Global entropy generation rate, <N$_s$>, is found as:

$$< N_s >= \frac{n^3}{16(2+5n)(1+2n)^2}\left(\frac{4\varsigma}{\langle n}\right)^{2n+2} + \frac{n}{\text{Œ}(1+2n)}\left(\frac{4\varsigma}{\langle n}\right)^{n+1} \tag{3.47}$$

Finally, Bejan number is obtained as:

$$Be = \frac{(\frac{\partial_{''}}{\partial y})^2}{(\frac{\partial_{''}}{\partial y})^2 + \frac{1}{\text{Œ}}\left|\frac{\partial u}{\partial y}\right|^{n+1}} \tag{3.48}$$

or

$$Be = \frac{(\frac{\partial_{''}}{\partial y})^2}{(\frac{\partial_{''}}{\partial y})^2 + \frac{1}{\text{Œ}}\left(\frac{4\varsigma}{\langle n}\right)^{n+1}(4y)^{\frac{n+1}{n}}} \tag{3.48}$$

3.2 Results and Discussion

This section includes the influence of slip coefficient and viscous dissipation on heat transfer characteristics of hydrodynamically and thermally fully developed non-Newtonian fluid flows between parallel-plates at both constant heat flux and constant wall temperature boundary conditions. First, constant heat flux boundary condition is considered. Thereafter, the results corresponding to constant wall temperature boundary condition are presented.

Shear thinning (or pseudoplastic) fluids with $0 \ n<1$ are non-Newtonian fluids, whose viscosity decreases with increasing shear rate, while the opposite is true for shear thickening (or dilatants) fluids with $n>1$. Figure 3.2 shows the dimensionless velocity distribution at different power-law indices, n, for the no-slip condition. It can be seen that the core velocity of the fluid increases with n, while its velocity gradient decreases. In other words, the velocity profile of shear-thinning fluids becomes more uniform with the decrease in n. It should be noted that a parabolic profile is obtained for Newtonian

fluids (n=1). On the other hand, the profile becomes more non-uniform for shear-thickening fluids (n>1).
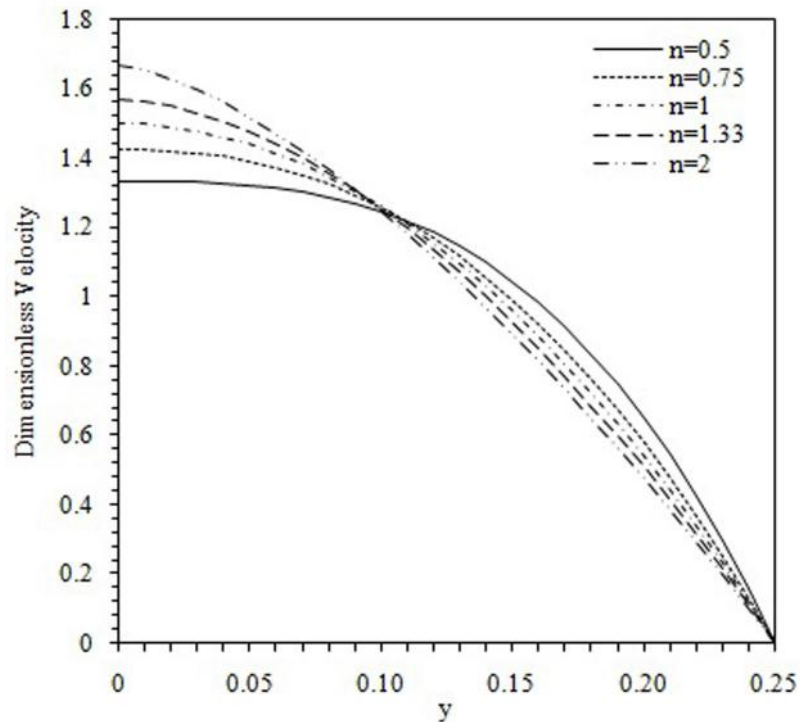
Fig. 3.2 Dimensionless fully developed velocity profiles for different values of n at
= 0

The effect of slip coefficient on the velocity distribution is displayed in Fig. 3.3 for a shear-thinning fluid (pseudoplastic) with n=0.5. As can be seen, in contrast to no-slip condition, there is a decrease in velocity gradient at both the wall and the core velocity with the increase of the slip velocity (increase in   ) for maintaining constant flow rate in the channel. For large values of   , the flow converges to "Plug flow", where the liquid acts like a solid slipping in the channel.

Figure 3.4 displays Nusselt number as a function of power-law index, n, at various slip coefficients in the absence of viscous heating (Br=0) for the constant heat flux case. It can be clearly observed that Nusselt number decreases with power-law index, which is due to the fact that the velocity gradients are greater near the wall for lower power-law index values (Fig. 3.2).
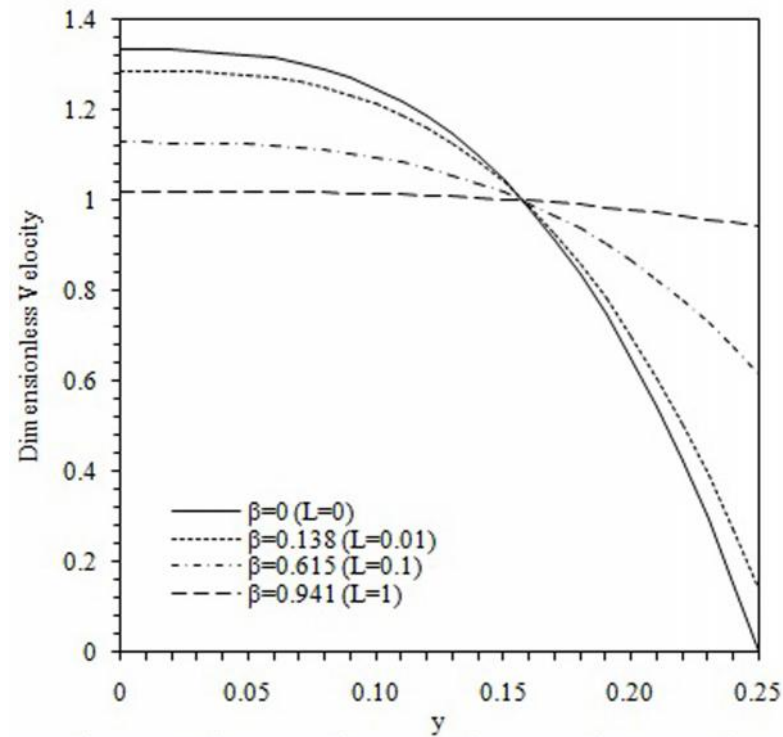
Fig. 3.3 Dimensionless fully developed velocity profiles for different values of   at n = 0.5

Furthermore, an increase in slip coefficient gives rise to the enhancement in heat transfer. This is in contrast to the results on slip flow for gas flows [134], where a temperature jump condition exists at the wall resulting in lower temperature gradients. However, no temperature jump condition exists for this case (liquid flow). In addition, the existence of slip condition in velocity increases convection by increasing streamwise velocity near walls leading to higher Nusselt number values. The effect of slip coefficient on Nusselt number is more dominant for shear-thickening fluids (n>1) than shear-thinning fluids (n<1). For example, the Nusselt number increase is around 26.6% for a shear-thickening fluid (n=1.5) for a slip coefficient of 0.6, while it is 20.3% for a shear-thinning fluid (n=0.5). Velocity profiles are more uniform for shear thinning fluids compared to shear thickening fluids. When a velocity slip condition exists at the wall, enhanced convection effects near the wall are therefore not as pronounced as in shear thickening fluids. As a result, a larger increase in heat transfer is apparent for shear thickening fluids for slip flows.
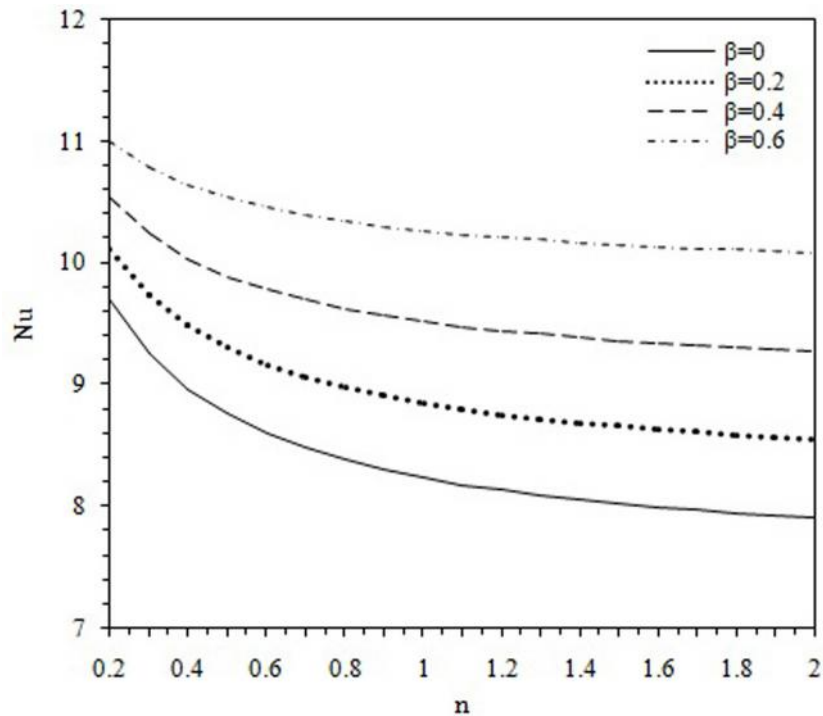
Fig. 3.4 Variation of Nusselt number versus n for different values of   at Br=0

Figures 3.5 and 3.6 illustrate Nusselt number as a function of slip coefficient at different Br for two n values, namely n=0.5 (Shear-thinning fluid), and n=1.5 (Shear-thickening fluid), respectively. As can be seen from these figures, Nusselt number increases dramatically with slip coefficient for these two n values. The increase in Br also leads to considerably lower Nusselt numbers due to increasing viscous dissipation effects. Indeed, viscous dissipation contributes to internal heating of the fluid and increases the mean temperature of the fluid. As a result, it increases the temperature difference between the wall and the mean fluid and therefore has a negative effect on convective heat transfer. Furthermore, the reduction in Nusselt number with Brinkman number for shear-thickening fluids is higher than that of shear-thinning fluids, which arises from the fact that viscous dissipation increases the mean temperature of shear-thickening fluids more. For instance, Nusselt number is decreased by 94.6% when Br goes from zero to 0.1 for n=1.5, whereas the decrease is 70.4% for n=0.5. Again, the decreasing trend in Nusselt number with n is observed in these figures, where viscous heating is also present.
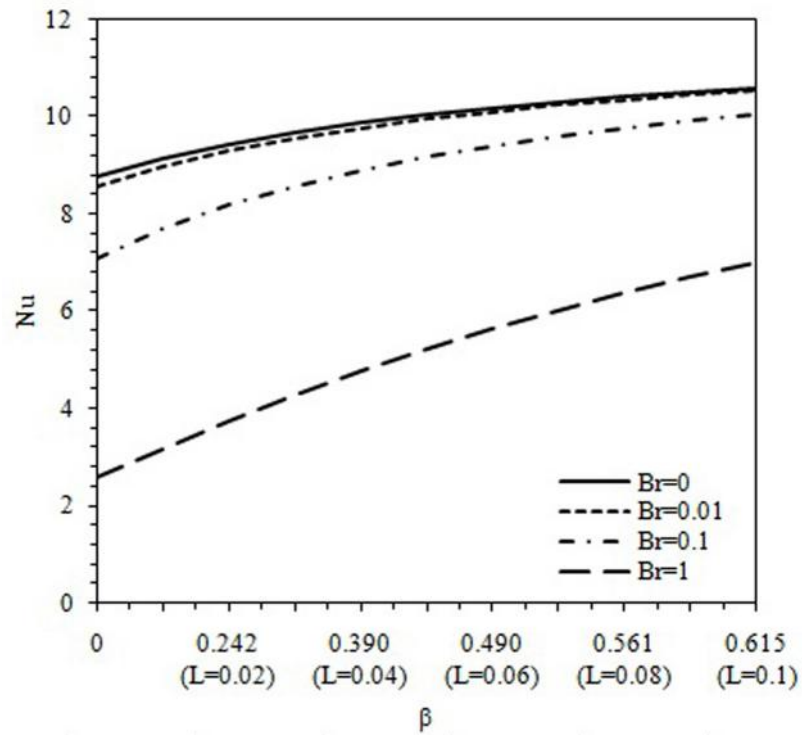
Fig. 3.5 Variation of Nusselt number versus β for different values of Br at n=0.5
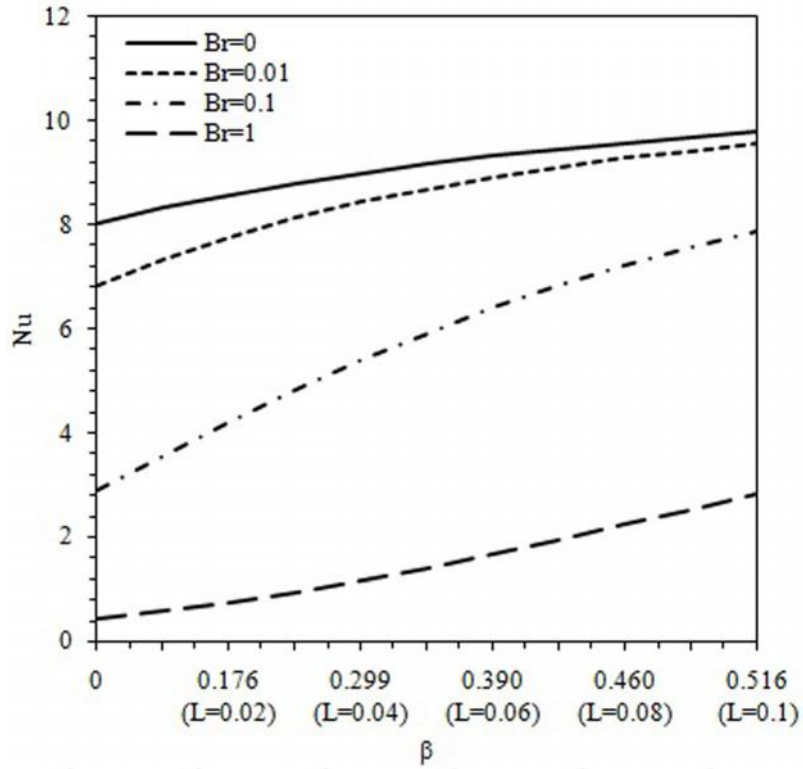
Fig. 3.6 Variation of Nusselt number versus β for different values of Br at n=1.5

26

Figures 3.7 and 3.8 display Nusselt number as a function of Br at different slip coefficient values for n=0.5 and n=1.5. One can observe the existence of some singularity points in Nusselt number for each . At these singular points, where the mean temperature reaches the wall temperature, the heat transfer between the fluid and wall cannot be expressed in terms of Nu. It is clear that by going away from singularities the absolute value of the Nusselt number asymptotically converges to zero, as expected from Nusselt number expression. Under slip flow conditions, the singularities occur at larger Br absolute values, while for shear-thickening fluids, they are close to each other.
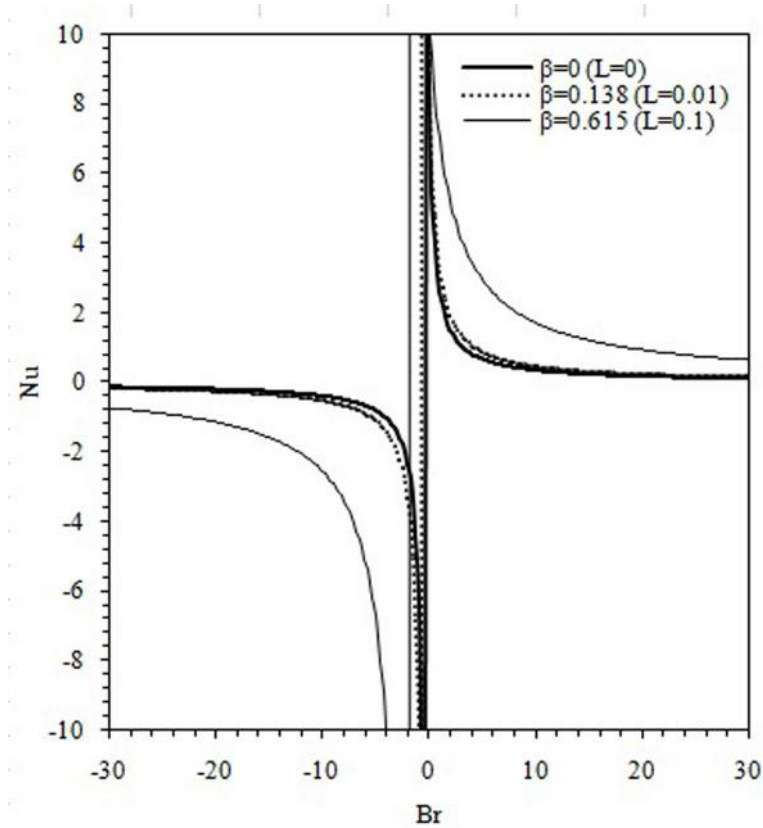
Fig. 3.7 The effect of Br on Nusselt number for different at n=0.5
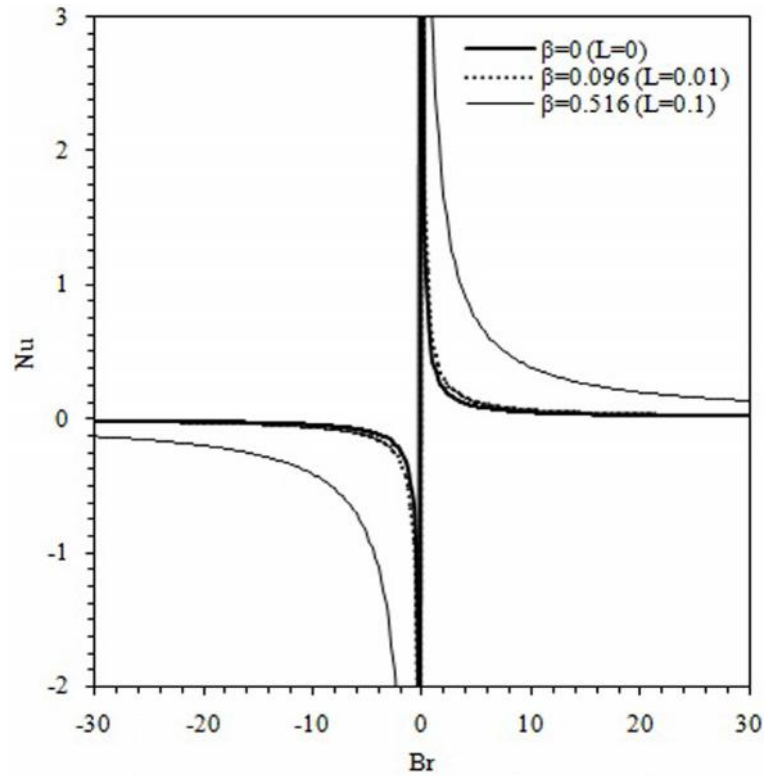
Fig. 3.8 The effect of Br on Nusselt number for different   at n=1.5

Tables 3.1 and 3.2 provide the values of global entropy generation rate $<N_s>$ at the wall isoflux case, while axial heat conduction is absent (i.e. Pe   ). Based on the results, either existence of slip condition or increasing slip coefficient causes the decrease in global entropy generation rate since slip condition leads to smaller velocity and temperature gradients particularly at the solid surface, which improves the performance of the system. On the other hand, the results show that an increase in Brinkman number leads to an increase in $<N_s>$. Therefore, the fluidic system with less Br would result in better working performance. It is known from the Brinkman number definition that it is directly proportional to the magnitude of velocity and has an inverse relationship with both heat flux and diameter of the channel. In other words, in order to minimize global entropy generation rate (i.e. irreversibility), lower magnitude of velocity with higher heat flux and larger channel height should be considered.

Moreover, shear-thickening fluids have larger $<N_s>$ values compared to shear-thinning fluids, which is due to larger gradients in velocity and temperature at walls, which are more influential regions in the domain for entropy generation distributions. The channel wall is a location, where maximum velocity and temperature gradients exist, while they are zero at the center. Accordingly, entropy generation rate, N_s, reaches its maximum

28

and minimum values at the wall and center, respectively. Consequently, Brinkman number and slip coefficient have a significant effect on entropy generation near the walls.

Table 3.1 The values of global entropy generation rate at =0.1, =0.2 and Pe

	Br			
	0	0.001	0.01	0.1
n				
0.2	0.396	0.456	1.000	6.443
0.3	0.411	0.487	1.171	8.013
0.4	0.422	0.516	1.364	9.851
0.5	0.430	0.546	1.589	12.036
0.6	0.436	0.578	1.856	14.650
0.7	0.442	0.615	2.174	17.789
0.8	0.446	0.657	2.554	21.567
0.9	0.449	0.705	3.011	26.121
1	0.452	0.763	3.560	31.613
1.1	0.455	0.831	4.222	38.239
1.2	0.457	0.913	5.019	46.238
1.3	0.459	1.011	5.979	55.896
1.4	0.461	1.128	7.137	67.562
1.5	0.462	1.269	8.532	81.656
1.6	0.463	1.438	10.215	98.691
1.7	0.465	1.642	12.245	119.288
1.8	0.466	1.887	14.692	144.206
1.9	0.467	2.182	17.643	174.367
2	0.468	2.538	21.203	210.902

Table 3.2 The values of global entropy generation rate at $\quad$ =0.1, Br=0.01 and Pe

	0	0.2	0.4	0.6
n				
0.2	1.203	1.000	0.807	0.626
0.3	1.448	1.171	0.913	0.679
0.4	1.735	1.364	1.028	0.732
0.5	2.079	1.589	1.157	0.789
0.6	2.496	1.856	1.304	0.850
0.7	3.006	2.174	1.473	0.917
0.8	3.632	2.554	1.670	0.991
0.9	4.402	3.011	1.899	1.073
1	5.350	3.560	2.166	1.165
1.1	6.518	4.222	2.478	1.267
1.2	7.958	5.019	2.842	1.382
1.3	9.734	5.979	3.269	1.510
1.4	11.925	7.137	3.767	1.654
1.5	14.628	8.532	4.351	1.816
1.6	17.962	10.215	5.035	1.998
1.7	22.076	12.245	5.836	2.202
1.8	27.154	14.692	6.773	2.431
1.9	33.420	17.643	7.871	2.688
2	41.154	21.203	9.157	2.977

Figures 3.9 and 3.10 demonstrate the distribution of Bejan number for different values of Br at $\quad$ =0, $\quad$ =0.1 in the cases of shear-thinning and shear-thickening fluids, respectively. For Br =0 (no viscous dissipation), Bejan number has the value of one regardless of transverse coordinate and power-law index, which means that the fluid friction irreversibility does not play a role in generation of the entropy, as expected from Eq. (34). As can be deduced from Eq. (34), Be is maximum at the center and has the value of one. There is a sharp drop in Bejan number from unity to smaller values for shear-thickening fluids by moving for a very small distance away from the center

particularly at higher Br. Small values of Be (Be<0.5) for these fluids indicate that the fluid friction irreversibility mainly dominates the heat transfer irreversibility. For shear-thinning fluids, the values of Be gradually decrease from unity at centerline, where there is zero velocity gradient, to relatively smaller values at the wall, where the velocity gradient is the largest. Be values are mostly lower than 0.5, beyond which heat transfer irreversibility exceeds fluid friction irreversibility. Accordingly, for shear thinning fluids (except for low Br) the contribution to the total entropy generation is mainly attributed to heat transfer irreversibility, while for shear-thickening fluids, irreversibility is mainly due to the fluid friction.
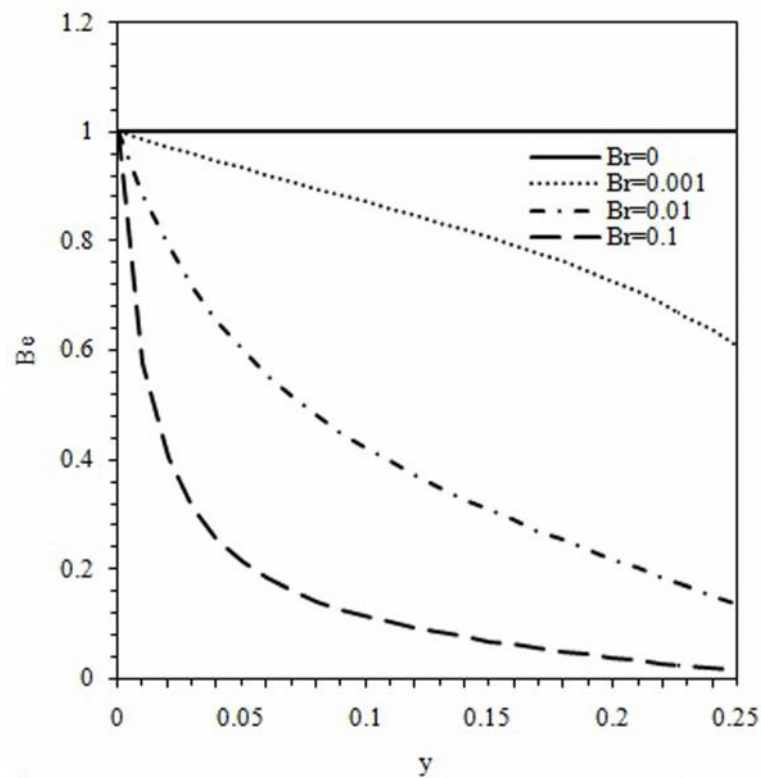
Fig. 3.9 Bejan number distribution for different Br at n=0.5, =0.1 and =0
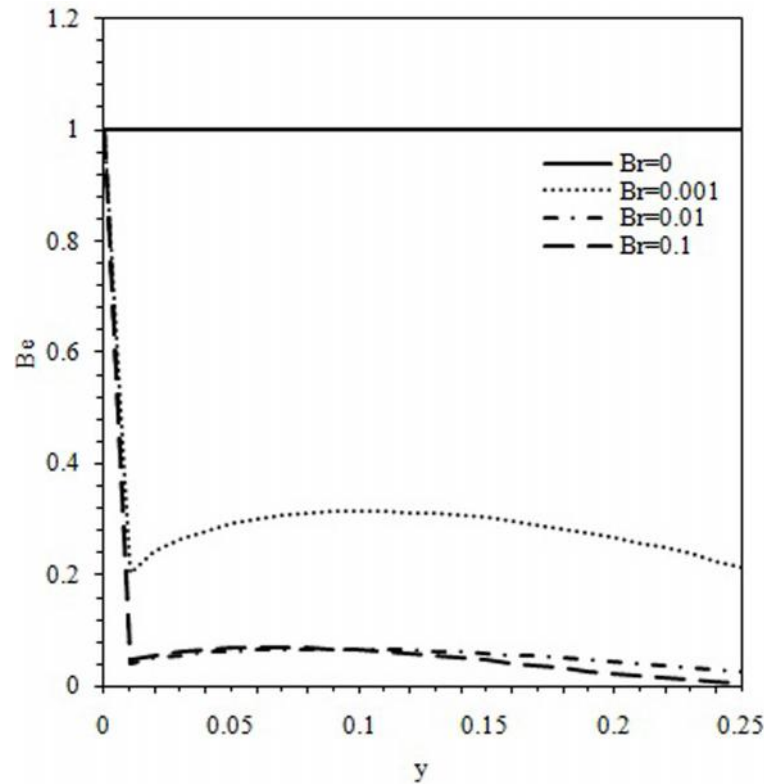
Fig. 3.10 Bejan number distribution for different Br at n=1.5, =0.1 and =0

The dependence of Bejan number distribution on slip coefficient at Br=0.01 and =0.1 is displayed in Figs. 3.11 and 3.12 for the cases of n=0.5 and n=1.5, respectively. An increase in from 0 to 0.615 for n=0.5 and from 0 to 0.516 for n=1.5 results in a reduction of the velocity gradient and a rise in the rate of heat transfer irreversibility (in terms of Be) up to 193% and 442% at the wall, respectively. However, irreversibilities due to fluid friction are still pronounced for shear-thickening fluids. Again, sharp drop from one to small values of Be in these figures indicates the dominance of fluid friction in irreversibility.

As mentioned before, the axial temperature gradient and Brinkman number do not appear in the energy equation for the isothermal wall boundary condition. Figure 3.13 displays the effect of slip coefficient on Nusselt number as a function of power-law index. The results indicate that similar to isoflux wall boundary condition, the increase in power-law index results in a decrease in Nusselt number. Furthermore, Nusselt number also increases when there is velocity slip on the surface, but this increase is more at higher n, similar to the constant heat flux boundary condition.
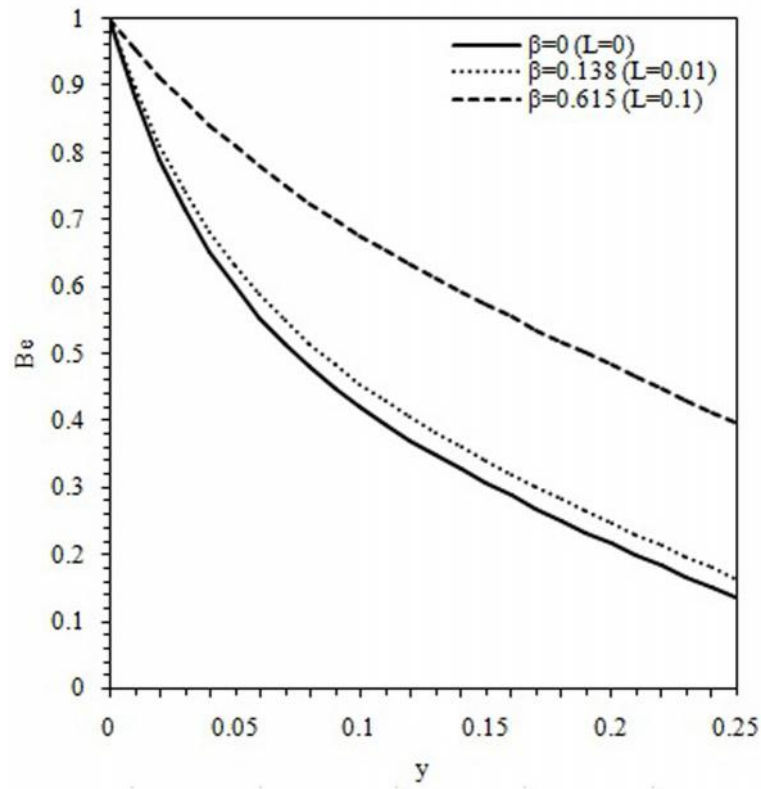
Fig. 3.11 Bejan number distribution for different   at n=0.5,   =0.1 and Br=0.01
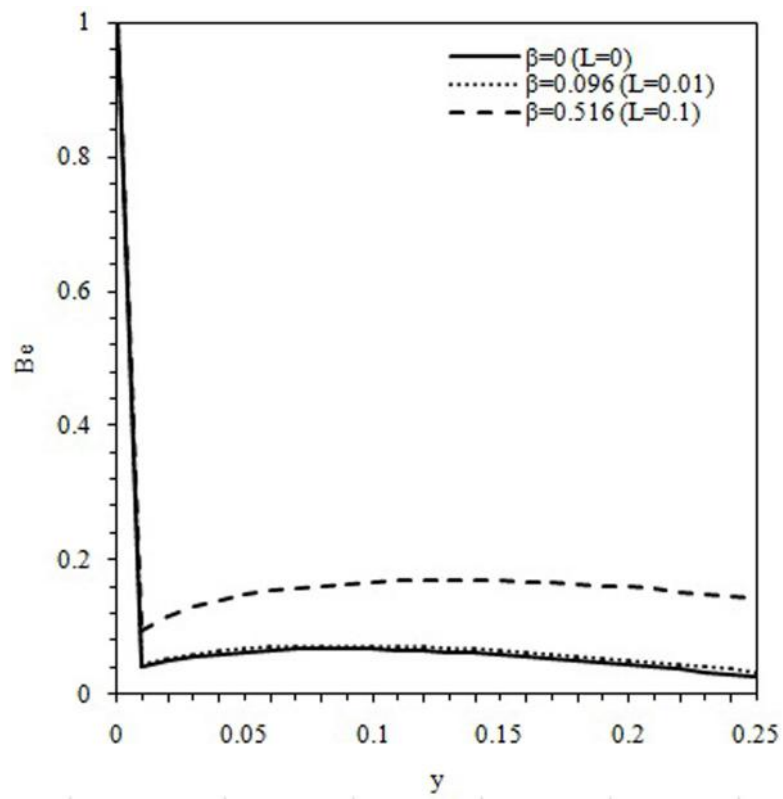
Fig. 3.12 Bejan number distribution for different   at n=1.5,   =0.1 and Br=0.01
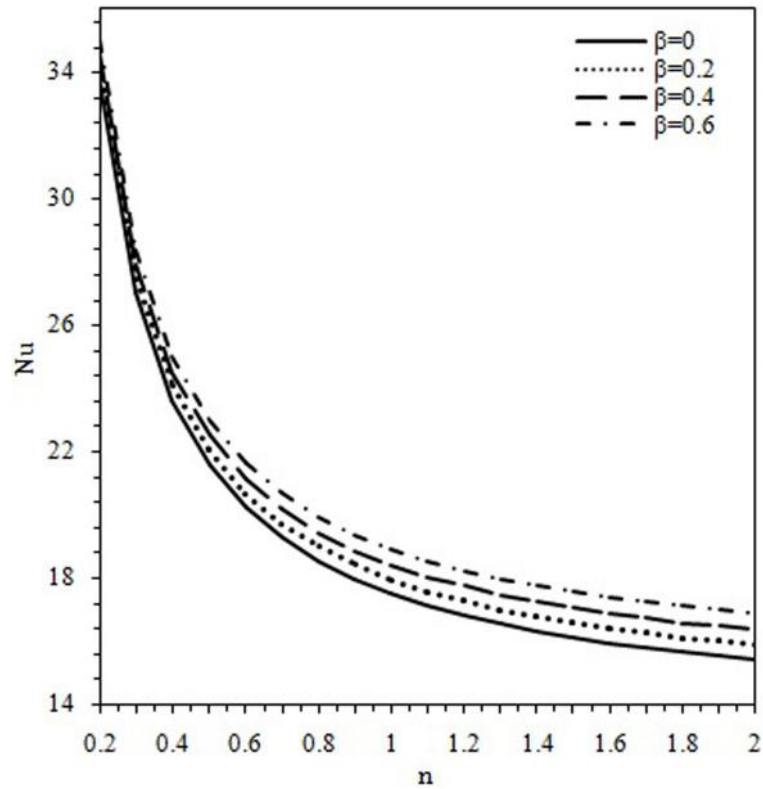
Fig. 3.13 Variation of Nusselt number versus n for different values of

The trends in N_s and Be for the isothermal wall condition and the corresponding discussion are relatively the same as those for the isoflux wall condition case and will not bring any additional insight. Therefore, their N_s and Be plots are not included.

3.3 Conclusions

An analysis on convective heat transfer and entropy generation was performed to examine the effects of slip coefficient, power-law index and viscous heating on heat transfer characteristics of hydrodynamically and thermally fully developed slip flows of non-Newtonian fluids between parallel-plates at isoflux and isothermal thermal boundary conditions. The effects of key parameters such as slip coefficient, , power-law index, n, and Brinkman number, Br, on Nusselt number, entropy generation rate

and Bejan number have been assessed. Major conclusions drawn from this study are as follows:

- Nusselt number and Bejan number decrease with the increase in either power-law index or Brinkman number, while they increase with slip coefficient.

- The global entropy generation rate increases with increasing both power-law index and Brinkman number, whereas a reduction in the global entropy generation rate is observed with the existence of slip condition and an increase in slip coefficient.

- The effect of key parameters on Nusselt number and the rate of entropy generation is more pronounced for shear-thickening fluids.

CHAPTER 4

SINGLE-PHASE NON-SLIP FLOW THROUGH MICROTUBE WITH TEMPERATURE-DEPENDENT PROPERTIES

4.1 Analysis:

In this study, hydrodynamically and thermally fully developed, steady state, incompressible and laminar flows of power-law fluids with constant and variable thermophysical properties are analyzed for circular channels under the isoflux thermal boundary condition applied to the tube wall (Fig. 4.1).
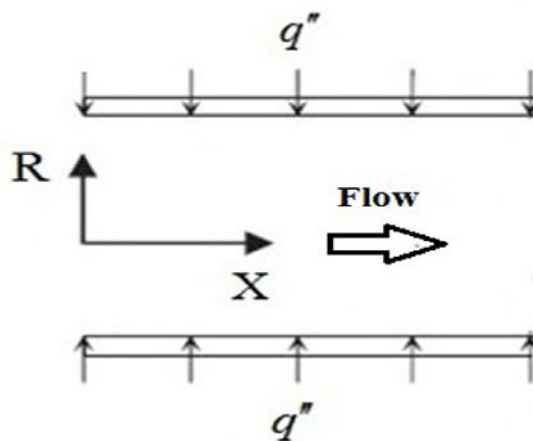
Fig. 4.1 Isoflux heating applied to a circular channel

For a power-law fluid, the following shear-stress power-law relationship is valid:

$$\ddagger = \text{\textmu} \left| \frac{\partial U}{\partial R} \right|^{n-1} \left(\frac{\partial U}{\partial R} \right)$$

(4.1)

where $\text{\textmu}_{ref} \left| \frac{\partial U}{\partial R} \right|^{n-1}$ is viscosity with the consistency factor at room temperature, $_{ref}$, and the power-law index, n. The governing equations are x-momentum and energy equations, which can be formulated respectively as

$$\frac{1}{R} \frac{\partial}{\partial R} \left({\sim} R \frac{\partial U}{\partial R} \right) - \frac{\partial P}{\partial X} = 0$$

(4.2)

$$_{\ldots} c_p U \frac{\partial T}{\partial X} = \frac{1}{R} \frac{\partial}{\partial R} \left(kR \frac{\partial T}{\partial R} \right) + {\sim} \left(\frac{\partial U}{\partial R} \right)^2$$

(4.3)

where is the density, P is the pressure, T is the temperature, c_p is the specific heat at constant pressure, k is the thermal conductivity, and U is velocity component in X direction.

In order to proceed with a solution, viscosity and thermal conductivity must be defined as a function of temperature. Reynolds [135] proposed an exponential model for the temperature-dependence of viscosity as:

$$\sim \; = \; \sim_{ref} \exp(-b'T)$$

(4.4)

where T is temperature, and μ_s and b are coefficients. Using a truncated Taylor series for exp(-bT) similar to Hooman and Ejlali [136], viscosity is expressed as:

$$\sim \; = \; \sim_{ref} \left(1 - \frac{\Delta T}{\sim_{ref}} \frac{d\sim}{dT} \frac{T - \overline{T_w}}{\Delta T} \right) = \; \sim_{ref} (1 - \text{v}_{\textit{n}}) = \text{\textmu}_{ref} (1 - \text{v}_{\textit{n}}) \left| \frac{\partial U}{\partial R} \right|^{n-1}$$

(4.5)

where

$$k = k_{ref}\left(1 + \frac{\Delta T}{\tilde{\sim}_{ref}}\frac{dk}{dT}\frac{T - \overline{T_w}}{\Delta T}\right) = k_{ref}(1 + \vee_{k''})$$ (4.6)

$$\vee = \frac{d\tilde{\sim}}{dT}\bigg|_{T_s}\frac{\Delta T}{\tilde{\sim}_{ref}}$$ (4.7)

$$\vee_k = \frac{dk}{dT}\bigg|_{T_s}\frac{\Delta T}{k_{ref}}$$ (4.8)

Here $\dfrac{T - \overline{T_w}}{\Delta T}$ is the dimensionless temperature, . ε_k is defined to be a coefficient of ε, i.e.

$\varepsilon_k = \Gamma\varepsilon$, in which Γ will be obtained for water as a working case through computational simulation.

The governing equations for x-momentum and energy equations can be stated as:

$$\frac{1}{R}\frac{\partial}{\partial R}\left(\tilde{\sim}_s(1 - \vee_{''})R\frac{\partial U}{\partial R}\right) - \frac{\partial P}{\partial X} = 0$$ (4.9)

or

$$\frac{1}{R}\frac{\partial}{\partial R}\left(R w_{ref}(1 - \vee_{''})\left|\frac{\partial U}{\partial R}\right|^{n-1}\left(\frac{\partial U}{\partial R}\right)\right) - \frac{\partial P}{\partial X} = 0$$ (4.10)

$$\dots c_p U\frac{\partial T}{\partial X} = \frac{1}{R}\frac{\partial}{\partial R}\left(k_s(1 + \vee_{k''})R\frac{\partial T}{\partial R}\right) + \left(w_{ref}\left|\frac{\partial U}{\partial R}\right|^{n-1}(1 - \vee_{''})\right)\left(\frac{\partial U}{\partial R}\right)^2$$ (4.11)

To facilitate an analytical solution, the governing equations are non-dimensionalized by using the following non-dimensional parameters and Reynolds number, Re, as:

$$u = \frac{U}{U_m} \qquad r = \frac{R}{r_o} \qquad x = \frac{X}{r_o} \qquad p = \frac{P}{\dots U_m^2} \qquad Re = \frac{\dots U_m^{2-n}D^n}{w_{ref}}$$

The dimensionless governing equations are analytically solved to obtain Nusselt number (Nu), as well as the velocity and temperature distributions. The closed form expressions for Nu corresponding to Newtonian liquid flow characteristics can also obtained by setting n=1.

The first step is to derive the velocity distribution. With the introduction of Reynolds number, the non-dimensionalized x-momentum equation becomes:

$$\frac{1}{r}\frac{\partial}{\partial r}\left[(1-v_{,,})r\left(\frac{\partial u}{\partial r}\right)^{n}\right]=\text{Re}\frac{\partial p}{\partial x}\qquad(4.12)$$

The above equation can be solved using the no-slip boundary condition at wall along with the symmetry condition at the center (via setting the axial velocity gradient at the center to zero (i.e., $\partial u/\partial r_{(\text{at }r=0)}=0$)).

After implementing the symmetry condition, and using Taylor series with the first order approximation, one can write:

$$\frac{\partial u}{\partial r}=\left(\text{Re}\frac{\partial p}{\partial x}\frac{r}{2}\right)^{\frac{1}{n}}(1+\frac{1}{n}{}_{,,}v)\qquad(4.13)$$

For most practical cases, the viscosity variation number is small compared to unity, i.e. $\ll 1$. This allows for a regular asymptotic expansion assumption (for dependent variables u and) in the following form

$$u=u_{0}+vu_{1}\qquad(4.14)$$

$$_{,,}=_{,,0}+v_{,,1}$$

As a result, Eq. (13) takes following form:

$$\frac{\partial u_{0}}{\partial r}+v\frac{\partial u_{1}}{\partial r}=\left(\text{Re}\frac{\partial p}{\partial x}\frac{r}{2}\right)^{\frac{1}{n}}(1+\frac{1}{n}{}_{,,0}v)\qquad(4.15)$$

Splitting the above equation into two following equations

$$\frac{\partial u_{0}}{\partial r}=\left(\frac{\text{Re}}{2}\frac{\partial p}{\partial x}\right)^{\frac{1}{n}}r^{\frac{1}{n}}\qquad(4.16)$$

$$v\frac{\partial u_{1}}{\partial r}=v\left(\frac{\text{Re}}{2}\frac{\partial p}{\partial x}\right)^{\frac{1}{n}}(\frac{1}{n}{}_{,,0})r^{\frac{1}{n}}\qquad(4.17)$$

39

the dimensionless fully developed axial velocity profile, u_0, under the no-slip boundary condition (i.e., $u_{(at\ r=1)} = 0$) is obtained as:

$$u_0 = -\frac{1+3n}{1+n}(r^{1+\frac{1}{n}} - 1)$$ (4.18)

In order to find u_1, it is required to proceed with $_0$. For the constant heat flux case, the energy equation containing viscous heating term (viscous dissipation term) should be solved under the no temperature-jump condition, while a constant heat flux is applied at the walls. In the energy equation, the longitudinal temperature gradient, $\partial T/\partial X$, can be obtained with the application of the first law of thermodynamics to an elemental control volume as [12,137]:

$$\dot{m}c_p\frac{\partial T}{\partial X} = q^{"}u + \int \sim \{dS$$ (4.19)

For a circular cross-section, it can be written as:

$$...U_m R^2 c_p \frac{\partial T}{\partial X} = 2q^{"}(R + \frac{W_{ref}}{q^{"}}\int_0^{r_0}\left|\frac{\partial U}{\partial R}\right|^{n+1}RdR)$$ (4.20)

The above equation can be solved by introducing Brinkman number, defined as $Br = \dfrac{W_{ref}U_m^{n+1}}{q^{"}D^n}$, and by performing the integral on the right side as:

$$\frac{\partial T}{\partial X} = \frac{q^{"}(A + \vee A')}{...U_m R c_p}$$ (4.21)

where the parameter A is expressed as:

$$A = 2\left(1 + Br\int_0^1\left|\frac{\partial u}{\partial r}\right|^{n+1}rdr\right)$$ (4.22)

or

40

$$A = 2 + Br\frac{n}{1+3n}\left|-\frac{1+3n}{n}\right|^{1+n} \tag{4.23}$$

$$A' = 2\frac{Br}{n}\left|-\frac{1+3n}{n}\right|^{1+n}\int_0^1 |_{''\,0}|\, r^{\frac{1+n}{n}}\, rdr \tag{4.24}$$

or

$$A' = Br\left|-\frac{1+3n}{n}\right|^n \left(\frac{\left(2+8n+Br\left|-\frac{1+3n}{n}\right|^{1+n} n\right)}{(1+3n)(1+5n)}\right) \tag{4.25}$$

Brinkman number, Br, is a dimensionless parameter representing viscous dissipation term. Its positive and negative values refer to wall heating (fluid is being heated) and wall cooling (fluid is being cooled), respectively.

Upon using the dimensionless temperature defined as $_{''} = \dfrac{T - \bar{T}_w}{r_0 q'' / k}$, the energy equation takes the following dimensionless form:

$$u_0 A + \mathsf{V}(u_0 A' + u_1 A) = \frac{1}{r}\frac{\partial}{\partial r}\left(r\frac{\partial_{''\,0}}{\partial r}\right) + Br\left|\frac{\partial u_0}{\partial r}\right|^{1+n} +$$
$$\mathsf{V}\left[\frac{1}{r}\frac{\partial}{\partial r}\left(r\frac{\partial_{''\,1}}{\partial r} + \Gamma r_{''\,0}\frac{\partial_{''\,0}}{\partial r}\right) + Br(1+n)\left|\frac{\partial u_0}{\partial r}\right|^n \frac{\partial u_1}{\partial r} - Br_{''\,0}\left|\frac{\partial u_0}{\partial r}\right|^{1+n}\right] \tag{4.26}$$

Or

$$u_0 A + \mathsf{V}(u_0 A' + u_1 A) = \frac{1}{r}\frac{\partial}{\partial r}\left(r\frac{\partial_{''\,0}}{\partial r}\right) + Br\left|-\frac{1+3n}{n}\right|^{1+n} r^{\frac{1+n}{n}} +$$
$$\mathsf{V}\left[\frac{1}{r}\frac{\partial}{\partial r}\left(r\frac{\partial_{''\,1}}{\partial r} + \Gamma r_{''\,0}\frac{\partial_{''\,0}}{\partial r}\right) + Br(1+n)\left|-\frac{1+3n}{n}\right|^n \left(\frac{\partial u_1}{\partial r}\right) r - Br_{''\,0}\left|-\frac{1+3n}{n}\right|^{1+n} r^{\frac{1+n}{n}}\right] \tag{4.27}$$

Splitting the above equation, the following equations are obtained:

$$u_0 A = \frac{1}{r}\frac{\partial}{\partial r}\left(r\frac{\partial_{''\,0}}{\partial r}\right) + Br\left|-\frac{1+3n}{n}\right|^{1+n} r^{\frac{1+n}{n}} \tag{4.28}$$

$$u_0 A' + u_1 A =$$

$$\left[\frac{1}{r}\frac{\partial}{\partial r}\left(r\frac{\partial \theta_1}{\partial r} + \Gamma r_{\theta_0}\frac{\partial \theta_0}{\partial r} \right) + Br(1+n)\left| -\frac{1+3n}{n} \right|^n \left(\frac{\partial u_1}{\partial r} \right) r - Br_{\theta_0}\left| -\frac{1+3n}{n} \right|^{1+n} r^{\frac{1+n}{n}} \right] \qquad (4.29)$$

These equations must be solved subject to the following boundary conditions

$$\text{At } r=1 \qquad \theta_0 = \theta_1 = 0 \qquad (4.30)$$

$$\text{At } r=0 \qquad \frac{\partial \theta_0}{\partial r} = \frac{\partial \theta_1}{\partial r} = 0$$

By substituting u_0, the dimensionless temperature distribution θ_0 is derived as:

$$\theta_0 = \frac{\left(-\dfrac{(1+3n)A}{1+n} - Br\left| -\dfrac{1+3n}{n} \right|^{1+n} \right)}{(3+\dfrac{1}{n})^2}\left(r^{3+\frac{1}{n}} - 1 \right) + \frac{(1+3n)A}{4(1+n)}\left(r^2 - 1 \right) \qquad (4.31)$$

Accordingly, the dimensionless fully developed axial velocity profile, u_1, is obtained as:

$$u_1 = \frac{\left[\begin{array}{l} -2n - 26n^2 - 132n^3 - 324n^4 - 378n^5 - 162n^6 \\[4pt] + \left(1 + 17n + 116n^2 + 406n^3 + 765n^4 + 729n^5 + 270n^6 \right) r^{\frac{1+n}{n}} \\[4pt] - \left(1 + 15n + 92n^2 + 294n^3 + 513n^4 + 459n^5 + 162n^6 \right) r^{\frac{1+3n}{n}} \\[4pt] + \left(2n^2 + 20n^3 + 72n^4 + 108n^5 + 54n^6 \right) r^{\frac{2+4n}{n}} + \\[4pt] Br\left| -\dfrac{1+3n}{n} \right|^{1+n} \left(\begin{array}{l} \left(n + 12n^2 + 56n^3 + 126n^4 + 135n^5 + 54n^6 \right)\left[r^{\frac{1+n}{n}} - r^{\frac{1+3n}{n}} \right] \\[6pt] + \left(n^2 + 10n^3 + 36n^4 + 54n^5 + 27n^6 \right)\left[r^{\frac{2+4n}{n}} - 1 \right] \end{array} \right) \end{array} \right]}{2n(1+n)^2(1+2n)(1+3n)^3} \qquad (4.32)$$

After substituting u_0, u_1, and θ_0 into Eq. (4.29) and performing several tedious manipulations, a long and complex expression is derived for θ_1 as follows:

$$\theta_1 = C_{41}\left(r^2 - 1\right) + C_{42}\left(r^4 - 1\right) + C_{43}\left(r^{3+\frac{1}{n}} - 1\right) + C_{44}\left(r^{5+\frac{1}{n}} - 1\right) + C_{45}\left(r^{6+\frac{2}{n}} - 1\right) \quad (4.33)$$

where

$$C_{41} = \frac{\begin{pmatrix} -2 + A' + (-12 + 8A')n + (-18 + 21A')n^2 + 18A'n^3 + \Gamma\left(1 + 10n + 31n^2 + 30n^3\right) \\ + Br\left|-\frac{1+3n}{n}\right|^{1+n}\left(-3n - 9n^2 + \Gamma\left(2n + 12n^2 + 16n^3\right)\right) + \\ Br^2\left|-\frac{1+3n}{n}\right|^{2+2n}\left(-n^2 + \Gamma\left(n^2 + 2n^3\right)\right) \end{pmatrix}}{4(1+n)(1+2n)(1+3n)} \quad (4.34)$$

$$C_{42} = -\frac{\Gamma\left(1 + 3n + Br\left|-\frac{1+3n}{n}\right|^{1+n}n\right)^2}{8(1+n)^2}$$

$$C_{43} = -\frac{\begin{pmatrix} -2n + (-16 + 2A')n^2 + (-30 + 12A')n^3 + 18A'n^4 + \Gamma\left(2n^2 + 16n^3 + 30n^4\right) \\ + Br\left|-\frac{1+3n}{n}\right|^{n}\left(1 + 10n + 32n^2 + 38n^3 + 15n^4\right) + Br\left|-\frac{1+3n}{n}\right|^{1+n}\begin{pmatrix} -3n^2 - 10n^3 + 5n^4 + \\ \Gamma\left(n^2 + 10n^3 + 21n^4\right) \end{pmatrix} \\ + Br^2\left|-\frac{1+3n}{n}\right|^{1+2n}\left(n + 5n^2 + 7n^3 + 3n^4\right) + Br^2\left|-\frac{1+3n}{n}\right|^{2+2n}\left(-n^3 + n^4 + \Gamma\left(n^3 + 3n^4\right)\right) \end{pmatrix}}{2(1+n)(1+3n)^3}$$

$$C_{44} = \frac{\left(1 + 3n + Br\left|-\frac{1+3n}{n}\right|^{1+n}n\right)\begin{pmatrix} -2n - 8n^2 - 6n^3 + \Gamma\left(2n^2 + 20n^3 + 50n^4\right) + \\ Br\left|-\frac{1+3n}{n}\right|^{n}\left(1 + 8n + 22n^2 + 24n^3 + 9n^4\right) \\ + Br\left|-\frac{1+3n}{n}\right|^{1+n}\left(-n^2 + 2n^3 + 3n^4 + \Gamma\left(n^2 + 10n^3 + 25n^4\right)\right) \end{pmatrix}}{2(1+n)^2(1+3n)(1+5n)^2}$$

$$C_{45} = -\frac{n^2\left(2+Br\left|-\dfrac{1+3n}{n}\right|^{1+n}\right)}{4(1+n)^2(1+2n)(1+3n)^3}\left(\begin{array}{l} -n-4n^2-3n^3+\Gamma\!\left(4n^2+20n^3+24n^4\right) \\[6pt] +Br\left|-\dfrac{1+3n}{n}\right|^{n}\left(1+7n+17n^2+17n^3+6n^4\right) \\[6pt] +Br\left|-\dfrac{1+3n}{n}\right|^{1+n}\left(2n^3+2n^4+\Gamma\!\left(2n^2+10n^3+12n^4\right)\right) \end{array}\right)$$

Determined velocities (u_0, u_1) and temperatures (θ_0 and θ_1) are utilized to find the dimensionless bulk or mean temperature given as:

$$\theta_m = \frac{\int u\,\theta\,dS}{\int u\,dS} = 2\int_0^1 \left[u_0\theta_0 + V(u_0\theta_1 + u_1\theta_0)\right] r\,dr \tag{4.35}$$

Nusselt number is defined as $Nu = \dfrac{Dq''}{k(\bar{T}_w - T_m)}$ and can be also written in terms of the dimensionless temperature as:

$$Nu = \frac{-2}{\theta_m} \tag{4.36}$$

In the case of constant properties, Nusselt number can be expressed in the following form as:

$$Nu = \frac{-8(1+3n)(1+5n)}{-1-12n-31n^2+Br\left(-4n-16n^2+\left(1+12n+31n^2\right)\left|-\dfrac{1+3n}{n}\right|^{n}\right)} \tag{4.37}$$

To the authors' best knowledge, there are no other studies in the literature, in which the viscous dissipation term is present. However, the results of Eq. (4.37) are in excellent agreement with those of Barkhordari and Etemad [68] in the absence of viscous heating and with those of Hooman [12] in the presence of viscous heating and n=1.

For the variable property case, it is not possible to give an explicit expression for Nusselt number. Therefore, a numerical analysis is needed.

In order to have a better design and improvement in thermo-fluidic systems, the second law analysis constitutes an important part of analysis. In this point of view, the entropy

generation, which is dependent on irreversibilities in fluid friction and heat transfer due to existence of gradients in velocity and temperature, plays a significant role in such systems. Therefore, minimization of entropy generation through reducing the irreversibilities would be a desirable goal for thermo-fluid researchers to augment the system efficiency. In this regard, the second law analysis is investigated in the current study to provide some insight on how the governing parameters affect the entropy generation rate. The volumetric rate of entropy generation can be expressed as [133]:

$$\dot{S} = \frac{k}{T^2}(\nabla T.\nabla T) + \frac{\tilde{\zeta}}{T} \tag{4.38}$$

where the first and second terms on the right side are (volumetric) Heat Transfer Irreversibility and Fluid Friction Irreversibility, respectively.

For the case of non-Newtonian fluids, entropy generation rate is derived as:

$$\dot{S} = \frac{k_s(1+v_{k''})}{T_i^2}\left((\frac{\partial T}{\partial X})^2 + (\frac{\partial T}{\partial R})^2\right) + \frac{w}{T_i}(1-v_{''})\left|\frac{\partial U}{\partial R}\right|^{n-1}\left(\frac{\partial U}{\partial R}\right)^2 \tag{4.39}$$

In non-dimensional form, it can be expressed as:

$$N_s = \dot{S}\frac{r_0^2}{k_s\Omega^2} = (1+v_{k''})\left((\frac{A+vA'}{Pe})^2 + (\frac{\partial_{''0}}{\partial r} + v\frac{\partial_{''1}}{\partial r})^2\right) +$$
$$\frac{Br}{\Omega}(1-v_{''})\left|\frac{\partial u_0}{\partial r} + v\frac{\partial u_1}{\partial r}\right|^{n+1} \tag{4.40}$$

After simplifications and rearrangements, and neglecting higher-order terms $o(\varepsilon^2)$, it becomes:

$$N_s = \dot{S}\frac{r_0^2}{k\Omega^2} = (\frac{A}{Pe})^2 + (\frac{\partial_{''0}}{\partial r})^2 + \frac{Br}{\Omega}\left|\frac{\partial u_0}{\partial r}\right|^{n+1} +$$
$$v\begin{pmatrix}\Gamma_{''0}(\frac{A}{Pe})^2 + \Gamma_{''0}(\frac{\partial_{''0}}{\partial r})^2 + \frac{2AA'}{Pe^2} + 2\frac{\partial_{''0}}{\partial r}\frac{\partial_{''1}}{\partial r} \\ -\frac{Br}{\Omega}_{''0}\left|\frac{\partial u_0}{\partial r}\right|^{n+1} + \frac{Br}{\Omega}(1+n)\frac{\partial u_1}{\partial r}\left|\frac{\partial u_0}{\partial r}\right|^{n}\end{pmatrix} \tag{4.41}$$

45

where $\quad = q^{"}r_0/T_i k$ and Pe is Peclet number. The temperature and velocity gradients are as follows:

$$\frac{\partial u_0}{\partial r} = -\frac{1+3n}{n} r^{\frac{1}{n}} \tag{4.42}$$

$$\frac{\partial u_1}{\partial r} = \frac{\left[\begin{array}{l} \left(\frac{1+n}{n}\right)\left(1+17n+116n^2+406n^3+765n^4+729n^5+270n^6\right)r^{\frac{1}{n}} \\[2mm] -\left(\frac{1+3n}{n}\right)\left(1+15n+92n^2+294n^3+513n^4+459n^5+162n^6\right)r^{\frac{1+2n}{n}} \\[2mm] +\left(\frac{2+4n}{n}\right)\left(2n^2+20n^3+72n^4+108n^5+54n^6\right)r^{\frac{2+3n}{n}} + \\[2mm] Br\left|-\frac{1+3n}{n}\right|^{1+n}\left(\begin{array}{l}\left(n+12n^2+56n^3+126n^4+135n^5+54n^6\right)\left[\begin{array}{l}\left(\frac{1+n}{n}\right)r^{\frac{1}{n}}\\[2mm]-\left(\frac{1+3n}{n}\right)r^{\frac{1+2n}{n}}\end{array}\right] \\[4mm] +\left(n^2+10n^3+36n^4+54n^5+27n^6\right)\left[\left(\frac{2+4n}{n}\right)r^{\frac{2+3n}{n}}\right]\end{array}\right)\end{array}\right]}{2n(1+n)^2(1+2n)(1+3n)^3}$$

$$\frac{\partial_{"0}}{\partial r} = \frac{\left(-\frac{(1+3n)A}{1+n}-Br\left|-\frac{1+3n}{n}\right|^{1+n}\right)}{3+\frac{1}{n}}r^{2+\frac{1}{n}}+\frac{(1+3n)A}{2(1+n)}r$$

$$\frac{\partial_{"1}}{\partial r} = 2C_1 r + 4C_2 r^3 + C_3\frac{1+3n}{n}r^{\frac{1+2n}{n}} + C_4\frac{1+5n}{n}r^{\frac{1+4n}{n}} + C_5\frac{2+6n}{n}r^{\frac{2+5n}{n}}$$

The main aim of second law analysis is to find parameters minimizing global entropy generation rate, denoted by $<N_s>$, which is related to the whole dissipations generated by irreversibilities in the channel. Therefore, it is required to integrate N_s across the cross-sectional area occupied by the fluid through $<N_s>=\int N_s dS/S$, and can be written as:

$$<N_s> = \int_0^1 2N_s r dr \tag{4.43}$$

46

Again, it is needed to perform numerical analysis to obtain the global entropy generation.

4.2 Results and Discussion

As pointed out earlier, viscosity and thermal conductivity vary with temperature so that a rise in temperature leads to a decrease in viscosity and an increase in thermal conductivity. This section includes the effect of variable properties and viscous dissipation on the entropy generation rate and heat transfer characteristics of hydrodynamically and thermally fully developed non-Newtonian flows in tubes at isoflux boundary condition while assuming a power-law fluid model.

Shear thinning (or pseudoplastic) fluids having power-law index in the range $0 < n < 1$ behaves in such a way that their viscosity decreases with shear rate, while this behavior is otherwise for shear thickening (or dilatants) fluids having power-law index larger than unity $(n > 1)$.

In order to verify the analytical results in the case of variable property, a numerical simulation was carried out by employing ANSYS FLUENT 14.0 software that compares the numerical and analytical results of fully developed dimensionless velocity profile. The temperature-dependent viscosity equation based on the experimental data expression given in Ref. [138] was implemented in the software through a User-Defined Function (UDF) as following

$$\sim(T) = 0.00002414 \times 10^{\frac{247.8}{T-140}} \qquad (4.44)$$

where T has units of Kelvin, and μ has units of N·s/m².

Fig. 4.2 demonstrates the comparison between numerical (at Re=10) and analytical solutions, which shows a good agreement. It is notable that analytical results correspond to =0.064, which was acquired by Eq. (4.7) from the numerical analysis. The value of   can be also obtained by the numerical simulation, which is dependent on the heat flux

47

applied. For the sake of simplicity and consistency, throughout this study it is taken to be =0.2.
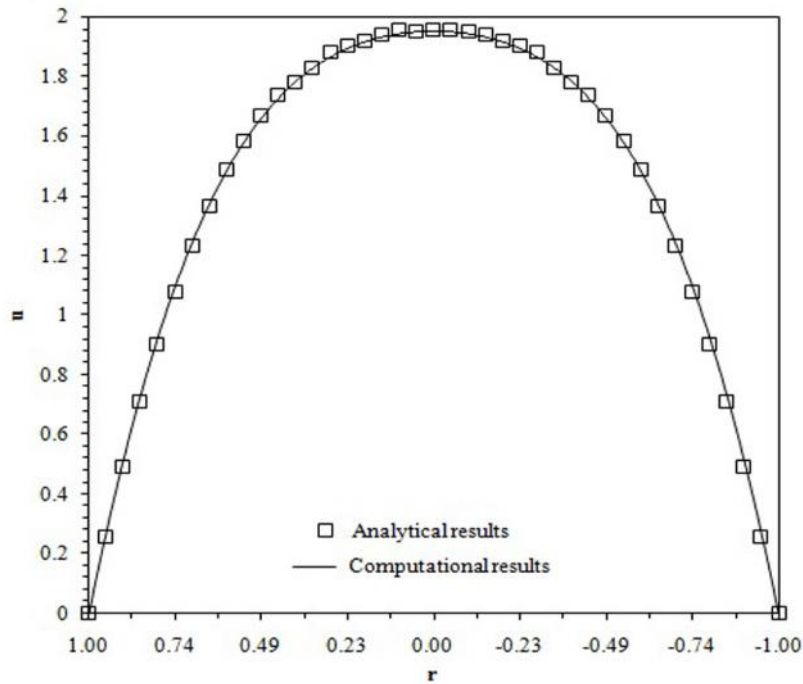
Fig. 4.2 Comparison between numerical results of temperature-dependent viscosity of water given in Ref. [138] and analytical result corresponding to =0.064

Fig. 4.3 illustrates the dimensionless velocity distribution at various power-law indices, n, for both constant and variable properties at Br=0.01. As seen, regardless of the property, the core velocity of the flow moves faster when the power-law index increases, while its velocity near the walls takes the smaller values to keep the flow rate constant. Generally, the parabolic profile regarding to Newtonian fluid (n = 1) deforms to a more uniform profile compared to shear-thinning fluids and to a more non-uniform profile compared to shear-thickening fluids. Furthermore, the consideration of temperature-dependent properties slightly decreases the velocity values at the core region. This trend is due to the decreasing viscosity with temperature hence giving rise to lower pressure drop and accordingly lower velocities.
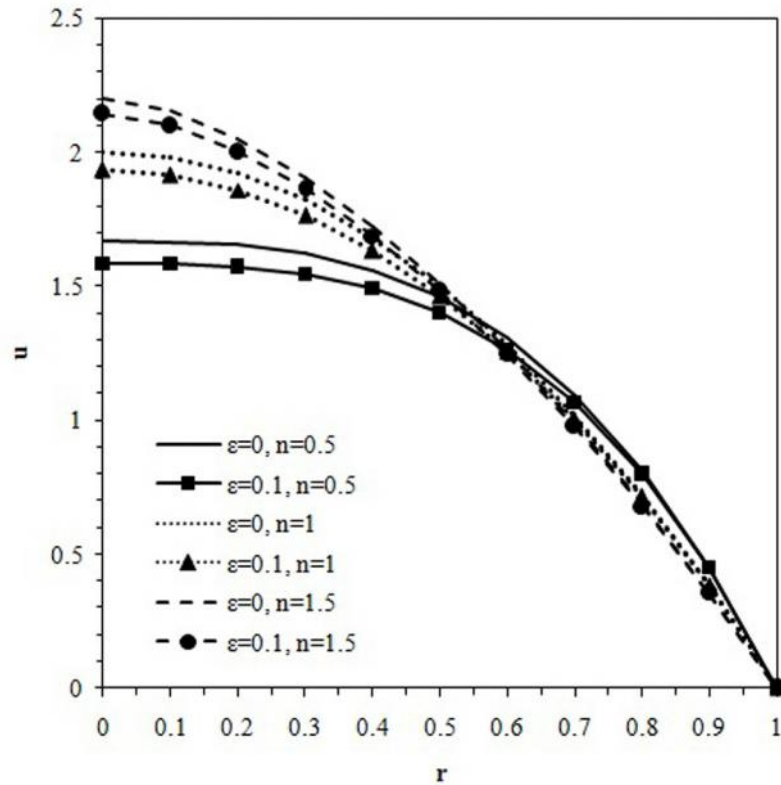
Fig. 4.3 Dimensionless fully developed velocity profiles for different values of n for constant and variable property case at Br=0.01

Figure 4.4 shows the dimensionless temperature distribution of the flow for different values of n in the cases of ε=0 and ε=0.1 at Br=0.01. Similar to velocity profiles, the temperature develops in the core region for increasing power-law index. It was also observed that a slight increase in the fluid temperature exists for all types of the fluids, but more effectively for shear-thinning fluid, at the core region by taking the variable properties. The temperature increment may be ascribed to the enhancing effect of thermal conductivity of the fluid owing to temperature variation.

Figure 4.5 shows the variation of Nusselt number as a function of power-law index for different Brinkman numbers in the case of both constant (=0) and variable property (=0.1) cases. It can be observed that Nusselt number decreases with both the power-law index and Brinkman number, regardless of the property. However, this decreasing trend is more significantly seen at higher Brinkman numbers, which is because of Brinkman number appearing as a coefficient in the viscous dissipation term leads to viscous heating, and accordingly, it gives rise to an increase in the mean temperature of the fluid through the internal heating and ultimately to the decrease in Nusselt number.
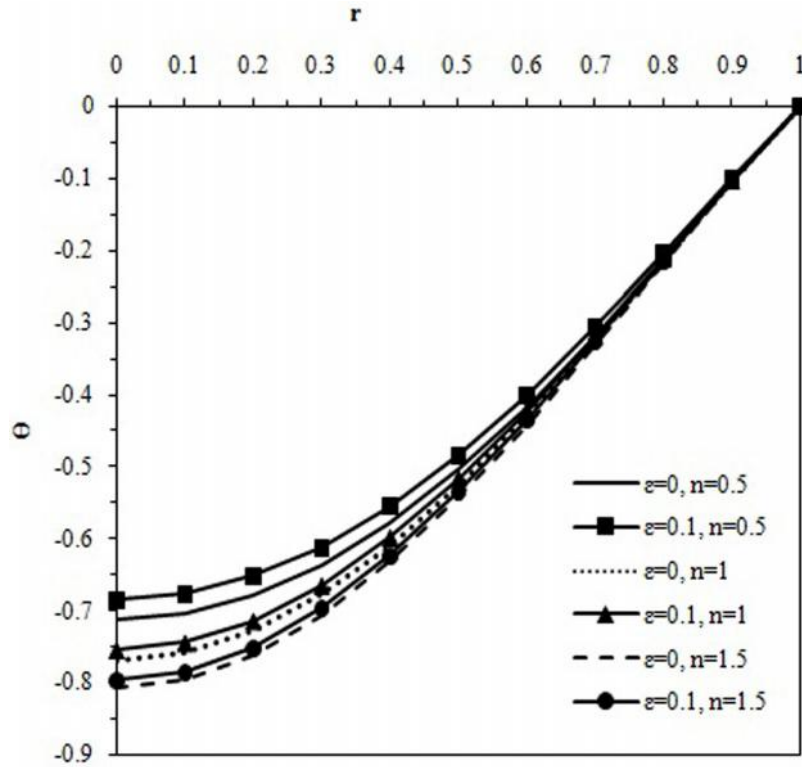
Fig. 4.4 Dimensionless fully developed temperature profiles for different values of n for constant and variable property cases at Br=0.01

It is also noticeable that the effect of Brinkman number on Nu becomes more significant for shear-thickening fluids, which is attributed to higher mean temperatures. In the case of the variable thermophysical property case, the values of Nusselt number are larger compared to the constant property case. However, the effect of property variation on the heat transfer rate becomes less significant when the power law index goes higher in the shear-thickening fluid range for low Br. For example, for n=2 and Br=0.1, the change in Nusselt number is about 8% due to the consideration of the variable properties. On the other hand, for shear-thinning fluid, the values of Nusselt number are significantly underestimated by neglecting the temperature-variation effect. For instance, at n=0.2 and Br=0.1, the deviation becomes more and reaches about 13%. Indeed, the viscosity decreases with temperature, which causes an increase in Reynolds number and consequently has a positive effect on heat transfer and Nusselt number. On the other hand, the thermal conductivity has an increasing trend with temperature, and has a negative effect on Nusselt number (Nu=hd/k). As a result, there is an interplay between viscosity and thermal conductivity effects, where the viscosity dominates giving rise to an increase in Nusselt number.
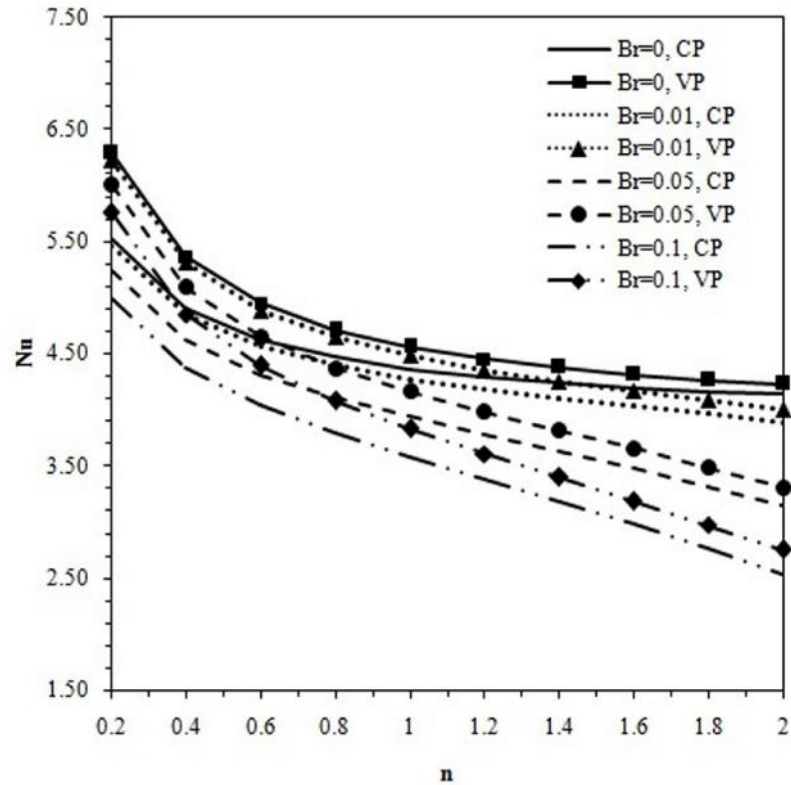
Fig. 4.5 Nusselt number as a function of n for different values of Br at the constant (at =0) and variable property (at =0.1) cases

The effect of property variation (perturbation parameter) on the heat transfer rate for different n and Br=0.01 is displayed in Fig. 6. As mentioned earlier, heat transfer is reduced when the power-law index is increased. It can be seen that heat transfer rate (Nusselt number value) increases for the variable thermophysical property case with at which the deviation from constant properties might reach about 21%. However, the effect of property diminishes as the power-law index becomes more, in particular for shear-thickening fluids where a very small change is observed for n=2.

Table 4.1 presents global entropy generation rate, <Ns>, versus power-law index at =0.1 and various Brinkman numbers in absence of axial heat conduction term corresponding to Pe . As can be seen from the table, except for Br=0.01 which will be depicted in the next figure, the global entropy generation rate increases with power-law index for both constant property and variable property cases particularly for higher Br. Since lower value of entropy generation would imply a better working performance, the fluidic system with smaller Br (or smaller viscous heating) is desirable, which leads to a more efficient convective heat transfer as well.

51
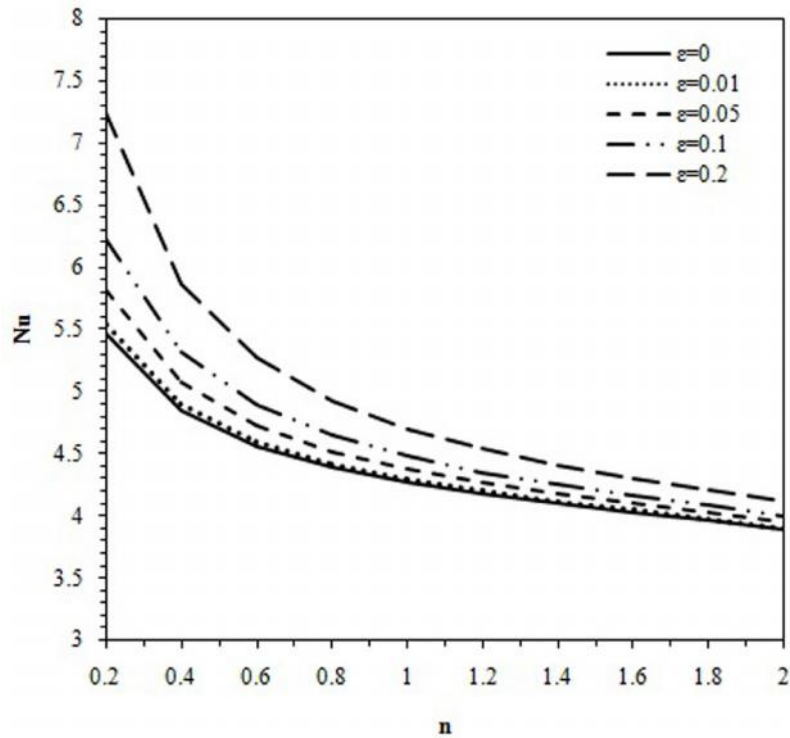
Fig. 4.6 Nusselt number as a function of n for different values of ε at Br=0.01

Furthermore, lower values of global entropy generation rate are obtained for lower n (i.e. shear-thining fluids), which is due to smaller velocity and temperature gradients at the walls, where the entropy generation is more pronounced. Entropy generation rate reaches its maximum and minimum values at the wall and center, respectively, where the maximum and minimum (zero for this case) velocity and temperature gradients are present.

From this table, it can be also understood that the property variation with temperature causes an increase in <Ns> for low values of Br, while the opposite remains valid for higher Br. In this case, the perturbed term contributes to the global entropy generation by increasing the irreversibility caused by viscous heating through the velocity gradient portion. However, the table reports a reduction in <Ns> for larger Brinkman number when the properties are varied with temperature.

52

Table 4.1 The values of global entropy generation rate
at   = 0.1, Pe =   for different Br and n

	constant property					variable property (=0.1)			
	Br					Br			
	0	0.01	0.05	0.1		0	0.01	0.05	0.1
n									
0.2	0.725	0.526	0.986	2.373		0.636	0.45	0.954	2.273
0.4	0.815	0.806	1.906	3.767		0.745	0.739	1.82	3.61
0.6	0.864	1.15	2.982	5.5		0.808	1.085	2.861	5.286
0.8	0.895	1.49	4.09	7.41		0.849	1.426	3.945	7.148
1	0.917	1.757	5.13	9.37		0.877	1.696	4.971	9.07
1.2	0.932	1.889	6.031	11.293		0.898	1.833	5.871	10.974
1.4	0.944	1.837	6.789	13.181		0.914	1.791	6.643	12.874
1.6	0.954	1.591	7.537	15.214		0.927	1.561	7.422	14.96
1.8	0.961	1.267	8.619	17.847		0.938	1.259	8.545	17.679
2	0.968	1.355	10.551	21.83		0.947	1.361	10.497	21.724

The variation in the global entropy generation as a function of power-law index at Br=0.01,   =0.1, and different values of   is depicted in Fig. 4.7. The global entropy generation increases with n to its maximum value around n=1.2 and then starts decreasing until n=1.8. An unexpected trend after this point is seen where the value of $<Ns>$ again increases with n, except for   =0.1 and 0.2. Additionally, one can observe that an increment in   leads to an increase in $<Ns>$, except for very high values of n.

Table 4.2 exhibits the values of the global entropy generation rate, $<N_s>$, as a function of power-law index at Br=0.01,   =0.1 and different values of Peclet number, Pe, which represents axial heat conduction effect on entropy generation. It is worthwhile noting that Peclet number does not play any role in the heat transfer analysis of fully developed flows due to the constant axial temperature gradient. The results in the table also reveal that the increase of Pe (axial heat conduction portion) generally decreases the values of $<N_s>$. For very low values of Pe (here Pe=0.1) the global entropy generation rate increases with n, which means that shear-thickening fluids generate more irreversibilities compared to shear-thinning ones. However, for other Pe values, the trend is very similar to that of Fig. 4.7.
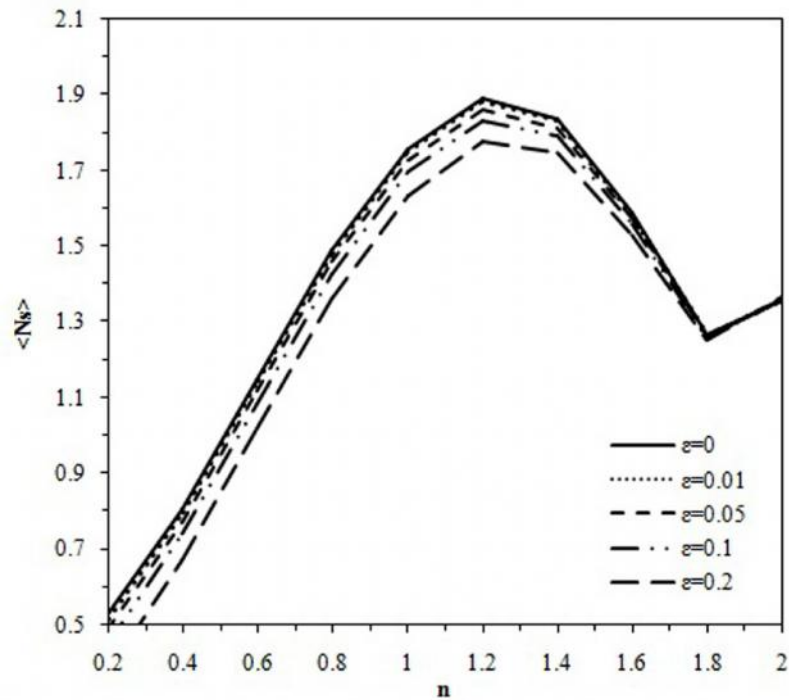
Fig. 4.7 Global entropy generation rate as a function of n for different values of   at
=0.1and Br=0.01

Furthermore, the values of $\langle N_s \rangle$ increase with inclusion of temperature-dependent properties, except for very high values of n, even though the viscosity has a decreasing trend with temperature in contrast to the thermal conductivity. This means that irreversibility due to heat transfer dominates over fluid friction. Therefore, the results suggest that if thermophysical properties are not considered as variable there will be an underestimation of $\langle N_s \rangle$.

Table 4.2 The values of global entropy generation rate at   = 0.1, Br = 0.01 for
different n and

n	=0, Pe=0.1	=0, Pe=10	=0, Pe=100	=0.1, Pe=0.1	=0.1, Pe=10	=0.1, Pe=100
0.2	412.713	0.565	0.526	410.834	0.489	0.451
0.4	416.69	0.843	0.806	414.599	0.776	0.739
0.6	421.46	1.188	1.15	419.259	1.123	1.086
0.8	427.304	1.531	1.49	425.041	1.467	1.426
1	434.397	1.8	1.758	432.098	1.739	1.696
1.2	442.923	1.931	1.89	440.607	1.875	1.834
1.4	453.199	1.872	1.838	450.881	1.826	1.792
1.6	465.82	1.608	1.591	463.51	1.577	1.561
1.8	481.799	1.248	1.267	479.5	1.239	1.259
2	502.647	1.305	1.355	500.356	1.311	1.36

4.3 Conclusion

Convective heat transfer analysis and second law analysis were performed to reveal the effects of variable thermophysical properties, namely viscosity and thermal conductivity, power-law index and viscous dissipation on heat transfer characteristics of hydrodynamically and thermally fully developed power-law fluid flows in tubes under uniform heat flux thermal boundary conditions. Aside from deriving the velocity and temperature distributions, Nusselt number and entropy generation rate have been examined along with their trends with key parameters being power-law index, Brinkman number, and property variation. Major conclusions of this study are as follows:

- Nusselt number decreases with increasing both power-law index and Brinkman number, regardless of the change in thermophysical properties with temperature, while this trend is more pronounced for variable properties.

- The variation in thermophysical properties with temperature has an increasing effect on Nusselt number compared to the constant property case.

- Except for few cases, the rate of global entropy generation, $\langle N_s \rangle$, increases with power-law index, Brinkman number, whereas thermophysical property variation effect causes the augmentation of $\langle N_s \rangle$ only for lower values of Brinkman number.

CHAPTER 5

SINGLE-PHASE SLIP FLOW AND PLUG FLOW WITH VARIABLE THERMOPHYSICAL PROPERTIES IN PARALLEL-PLATES AND CIRCULAR MICROCHANNELS

5. Analysis:

5.1 Power-law fluid flow

In this section, the analytical solutions are derived to obtain velocity and temperature distributions and heat transfer characteristics of power-law fluid flows inside parallel-plate and circular microchannels. To achieve this, it is assumed that the flow is hydrodynamically and thermally fully developed, steady state, incompressible and laminar with constant and variable thermophysical properties under wall uniform heat flux thermal boundary condition (Fig. 5.1). The viscous dissipation term is also included in the analysis to examine the viscous heating effect.
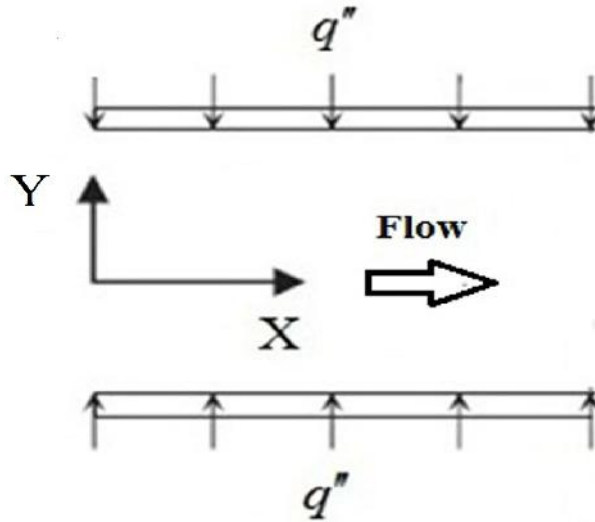
Fig. 5.1 Isoflux heating applied to circular and parallel-plates channels

The following shear-stress power-law relationship is applicable for a power-law fluid:

$$\ddagger = w \left| \frac{\partial U}{\partial Y} \right|^{n-1} \left(\frac{\partial U}{\partial Y} \right)$$

(5.1)

where $w_{ref} \left| \frac{\partial U}{\partial Y} \right|^{n-1}$ is viscosity the consistency factor at room temperature, $_{ref}$, and the power-law index, n. The governing equations, being x-momentum and energy equations, are formulated respectively as

$$\frac{1}{Y^m} \frac{\partial}{\partial Y} \left(\sim Y^m \frac{\partial U}{\partial Y} \right) - \frac{\partial P}{\partial X} = 0$$

(5.2)

$$\dots c_p U \frac{\partial T}{\partial X} = \frac{1}{Y^m} \frac{\partial}{\partial Y} \left(k Y^m \frac{\partial T}{\partial Y} \right) + \sim \left(\frac{\partial U}{\partial Y} \right)^2$$

(5.3)

where is the density, P is the pressure, T is the temperature, c_p is the specific heat at constant pressure, k is the thermal conductivity, U is velocity component in X direction, and m takes values between 0 and 1 for parallel-plate and circular channels, respectively.

In order to proceed with a solution, viscosity, thermal conductivity and density must be defined as a function of temperature. Reynolds [135] proposed an exponential model for the temperature-dependence of viscosity as:

$$\sim = \sim_{ref} \exp(-b'T) \tag{5.4}$$

where T is temperature, and μ_s and b are coefficients. Using a truncated Taylor series for exp(-bT) similar to our previous work [85], viscosity is expressed as:

$$\sim = \sim_s \exp(-bT) = \sim_s \left(1 - \frac{\Delta T}{\sim_s} \frac{d\sim}{dT} \frac{T - \overline{T_w}}{\Delta T} \right) = \sim_s (1 - v_n) = w_{ref}(1 - v_n) \left| \frac{\partial U}{\partial R} \right|^{n-1} \tag{5.5}$$

and

$$k = k_s \left(1 + \frac{\Delta T}{k_s} \frac{dk}{dT} \frac{T - \overline{T_w}}{\Delta T} \right) = k_s (1 + v_{kn}) \tag{5.6}$$

where

$$v = \frac{d\sim}{dT} \frac{\Delta T}{\sim_{ref}} \tag{5.7}$$

$$v_k = \frac{dk}{dT} \frac{\Delta T}{k_{ref}} \tag{5.8}$$

and

$$\Gamma = \frac{v_k}{v} \tag{5.9}$$

Here $\frac{T - \overline{T_w}}{\Delta T}$ is the dimensionless temperature, . It should be noted that the effects of density and heat capacity as variable properties cancel out in the analytical solution, and therefore, the viscosity and the thermal conductivity temperature-dependent properties appear in the analysis.

The governing equations for x-momentum and energy equations can be stated as:

$$\frac{1}{Y^m} \frac{\partial}{\partial Y} \left(\sim_s (1 - v_n) Y^m \frac{\partial U}{\partial Y} \right) - \frac{\partial P}{\partial X} = 0 \tag{5.10}$$

58

or

$$\frac{1}{Y^m}\frac{\partial}{\partial Y}\left(Y^m W_{ref}(1-v_\mu)\left|\frac{\partial U}{\partial Y}\right|^{n-1}\left(\frac{\partial U}{\partial Y}\right)\right)-\frac{\partial P}{\partial X}=0 \tag{5.11}$$

$$...c_p U\frac{\partial T}{\partial X}=\frac{1}{Y^m}\frac{\partial}{\partial Y}\left(k_s(1+v_{k\mu})Y^m\frac{\partial T}{\partial Y}\right)+\left(w\left|\frac{\partial U}{\partial Y}\right|^{n-1}(1-v_\mu)\right)\left(\frac{\partial U}{\partial Y}\right)^2 \tag{5.12}$$

To facilitate an analytical solution, the governing equations are non-dimensionalized by using the following non-dimensional parameters and Reynolds number, Re, as:

$$u=\frac{U}{U_m} \qquad y=\frac{Y}{R} \text{ or } y=\frac{Y}{r_0} \qquad x=\frac{X}{r_0} \text{ or } x=\frac{X}{H} \qquad p=\frac{P}{...U_m^2}$$

$$Re\big|_{pp}=\frac{...U_m^{2-n}r_0^n}{W_{ref}} \qquad Re\big|_{CC}=\frac{...U_m^{2-n}H^n}{W_{ref}}$$

The dimensionless governing equations are analytically solved to obtain Nusselt number (Nu), as well as the velocity and temperature distributions. The closed form expressions for Nu corresponding to Newtonian liquid flow characteristics can also obtained by setting n=1.

The first step is to derive the velocity distribution. With the introduction of Reynolds number, the non-dimensionalized x-momentum equation becomes:

$$\frac{1}{y^m}\frac{\partial}{\partial y}\left((1-v_\mu)y^m\left(\frac{\partial u}{\partial y}\right)^n\right)=Re\frac{\partial p}{\partial x} \tag{5.13}$$

Using the above equation subject to the symmetry condition at the center (via setting the axial velocity gradient at the center to zero (i.e., u/ y $_{(at\ y=0)}$ =0)) and using Taylor series with the first order approximation, the following expression can be derived:

$$\frac{\partial u}{\partial y}=\left(Re\frac{\partial p}{\partial x}\frac{y}{(1+m)}\right)^{\frac{1}{n}}(1+\frac{1}{n}_\mu v) \tag{5.14}$$

For most practical cases, the viscosity variation number is small compared to unity, i.e. $\ll 1$. This allows for a regular asymptotic expansion assumption (for dependent variables u and) in the following form

59

$$u = u_0 + vu_1 \tag{5.15}$$

$$v = v_0 + v v_1$$

As a result, Eq. (5.14) takes the following form:

$$\frac{\partial u_0}{\partial y} + v\frac{\partial u_1}{\partial y} = \left(\mathrm{Re}\frac{\partial p}{\partial x}\frac{y}{(1+m)} \right)^{\frac{1}{n}}(1 + \frac{1}{n}v_0 v) \tag{5.16}$$

Splitting the above equation into two equations:

$$\frac{\partial u_0}{\partial y} = \left(\frac{\mathrm{Re}}{(1+m)}\frac{\partial p}{\partial x} \right)^{\frac{1}{n}} y^{\frac{1}{n}} \tag{5.17}$$

$$v\frac{\partial u_1}{\partial y} = v\left(\frac{\mathrm{Re}}{(1+m)}\frac{\partial p}{\partial x} \right)^{\frac{1}{n}}(\frac{1}{n}v_0)y^{\frac{1}{n}} \tag{5.18}$$

As shown by the experimental observations for molten polymers, polymer solutions [89,139,140] and pastes [141], an adopted nonlinear slip boundary condition relating the velocity slip to shear stress can reasonably approximate the slip behavior of several non-Newtonian fluids, which is in the following form:

$$u_{ws} = f\tau_w^{G} \tag{5.19}$$

where f is slip-friction coefficient (with SI unit $Pa^{-G}m/s$), τ_w is the wall shear stress and G is a power-law exponent.

The dimensionless form of Eq. (5.19) for power law fluids is expressed as:

$$S = F\left(\left.\frac{\partial u}{\partial y}\right|_{y=1} \right)^{nG} \tag{5.20}$$

60

where   is the relative wall slip velocity to mean velocity, U_{ws}/U_m, and F is dimensionless slip-friction coefficient defined as $f_W{}^G(U_m/D)^{nG}$.

The quadratic and cubic power-law exponents were reported by Ramamurthy [140] and Hatzikiriakos and Dealy (relevant to a power-law fluid) [89], respectively, for molten polymers as well as the linear slip boundary for Newtonian fluids [25] and non-Newtonian fluids [141].

Another suitable wall boundary condition for non-Newtonian fluids, which is an easy condition for obtaining an analytical solution, is taking the relative wall slip velocity as mean velocity, i.e.   . Due to cumbersome nature of non-linear slip boundary condition for achieving an analytical solution, first the relative wall slip velocity is applied at the solid boundary. Then the inverse solution is used to obtain corresponding dimensionless friction coefficient in the non-linear slip boundary equation.

The dimensionless fully developed axial velocity profile, u_0, under the slip boundary condition (i.e., u $_{(at\ y=1)}$ =   ) is obtained as:

$$u_0 = \mathsf{s} + \mathsf{y}(y^{1+\frac{1}{n}} - 1) \tag{5.21}$$

where   is

$$\mathsf{y} = \frac{(-1+\mathsf{s})(1+2n+mn)}{1+n} \tag{5.22}$$

In order to find u_1, it is required to proceed with $_0$. For the constant heat flux case, the energy equation containing viscous heating term (viscous dissipation term) should be solved under the no temperature-jump condition, while a constant heat flux is applied at the walls. In the energy equation, the longitudinal temperature gradient, T/ X, can be obtained with the application of the first law of thermodynamics to an elemental control volume as [12,137]:

$$\overset{\bullet}{m}c_p \frac{\partial T}{\partial X} = q^{''}\Gamma + \int \sim \{dS \tag{5.23}$$

The above equation can be written as:

$$\ldots U_m \left(\frac{D}{2}\right)^{1+m} c_p \frac{\partial T}{\partial X} = (1+m)q^{"} \left(\left(\frac{D}{2}\right)^m + \frac{W_{ref}}{q^{"}} \int_0^{\frac{D}{2}} \left|\frac{\partial U}{\partial Y}\right|^{n+1} Y^m dY\right) \tag{5.24}$$

The above equation can be solved by introducing Brinkman number, defined as $Br = \dfrac{wU_m^{n+1}}{q^{"}D^n}$, and by performing the integral on the right side as:

$$\frac{\partial T}{\partial X} = \frac{q^{"}(A + vA')}{\ldots U_m c_p \dfrac{D}{2}} \tag{5.25}$$

where the parameter A is expressed as:

$$A = (1+m)\left(1 + Br\int_0^1 \left|\frac{\partial u}{\partial y}\right|^{n+1} y^m dy\right) \tag{5.26}$$

or

$$A = (1+m)\left(1 + Br\frac{n}{1+2n+mn}\left|y\frac{1+n}{n}\right|^{1+n}\right) \tag{5.27}$$

$$A' = Br(1+m)\left|y\frac{1+n}{n}\right|^{1+n} \frac{1}{n}\int_{0_{"}0}^1 \left|y^{\frac{1+mn+n}{n}}\right| dy \tag{5.28}$$

or

$$A' = -Br\left|y\frac{1+n}{n}\right|^{1+n} \left(\frac{\begin{array}{c} A(-2y+2s)n + A(-8y+9s-2ym+3sm)n^2 \\ + A(-6y+10s-2ym+7sm+sm^2)n^3 \\ -Br\left|y\left(1+\dfrac{1}{n}\right)\right|^{1+n}(n^2+mn^2+4n^3+5mn^3+m^2n^3) \end{array}}{(1+2n+mn)^2(1+4n+mn)(2+5n+mn)}\right) \tag{5.29}$$

Brinkman number, Br, is a dimensionless parameter representing viscous dissipation term. Its positive and negative values refer to wall heating (fluid is being heated) and wall cooling (fluid is being cooled), respectively.

Upon using the dimensionless temperature defined as $\theta = \dfrac{T - \bar{T}_w}{Dq''/2k}$, the energy equation takes the following dimensionless form:

$$u_0 A + V(u_0 A' + u_1 A) = \frac{1}{y^m}\frac{\partial}{\partial y}\left(y^m \frac{\partial \theta_0}{\partial y}\right) + Br\left|\frac{\partial u_0}{\partial y}\right|^{1+n} +$$

$$V\left[\frac{1}{y^m}\frac{\partial}{\partial y}\left(y^m \frac{\partial \theta_1}{\partial y} + y^m_{\ \theta 0}\frac{\partial \theta_0}{\partial y}\right) + Br(1+n)\left|\frac{\partial u_0}{\partial y}\right|^n \frac{\partial u_1}{\partial y} - Br_{\theta 0}\left|\frac{\partial u_0}{\partial y}\right|^{1+n}\right] \qquad (5.30)$$

or

$$u_0 A + V(u_0 A' + u_1 A) = \frac{1}{y^m}\frac{\partial}{\partial y}\left(y^m \frac{\partial \theta_0}{\partial y}\right) + Br\left|y\left(1+\frac{1}{n}\right)\right|^{1+n} y^{\frac{1+n}{n}} +$$

$$V\left[\begin{array}{l}\dfrac{1}{y^m}\dfrac{\partial}{\partial y}\left(y^m \dfrac{\partial \theta_1}{\partial y} + y^m_{\ \theta 0}\dfrac{\partial \theta_0}{\partial y}\right) + Br(1+n)\left|y\left(1+\dfrac{1}{n}\right)\right|^{n}\left(\dfrac{\partial u_1}{\partial y}\right)y \\[4mm] - Br_{\theta 0}\left|y\left(1+\dfrac{1}{n}\right)\right|^{1+n} y^{\frac{1+n}{n}}\end{array}\right] \qquad (5.31)$$

Splitting the above equation, the following equations are obtained:

$$u_0 A = \frac{1}{y^m}\frac{\partial}{\partial y}\left(y^m \frac{\partial \theta_0}{\partial y}\right) + Br\left|y\left(1+\frac{1}{n}\right)\right|^{1+n} y^{\frac{1+n}{n}} \qquad (5.32)$$

$$V(u_0 A'' + u_1 A) =$$

$$V\left[\begin{array}{l}\dfrac{1}{y^m}\dfrac{\partial}{\partial y}\left(y^m \dfrac{\partial \theta_1}{\partial y} + y^m_{\ \theta 0}\dfrac{\partial \theta_0}{\partial y}\right) + Br(1+n)\left|y\left(1+\dfrac{1}{n}\right)\right|^{n}\left(\dfrac{\partial u_1}{\partial y}\right)y \\[4mm] - Br_{\theta 0}\left|y\left(1+\dfrac{1}{n}\right)\right|^{1+n} y^{\frac{1+n}{n}}\end{array}\right] \qquad (5.33)$$

These equations must be solved subject to the following boundary conditions

$$\text{At } y=1 \qquad \theta_0 = \theta_1 = 0 \qquad (5.34)$$

$$\text{At } y=0 \qquad \frac{\partial \theta_0}{\partial y} = \frac{\partial \theta_1}{\partial y} = 0$$

By substituting u_0, the dimensionless temperature distribution θ_0 is derived as:

63

$$u_0 = \frac{Ayn^2}{(1+3n)(1+2n+mn)}\left(y^{3+\frac{1}{n}}-1\right)-\left(\frac{A(y-s)}{2(1+m)}\right)\left(y^2-1\right)$$

$$- Br\frac{\left|\frac{y(1+n)}{n}\right|^{1+n}n^2}{(1+3n)(1+2n+mn)}\left(y^{3+\frac{1}{n}}-1\right)$$

(5.35)

Accordingly, the dimensionless fully developed axial velocity profile, u_1, is obtained as:

$$u_1 = \left(\frac{Ay(y-s)}{2(n+mn)}-\frac{Ay^2n}{(1+3n)(1+2n+mn)}\right)\left(y^{\frac{1+n}{n}}-1\right)$$

$$-\left(\frac{Ay(y-s)(1+n)}{2(n+mn)(1+3n)}\right)\left(y^{\frac{1+3n}{n}}-1\right)$$

$$+\frac{Ay^2(n+n^2)}{2(1+2n)(1+3n)(1+2n+mn)}\left(y^{\frac{2+4n}{n}}-1\right)+$$

(5.36)

$$Bry\left|\frac{y(1+n)}{n}\right|^{1+n}\left[\frac{n}{(1+3n)(1+2n+mn)}\left(y^{\frac{1+n}{n}}-1\right)\right.$$

$$\left.-\frac{(n+n^2)}{2(1+2n)(1+3n)(1+2n+mn)}\left(y^{\frac{2+4n}{n}}-1\right)\right]$$

After substituting u_0, u_1, and θ_0 into Eq. (5.33) and performing several tedious manipulations, a long and complex expression is derived for θ_1 as follows:

$$\theta_1 = C_{51}\left(y^2-1\right)+C_{52}\left(y^4-1\right)+C_{53}\left(y^{3+\frac{1}{n}}-1\right)+C_{54}\left(y^{5+\frac{1}{n}}-1\right)+C_{55}\left(y^{6+\frac{2}{n}}-1\right)$$

(5.37)

where

$$C_{51} = -\frac{y\left(A^2(y-s)+A'(1+m+3n+3mn)\right)}{4(1+m)(1+3n)}+\frac{Ayn\left(Ay-Br\left|\frac{y(1+n)}{n}\right|^{1+n}\right)}{8(1+2n)(1+2n+mn)}$$

$$+\Gamma\left(\frac{A^2(y-s)^2}{4(1+m)^2}-\frac{A(y-s)\left(Ay-Br\left|\frac{y(1+n)}{n}\right|^{1+n}\right)n^2}{2(1+m)(1+3n)(1+2n+mn)}\right)$$

(5.38)

$$C_{52} = -\frac{\Gamma A^2 (y-s)^2}{8(1+m)^2}$$

$$C_{53} = \frac{A^2 y(y-s)n + 2yA'(1+m)n^2 + Br\left|\frac{y(1+n)}{n}\right|^{1+n} A(y-s)n^2 - Br\left|\frac{y(1+n)}{n}\right|^{n} Ay(y-s)(1+n)}{2(1+m)(1+3n)^2}$$

$$-\frac{\left(Ay - Br\left|\frac{y(1+n)}{n}\right|^{1+n}\right)\left[Ayn^3 - Br\left|\frac{y(1+n)}{n}\right|^{n} y(1+n)(n^2+n^3) + Br\left|\frac{y(1+n)}{n}\right|^{1+n} n^4\right]}{(1+3n)^3(1+2n+mn)}$$

$$+\Gamma\left[-\frac{A(y-s)\left(Ay - Br\left|\frac{y(1+n)}{n}\right|^{1+n}\right)n^2}{2(1+m)(1+3n)(1+2n+mn)} + \frac{\left(Ay - Br\left|\frac{y(1+n)}{n}\right|^{1+n}\right)^2 n^4}{(1+3n)^2(1+2n+mn)^2}\right]$$

$$C_{54} = -\frac{A(y-s)\left(Ay(n+n^2) + Br\left|\frac{y(1+n)}{n}\right|^{1+n}(n^2+3n^3) - Br\left|\frac{y(1+n)}{n}\right|^{n} y(1+n)(1+4n+3n^2)\right)}{2(1+m)(1+3n)(1+5n)^2}$$

$$+\Gamma\frac{A(y-s)\left(Ay - Br\left|\frac{y(1+n)}{n}\right|^{1+n}\right)n^2}{2(1+m)(1+3n)(1+2n+mn)}$$

$$C_{55} = \frac{y\left(Ay - Br\left|\frac{y(1+n)}{n}\right|^{1+n}\right)\left(An - Br\left|\frac{y(1+n)}{n}\right|^{n}(2+6n+4n^2)\right)(n^2+n^3)}{8(1+2n)(1+3n)^3(1+2n+mn)}$$

$$+\frac{Br\left|\frac{y(1+n)}{n}\right|^{1+n}\left(Ay - Br\left|\frac{y(1+n)}{n}\right|^{1+n}\right)n^4}{4(1+3n)^3(1+2n+mn)} - \Gamma\frac{\left(Ay - Br\left|\frac{y(1+n)}{n}\right|^{1+n}\right)^2 n^4}{2(1+3n)^2(1+2n+mn)^2}$$

Determined velocities (u_0, u_1) and temperatures (θ_0 and θ_1) are utilized to find the dimensionless bulk or mean temperature given as:

$$\theta_m = \frac{\int u\,\theta\,dS}{\int u\,dS} = \int_0^1 (1+m)\left(u_0\theta_0 + v\,(u_0\theta_1 + u_1\theta_0)\right)y^m dy \tag{5.39}$$

Nusselt number is defined as $Nu = \frac{Dq''}{k(\bar{T}_w - T_m)}$, which can be written in terms of the dimensionless temperature as:

$$Nu = \frac{-4}{(1+m)_{''\ m}}$$

(5.40)

In the case of constant properties and no-slip condition, Nusselt number for circular channel (m=1) can be expressed in the following form as:

$$Nu = \frac{8(1+3n)(1+5n)}{1+12n+31n^2 + Br(1+3n)(1+5n)\left(\dfrac{1+3n}{n}\right)^n}$$

(5.41)

Nusselt number is obtained from the following relation for constant properties and slip condition as:

$$Nu = \frac{4(3+m)(1+2n+mn)(1+4n+mn)(2+5n+mn)}{[1+m]\left\langle \begin{array}{l}(1+2n+mn)\left(\begin{array}{l}2+(17+7mn)n+(32+25m+5m^2)n^2\\+s[(-4-4m)n+(-14-20m-6m^2)n^2]\\+s^2(2+4m+2m^2)n^2\end{array}\right)\\+Br\left|\dfrac{(1+s)(1+2n+mn)}{n}\right|^{1+n}(-2+(-7-3m)n+s(2+2m)n)\\(-n-(2+m)n^2+s(1+m)n^2)\end{array}\right\rangle}$$

(5.42)

The results of Eq. (5.42) are in excellent agreement with those of Barkhordari and Etemad [68] in the absence of viscous dissipation (for m=1) and our previous study [142] (for m=0).

For the variable property case, an explicit expression for Nusselt number cannot be obtained, and therefore, a numerical calculation was employed to calculate the results.

5.2 Plug flow

For plug flows, as known, the velocity has a uniform velocity profile [143]. The longitudinal temperature gradient for plug flows is written as:

$$\frac{\partial T}{\partial X} = \frac{q^{''}(1+m)}{\ldots U c_p \frac{D}{2}}$$

(5.43)

For plug flows, the velocity gradient term vanishe,s and the type of fluid (being Newtonian or non-Newtonian liquids) is not important. The energy equation in dimensional form is as follows:

$$\ldots c_p U \frac{\partial T}{\partial X} = \frac{1}{Y^m} \frac{\partial}{\partial Y}\left(k_s (1+v_{''})Y^m \frac{\partial T}{\partial Y} \right)$$

(5.44)

Substituting Eq. (5.43) into Eq. (5.44) along with dimensionalization, the two parts of the energy equation corresponding to the plug flow are derived as:

$$\frac{1}{y^m} \frac{\partial}{\partial y}\left(y^m \frac{\partial_{''0}}{\partial y} \right) = 1+m$$

(5.45)

$$\frac{\partial}{\partial y}\left(y^m \frac{\partial_{''1}}{\partial y} + y^m_{''0} \frac{\partial_{''0}}{\partial y} \right) = 0$$

(5.46)

These equations under the implementation of boundary conditions given in Eq. (5.34), one obtains the solution ($= _0 + _k \, _1$) as follows:

$$_{''0} = \frac{y^2 - 1}{2}$$

(5.47)

and

$$_{''1} = \frac{y^4 - 2y^2 + 1}{8}$$

(5.48)

The mean temperature becomes

$$u_m = \frac{\int u_n \, dS}{\int u \, dS} = \int_0^1 (1+m)(u_0 + v_{u1}) y^m dy = \frac{-5-m+v_k}{(3+m)(5+m)} \tag{5.49}$$

Nusselt number, Nu=-4/(u_m(1+m)), reads

$$Nu = \frac{-4(3+m)(5+m)}{(1+m)(-5-m+v_k)} \tag{5.50}$$

The values of Nusselt number calculated from this expression for circular (m=1) and Parallel-plates (m=0) channels in the constant property case converges to that of reported in [143].

5.3 Numerical Simulations

Numerical simulations were performed by using the ANSYS FLUENT 14.0 software at which the thermal conductivity and the viscosity were taken to be variable with temperature through integrated User-defined Functions (UDFs). A microchannel of 100×1000 μm^2 (Height×length) was modeled (having mesh size 100×500 with double sided ratio of 1.15) under a constant heat flux of 50000 W/m^2 and different slip velocities at the walls, while the Reynolds number was fixed at 10. Water (i.e. Newtonian fluid with n=1) was considered as the working fluid, whose thermal conductivity and viscosity expressions exist as a function of temperature in the literature [138,144] as follows:

$$\sim(T) = 0.00002414 \times 10^{\frac{247.8}{T-140}} \tag{5.51}$$

$$k(T) = 0.6065 \times \left(-1.48445 + 4.12292\left(\frac{T}{298}\right) - 1.63866\left(\frac{T}{298}\right)^2 \right) \tag{5.52}$$

where T has the unit of Kelvin.

It should be noted that water was taken as the working fluid for numerical simulations since for the power-law fluids (non-Newtonian fluids) it is required to have the thermophysical properties of the fluids as a function of temperature while there are no such expressions in literature.

The simulations provide a comparison between the numerical and analytical results, verifying the analytical results in the case of variable properties as well as constant properties.

5.4 Results and Discussion

An increase in temperature along the channel during the wall heating process causes simultaneous variations in both the viscosity and the thermal conductivity. These property variations lead to a change in the convective heat transfer rate of the fluid flow. Therefore, this section displays how the temperature dependent properties affect Nusselt number in the hydrodynamically and thermally fully developed non-Newtonian power-law fluid flows in circular and parallel-plates microchannels at constant heat flux thermal boundary condition applied to the walls.

As known, a fluid is considered as shear thinning (or pseudoplastic) if its viscosity decreases with shear rate, and the corresponding power-law index is less than unity (n<1) for this type of fluid. Contrarily, shear thickening (or dilatant) fluids show opposite behavior and have the power-law index higher than 1 (i.e. n>1). In our previous study [142], the effects of power-law index and slip coefficient on the velocity profile for parallel- plates microchannels for constant thermophysical properties were discussed.

Figures 5.2 and 5.3 depict dimensionless velocity distributions of non-Newtonian fluid cases with n=0.5 and 1.5 for both constant and variable properties (=0.1) at different slip coefficients, , m=1 and Br=0.01. Unlike the constant property case, Brinkman number appears in the velocity distribution as well. As expected, an increase in decelerates the velocity core to keep the flow rate constant, which also implies that slip

velocity becomes more at the walls. In addition, there is a considerable decrease in values of core velocity, when the properties are considered as temperature-dependent, which is ascribed to the decreased viscosity, resulting in smaller shear stresses. It can be also observed that the property variation effect on the velocity profile is more influential for shear-thinning fluids. For example, for =0, the deviation of the center velocity of the variable property case from the constant property case is about 5.3% for n=0.5, while it is nearly 2.7% for n=1.5.

Fig. 5.2 Dimensionless fully developed velocity profiles of n =0.5for constant and variable property cases at different slip coefficients, m=1 and Br=0.01

Figure 5.4 compares the numerical (at Re=10) and analytical velocity distributions of fully developed velocities in the case of constant property and shows an excellent agreement. The results also match with analytical expressions available in the literature.

Figure 5.5 presents the deviation of numerical velocity profiles from the analytical ones for both constant and variable properties. As seen from the figure, for the case of constant property the deviation is nearly close to zero. The deviations become visible as the properties are varied with the temperature.
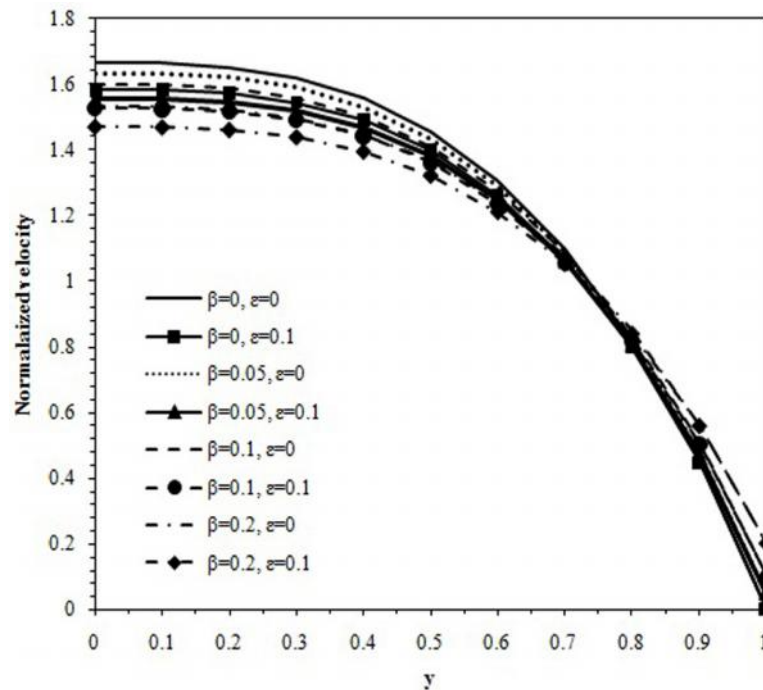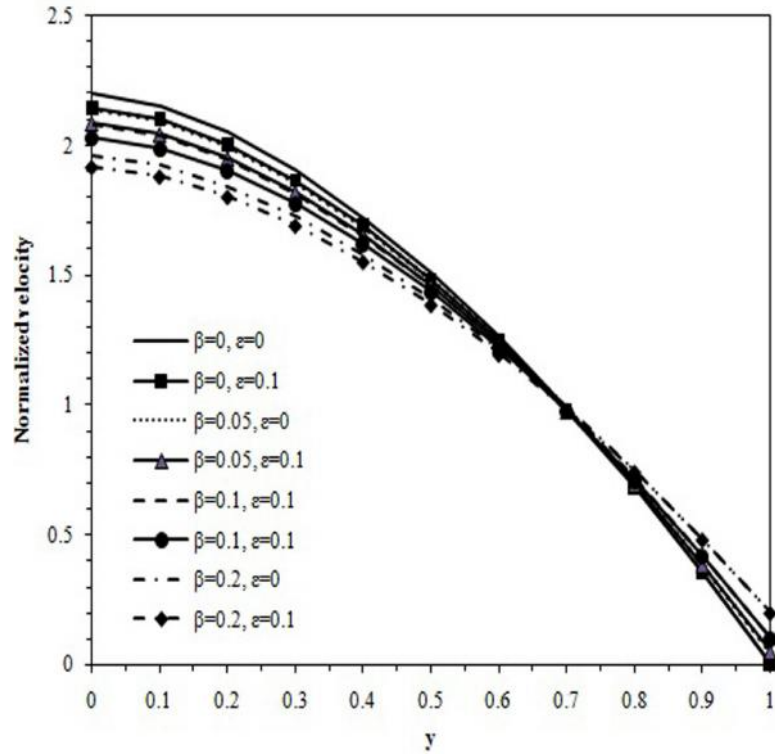
70

Fig. 5.3 Dimensionless fully developed velocity profiles of n =1.5for constant and variable property cases at different slip coefficients, m=1 and Br=0.01
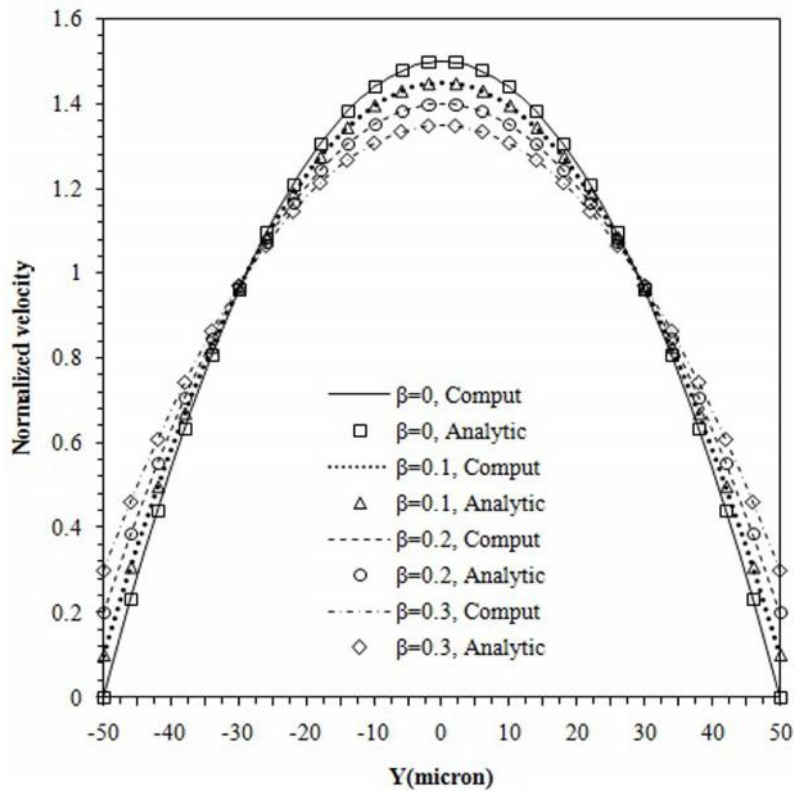

Fig. 5.4 Dimensionless fully developed velocity profiles of n =1 for constant property case at different slip coefficients and Br=0

71

However, this does not go beyond 0.011, which is acceptable and can be due to the use of first order perturbation method for analytical solution or the dependency of the numerical solution to heat flux, since the values of and change with heat flux. The deviation decreases, as the slip coefficient increases. It is worthwhile to note that the heat flux in numerical simulation must be applied so that obtained values of and $_k$ meet the assumption of <<1. Otherwise, the comparison with the analytical solution based on the perturbation method (with criterion of <<1) is not accurate.
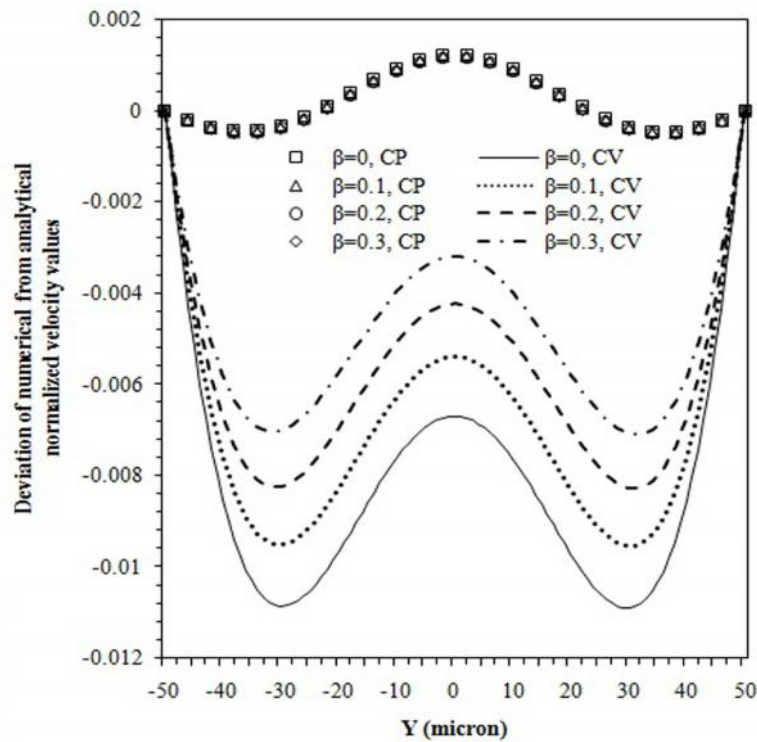
Fig. 5.5 Deviation of numerical from analytical normalized velocity values of n =1 for constant and variable property cases at different slip coefficients and Br=0

The dimensionless temperature distributions of cases n=0.5 and n=1.5 for different values of are displayed at ε=0 and ε=0.1 at m=1, Br=0.01 and =0.2 in Figures 5.6 and 5.7. Besides the fact that the shear-thickening fluid has higher temperature values across the channel than those of the shear-thinning one, in particular at core region, it can be seen that the dimensionless temperature in the core region is suppressed with either the increase in slip coefficient or inclusion of property variation. Similar to the velocity trend, the variable property effect on the dimensionless temperature of shear-thinning fluids is more than that of shear-thickening fluids. But in contrast to the velocity trend, there is no discontinuity between the temperature of wall and fluid particle adjacent to the wall (means there is no jump temperature at the walls) as it

72

exists in the gaseous slip flow case (see Refs [13,14,143,145,146]). The decreased temperatures with   and   are associated to the decreased velocity at core region because of the slip effect on the walls and to the property variation, respectively. When the slip velocity exists near wall, the fluid motion at that region takes contributes more to convection, and less heat is transferred into the core region, leading to smaller temperature values at the centerline. For the property variation case, the thermal conductivity and viscosity, which have no longer a constant profile, change in accordance to the temperature profile. These changes in the properties as well as affected velocity distributions have an interplay in the generation of the temperature profile such that the temperatures become smaller compared to the constant property case, especially at the core region. Further numerical investigation for water discloses that the dimensionless temperature at the center is decreased by either implementing temperature-dependent properties individually or both properties together.

Fig. 5.6 Dimensionless fully developed temperature profiles of n =0.5for constant and variable property cases at different slip coefficients, m=1,   =0.2 and Br=0.01
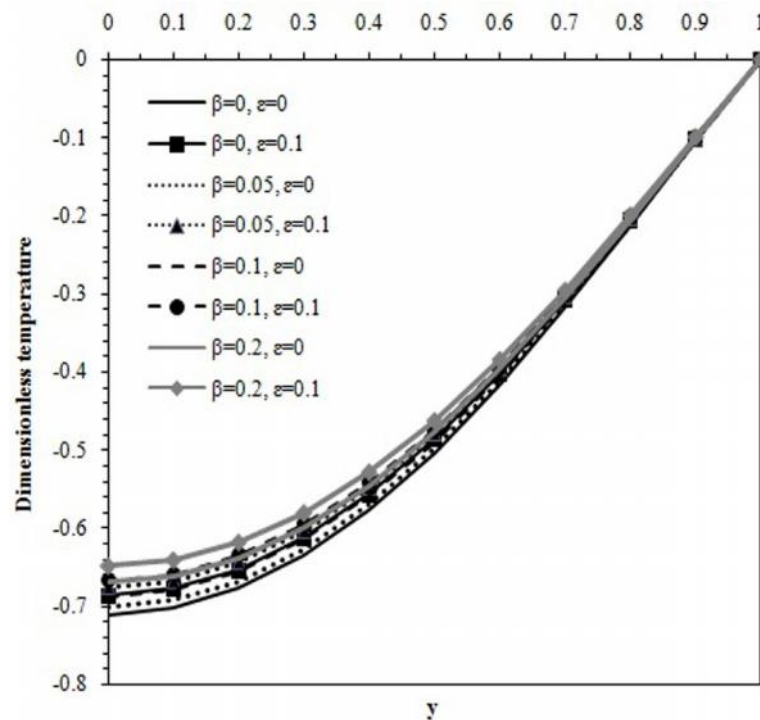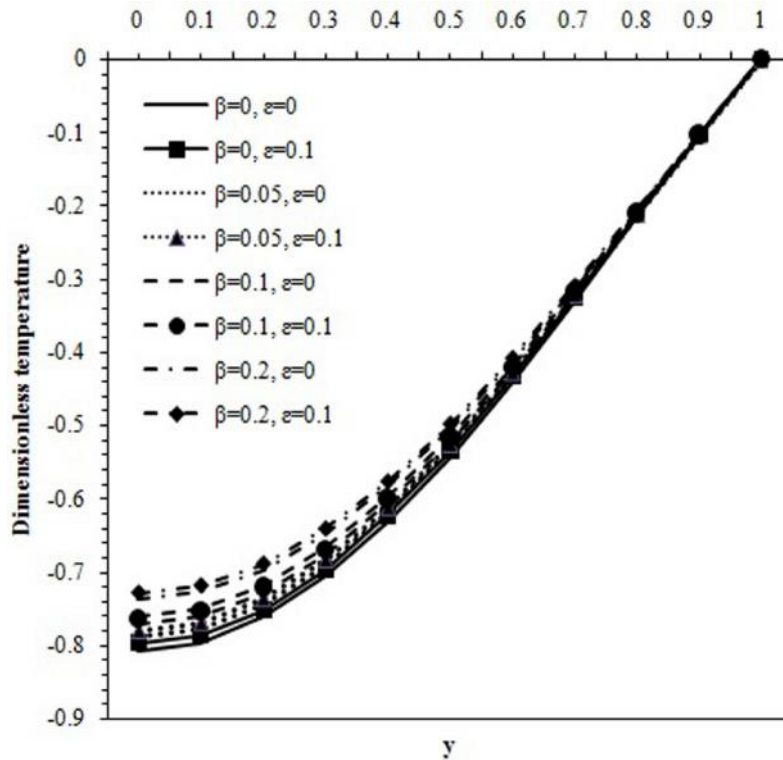
Fig. 5.7 Dimensionless fully developed temperature profiles of n =1.5for constant and variable property cases at different slip coefficients, m=1, =0.2 and Br=0.01

Table 5.1 provides the values of Nusselt number for different slip coefficients at constant and variable properties along with the calculated and by Eqs. (7-9). The percentage errors between the computational and numerical results are in the range of 0.08-0.56%, which indicates an excellent agreement.

Figures 5.8 and 5.9 illustrate Nusselt number as a function of the power-law index for various slip coefficients in the cases of constant (=0) and variable properties (=0.1) at Br=0 for m=0 (parallel-plates channel) and m=1 (circular channel). As can be observed, there is a sharp decrease in Nusselt number with the power-law index for shear thinning fluids. However, the decreasing trend becomes smaller for shear thickening fluids (n>1). The results indicate that an increase in the slip coefficient at the wall enhances heat transfer, as the slip velocity intensifies the fluid motion near the wall leading to enhanced advection effects. The difference between mean and wall temperatures due to inclusion of the wall slip condition reduces, which results in an increase in Nusselt number. It can be further seen that the consideration of temperature-dependency for properties increases the values of Nusselt number, which is mostly effective for the lower power-law index (i.e. shear-thinning fluid) and is the consequence of the same

trend in the velocity and temperature distributions. This suggests that if the property variation with temperature is neglected the heat transfer rate will be underestimated. The deviation can be as much as 8.8% (for =0 and n=0.2) and 1.4% (for =0 and n=2) in the case of m=0, while it can be as much as 12.2% (for =0 and n=0.2) and 2.2% (for =0 and n=2) in the case of m=1. For the slip flow case, the percentages become a bit lower.

Additionally, compared to shear-thickening fluids, Nusselt number is less sensitive to the slip coefficient at the lower power-law index (shear-thinning fluids) for the variable properties case. For example, Nusselt number for m=1 is increased nearly for 4.4% when goes from 0 to 0.2 for n=0.2, whereas it becomes about 12.3% for n=2.

Table 5.1 The analytical and computational values of Nusselt number
for constant and variable properties at different for Br =0 and n=1

		0	0.1	0.2	0.3
CV by Eqs. (7-9)		=0.037 =0.1369	=0.0365 =0.1368	=0.0353 =0.1366	=0.0341 =0.1364
Computional values of Nu					
CP		8.248	8.551	8.870	9.205
CV		8.284	8.585	8.901	9.234
Analytical values of Nu					
CP		8.235	8.533	8.846	9.174
CV		8.331	8.621	8.923	9.241
The error percentage (%) of numeric from analytic results					
CP		0.16	0.21	0.27	0.34
CV		0.56	0.42	0.25	0.08

Fig. 5.8 Nusselt number as a function of n for different values of   at constant (at =0)
and variable property (at =0.1) cases for m=0, Br=0 and =0.2

Fig. 5.9 Nusselt number as a function of n for different values of   at constant (at =0)
and variable property (at =0.1) cases for m=1, Br=0 and =0.2

Figures 5.10 and 5.11 exhibit Nusselt number as a function of the power-law index for different Brinkman number at =0 for m=0 and m=1 in the cases of constant (=0) and variable properties (=0.1). The variation trend is similar to those of Figures 8 and 9 with the difference that an increase in Brinkman number causes a decrease in Nusselt number since the Brinkman number, as a representative of viscous heating and contributing to the internal heating of the fluid, increases the dimensionless mean temperature, which leads to the decrease in Nusselt number.

Fig. 5.10 Nusselt number as a function of n for different values of Br at constant (at =0) and variable property (at =0.1) cases for m=0, =0 and =0.2

Figure 5.12 shows how Nusselt number varies with the slip coefficient at different values of for n=1, m=1, Br=0.01 and =0.2. It can be observe that larger would result in higher Nusselt number, particularly for lower slip coefficients. This implies that the heat transfer rate corresponding to the constant property case deviates more from the temperature dependent case, when the rate of change in thermal conductivity and viscosity with temperature increases. In addition, the slip coefficient has an enhancing effect on Nusselt number, as mentioned earlier.
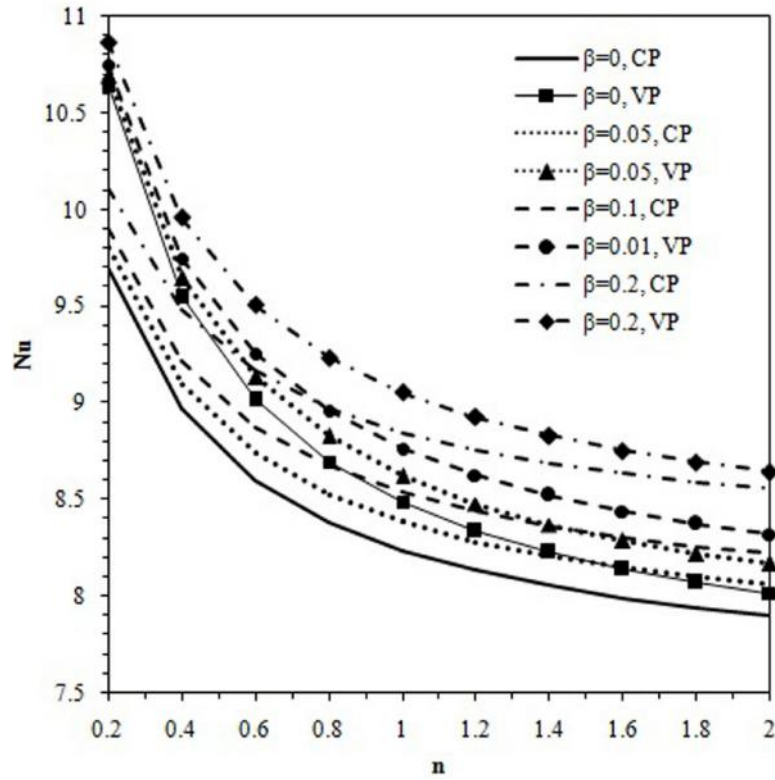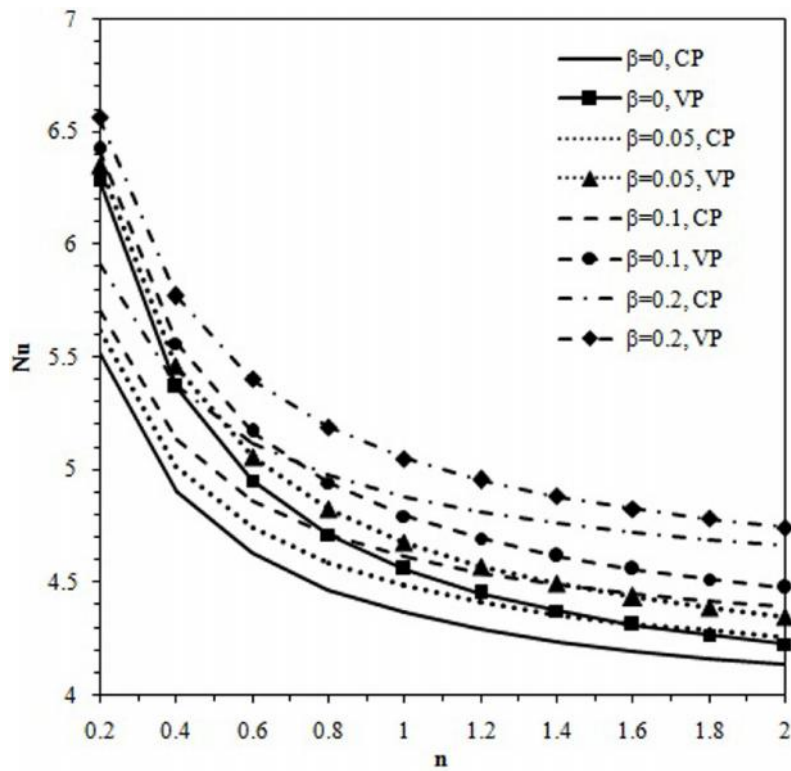
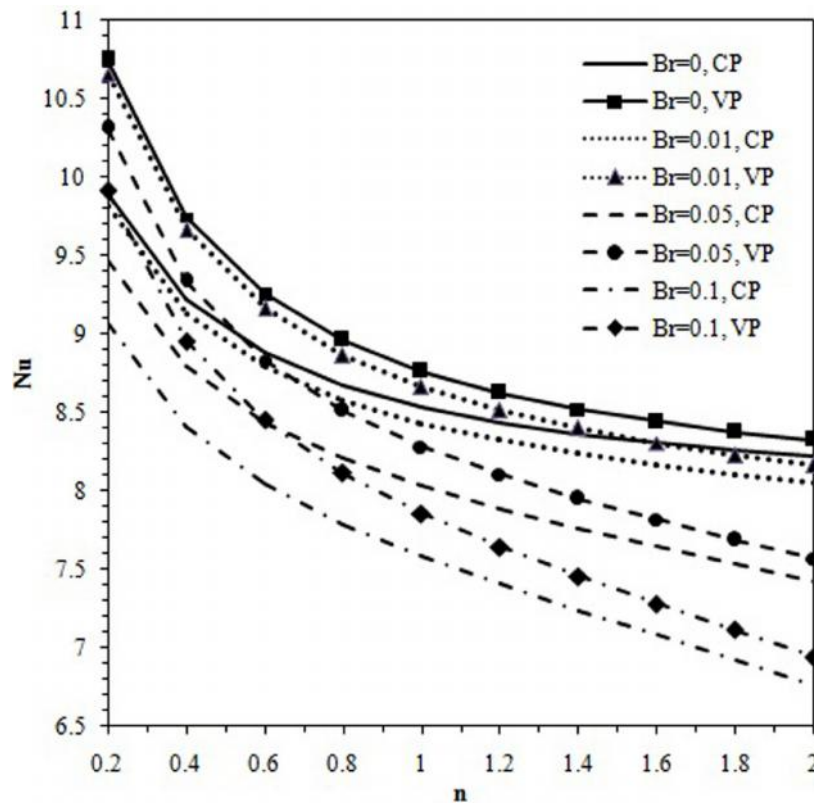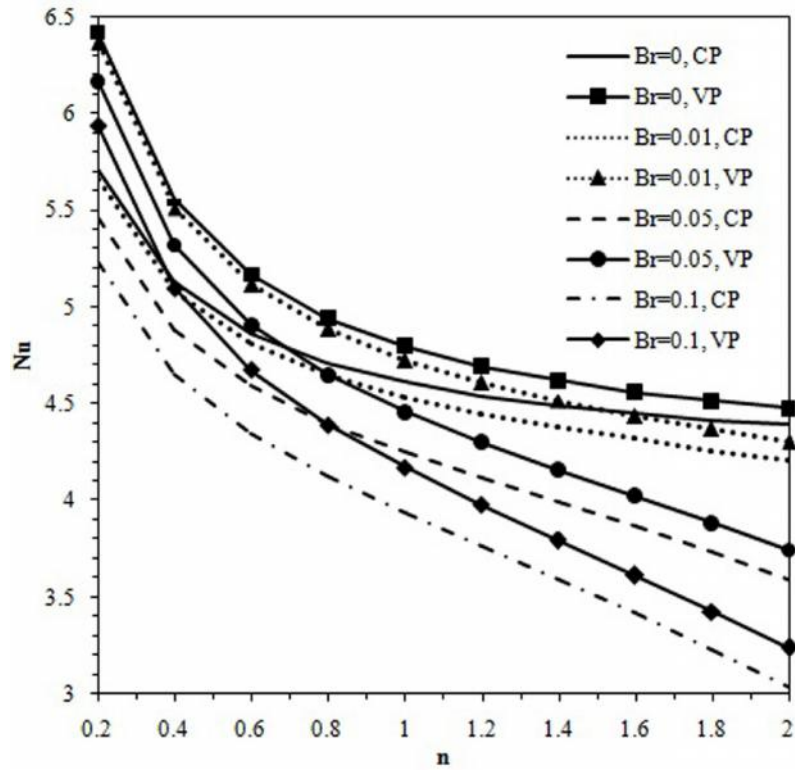Fig. 5.11 Nusselt number as a function of n for different values of Br at constant (at
=0) and variable property (at =0.1) cases for m=1, =0 and =0.2
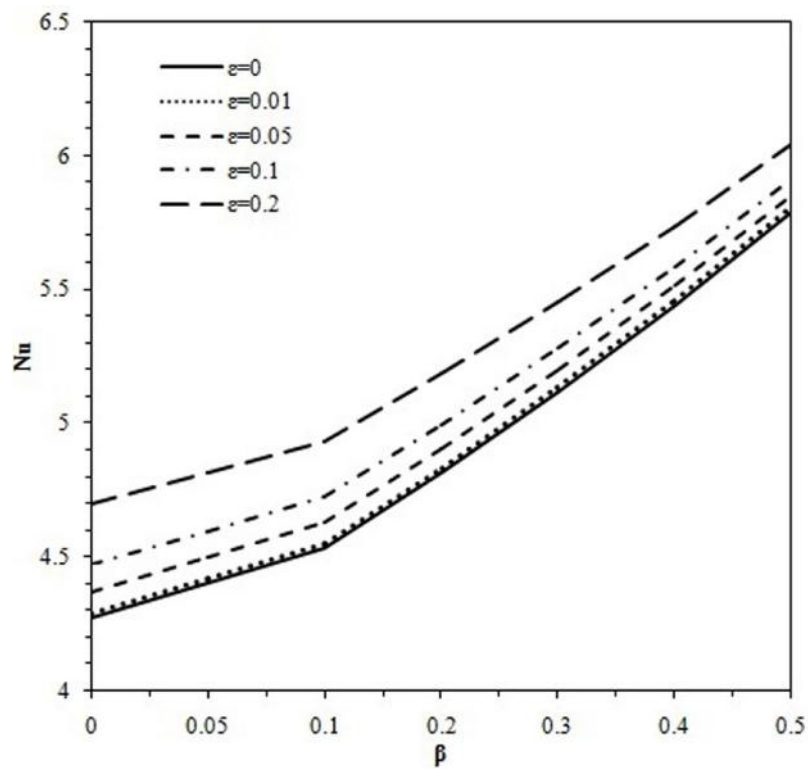
Fig. 5.12 Nusselt number as a function of for different values of at n=1, m=1,
Br=0.01 and =0.2

Figures 5.13 and 5.14 display Nusselt number as a function of the power-law-index (=0.1) and slip coefficient (n=1) for different values of   at Br=0.01, =0.1 and m=1. As seen from these figures heat transfer decreases with the increase in the power-law index and increases with the slip coefficient. One can observe that convective heat transfer (Nusselt number) decreases with the ratio of change in thermal conductivity with temperature to that of viscosity. Taking   equal to $_k$ (i.e. =1) is a poor assumption in both physical and mathematical aspects. However, its effect on the heat transfer rate for single-phase fluid flows studied here is not highly remarkable. For example, the value of Nusselt number changes for an amount of maximum 2.3%, when   varies from 0.2 to 1, which means that even if this ratio is unknown for a liquid, whose viscosity complies with the power-law fluid, it is acceptable to take any value in the range 0.2<   <1, while the deviation from the exact value will not exceed 2.3%. Since the heat transfer behavior associated with the parallel-plates case (m=0) is very similar to the circular channel case (m=1), the results are not included here to avoid repetition.
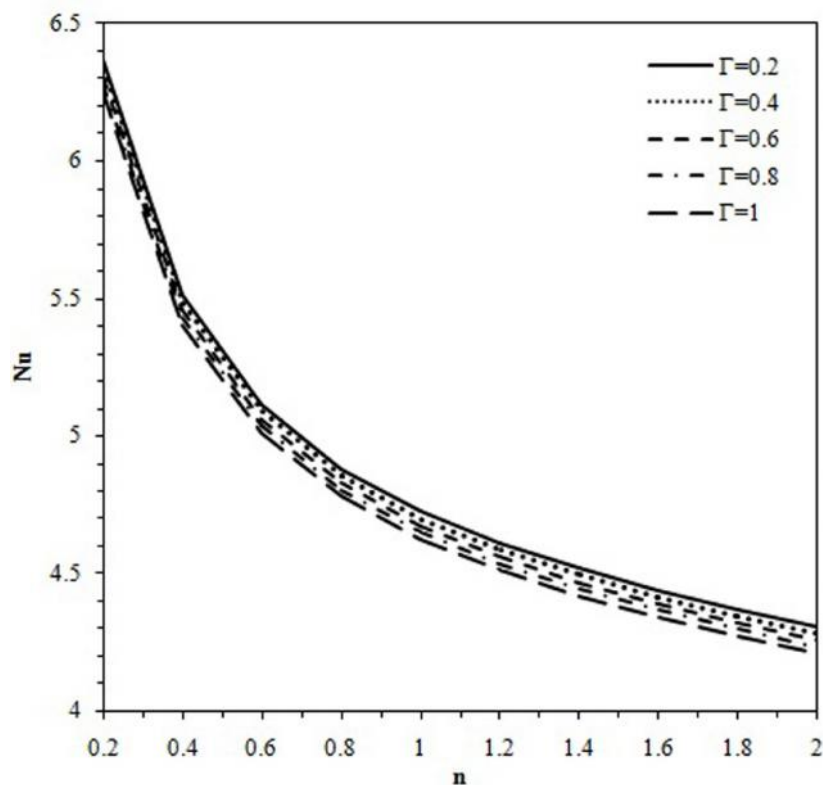
Fig. 5.13 Nusselt number as a function of n for different values of   at m=1, =0.1, Br=0.01 and =0.1
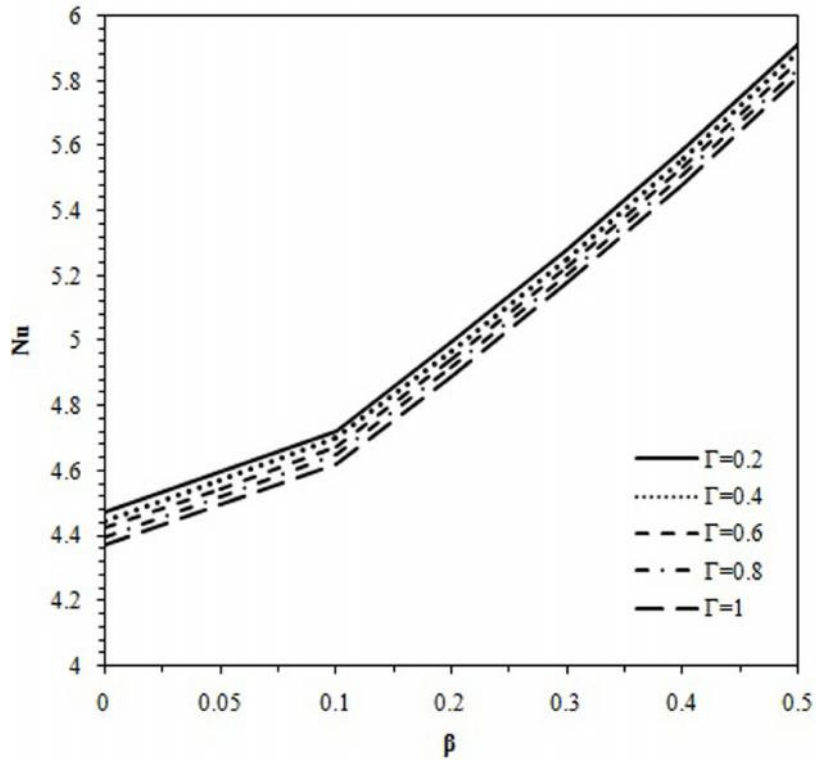
Fig. 5.14 Nusselt number as a function of   for different values of   at m=1, n=1, Br=0.01 and   =0.1

As mentioned earlier, the dimensionless non-linear slip boundary condition is =F(u/ y)^nG, and accordingly, the dimensionless friction coefficient, F, for power-law fluids is expressed as:

$$F = \frac{\text{s}}{\left[\dfrac{(1-\text{s})(1+2n+mn)}{n}\right]^{nG}}$$ (5.53)

which is tabulated in Table 5.2. In the case of n=1 and G=1, the values of F correspond to the dimensionless slip length pertinent to Newtonian liquids defined as the ratio of slip length to hydraulic diameter.

Table 5.2 The slip-friction coefficient values at different n for circular channel (m=1)

	G=1				G=2				G=3			
	0.05	0.1	0.2	0.3	0.05	0.1	0.2	0.3	0.05	0.1	0.2	0.3
n												
0.2	0.0333	0.0674	0.138	0.2126	0.0222	0.0454	0.0952	0.1506	0.0148	0.0306	0.0657	0.1067
0.4	0.0258	0.0527	0.1106	0.175	0.0133	0.0278	0.0611	0.102	0.0069	0.0147	0.0338	0.0595
0.6	0.0205	0.0423	0.0907	0.1475	0.0084	0.0179	0.0412	0.0725	0.0034	0.0076	0.0187	0.0356
0.8	0.0164	0.0342	0.0751	0.1254	0.0054	0.0117	0.0282	0.0524	0.0018	0.004	0.0106	0.0219
1	0.0132	0.0278	0.0625	0.1071	0.0035	0.0077	0.0195	0.0383	0.00091	0.0021	0.0061	0.0137
1.2	0.0106	0.0226	0.0521	0.0918	0.0022	0.0051	0.0136	0.0281	0.00048	0.0012	0.0035	0.0086
1.4	0.0086	0.0185	0.0435	0.0787	0.0015	0.0034	0.0095	0.0207	0.00025	0.00063	0.0021	0.0054
1.6	0.0069	0.0151	0.0364	0.0676	0.001	0.0023	0.0066	0.0152	0.00013	0.00034	0.0012	0.0034
1.8	0.0056	0.0123	0.0305	0.0581	0.00063	0.0015	0.0046	0.0113	0.00007	0.00019	0.00071	0.0022
2	0.0045	0.0101	0.0255	0.05	0.00041	0.00102	0.0033	0.0083	0.000037	0.0001	0.00042	0.0014

The wall shear stress is independent of temperature, i.e. independent of , and dimensionless slip-friction coefficient, F, is not a function of temperature. However, the experimental observations of Hatzikiriakos and Dealy [89] revealed that the slip-friction coefficient, F, changes with temperature, while G is practically independent of it.

Figure 5.15 displays Nusselt number for plug flow in the case of the temperature-dependent case for both circular and parallel-plates channels. As can be observed, the values of Nusselt number for the constant property case are constant (8 and 12 for circular channels and parallel-plates channels, respectively), similar to [143]. The temperature profile remains the same for both geometries, nevertheless, the values of Nusselt number are different. For plug flow, the viscosity variation does not play any role in heat transfer since the velocity gradient is zero in this case. On the other hand, the thermal conductivity variation with temperature comes into play. The results reveal that neglecting this variation would lead to an underestimation in heat transfer.
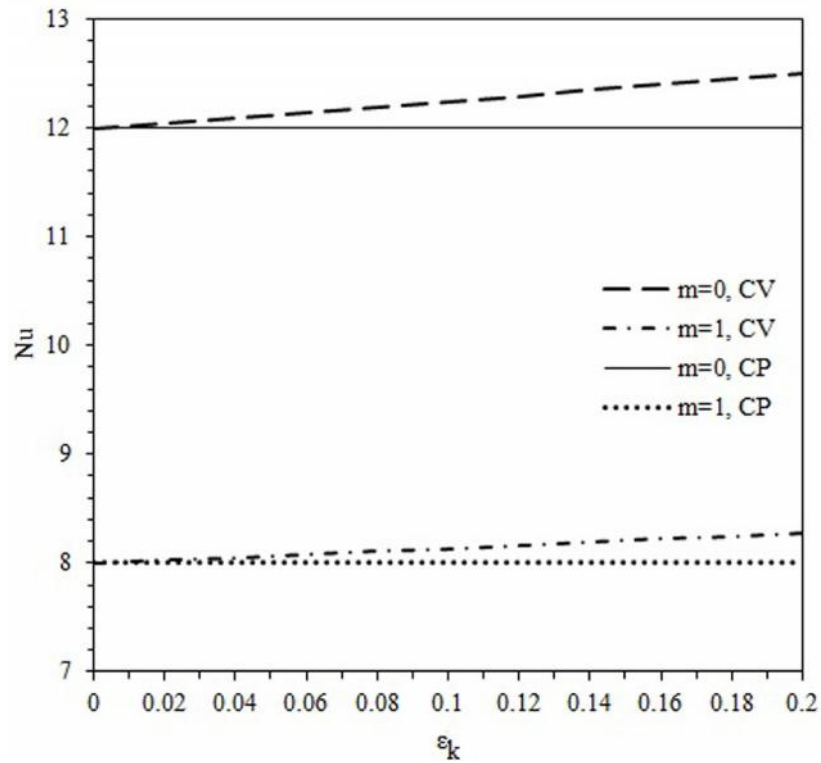
Fig. 5.15 Nusselt number of plug flow as a function of ε_k for circular (m=1) and parallel-plates (m=0) channels for constant and variable property cases

5.5 Conclusion

Convective heat transfer of hydrodynamically and thermally fully developed non-Newtonian power-law fluid flows inside parallel-plates and circular microchannels was analytically and numerically investigated under constant isoflux thermal condition, while the viscous heating, the wall slip condition and the thermophysical properties were taken into account as a function of temperature. Aside from the numerical simulations performed with the ANSYS FLUENT software, the expressions of velocity and temperature profiles and the constant property Nusselt number as a funcion of governing parameters were derived from governing equations, and variable property Nusselt numbers were obtained with numerical calculations.

For power-law fluids, it was found that regardless of temperature-dependent properties, Nusselt number has a decreasing trend with both the power-law index and Brinkman

number, where the Brinkman number effect becomes stronger for shear thickening fluids (i.e. higher power-law index). Nusselt number is underestimated by either neglecting slip condition or dependency of thermophysical properties on temperature, which is more pronounced for shear-thinning fluids. For plug flows, temperature dependent thermal conductivity significantly affects convective heat transfer.

CAPTER 6

NUCLEATE POOL BOILING OF POLYMERIC SOLUTIONS

6.1 Experimental Setup and Procedure

The schematic of the experimental setup is displayed in Fig. 6.1. The setup consists of different components such as Plexiglass block, Aluminium heater plate, holder plates, cartridge heaters, thermocouples, gasket sealers and a reflux condenser. The rectangular Plexiglass block has a dimension of $50\times50\times50$ mm^3 with a thickness of 6 mm. The heater plate with dimensions of $62\times62\times25$ mm^3 has four holes for inserting the cartridge heaters covering the whole heating surface region 18 mm below the surface. It also has three holes for thermocouples located about 0.8 mm below the surface. The cartridge heaters are press-fitted into cylindrical holes, while high quality conductive grease is utilized to fill the air gap between the cartridge heaters and inner areas of the holes. The holder plates are used to sandwich the Plexiglass block and the heater plate together. The upper plate has three holes, which are used for the connection with the condenser, introducing working fluid, and inserting a T-type thermocouple to measure the bulk fluid temperature. Plastic gasket sealing elements, which are resistant to high temperatures, are used between Plexiglass block edges and the plates (both heater and cap plates) to prevent any leakage as well as between the heater and holder plates to prevent heat dissipation. The reflux condenser is composed of concentric glass tubes of

22 mm and 40 mm (inner and outer diameters) of a length of 40 cm. The gap between the outer and inner tubes is filled with water to condense the vapor escaping through the inner tube, which is open to atmosphere to maintain the tests at atmospheric pressure.
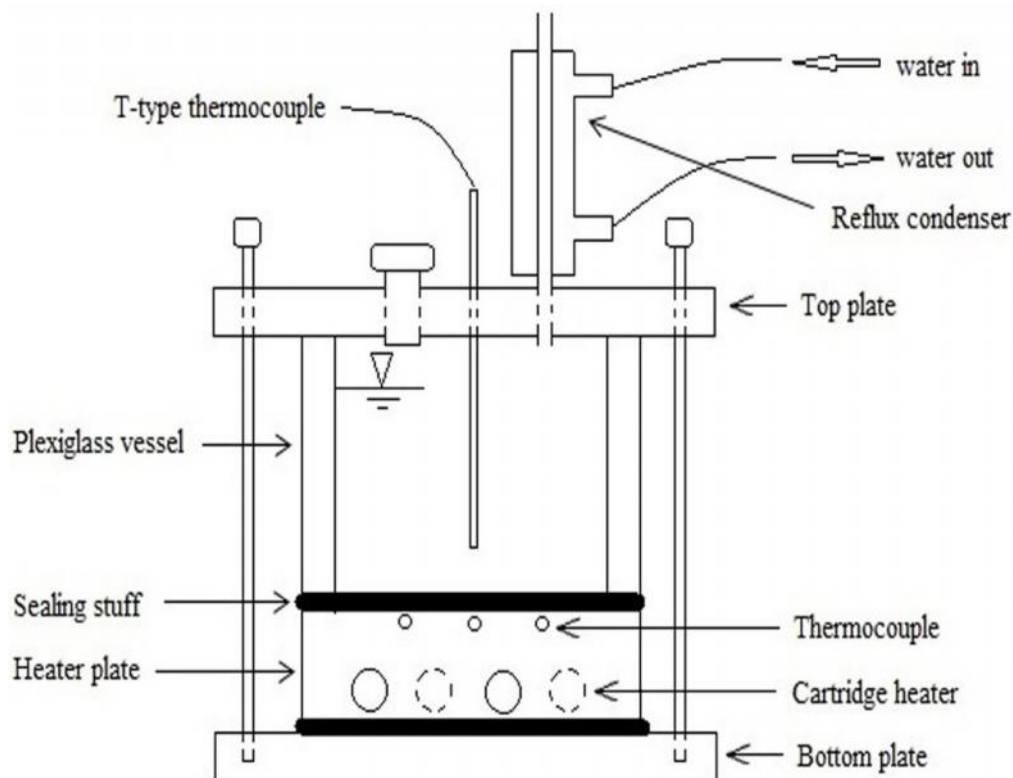
Fig. 6.1 Schematic of the experimental set-up

The mass of liquid were measured before and after of rests were measured to check for the change in the liquid amount. It was found that the mass of liquid remains nearly the same, which indicates effective operation of the reflux condenser. The cartridge heaters were connected to a power supply with high-precision digital multimeters, and voltage and current could be tuned and recorded. The power and bulk and surface temperatures were recorded under steady state conditions. Every liquid sample tested for several times to make sure the repeatability, and the averaged values were taken into consideration.

6.2 Data Reduction and Uncertainties

The net heat flux value of power input was calculated as:

$$q'' = \frac{VI - Q_{loss}}{A} \tag{6.1}$$

where A is the heated surface area. To account for heat losses, natural convection analysis was done for surrounding areas of the heater, which are in contact with ambient. After the assessment of heat losses, the net power was deduced. The heat losses were between 2.5-5% relative the electrical power.

The boiling heat transfer coefficient, h, was then found as:

$$h = \frac{q''}{(T_s - T_{sat})} \tag{6.2}$$

where T_s is the surface temperature and T_{sat} is the saturation temperature of the fluid. The surface temperatures were obtained by considering thermal contact resistance from the thermocouple to the surface R_c and the average of the thermocouple measurements T_{th}, as:

$$T_s = T_{th} - q'' \ R_c \tag{6.3}$$

The wall superheat, T_{sat}, is defined as the difference of saturation temperature, T_{sat}, and the average surface temperature, T_s.

The uncertainties in the measured values given in Table 6.1 were taken from the manufacturer's specification sheet, while the propagation of error method [147] was used to calculate the uncertainties in the derived parameters as seen in the Table 1.

Table 6.1 Uncertainty in experimental parameters

Uncertainty Parameter	Error %
$T_{superheat}$	0.27
q"	1.1
h	2.7

6.3 Material Preparation and Property Measurements

Aqueous polymeric solutions were prepared by adding Xanthan gum E415 powder in small amounts, which was measured by an electronic high precision weighing scale, into deionized water with different concentrations (100, 500, 1000, 4000 and 6000 mg/L). To achieve the desirable solutions in terms of homogeneity, each sample was treated in a pool of silicon while keeping the temperature at 55 °C, and magnetically stirring at 1000 rpm was performed for several hours.

In order to measure the contact angle and equilibrium surface tension (or equilibrium gas-liquid interfacial tension) of the polymeric solutions, Theta Lite Optical Tensiometer TL100 device was employed. The device contains a USB2 digital camera (160 frames/sec max) or a FireWire video camera (60 frames/sec), an adjustable sample stage and a LED light source. Each of prepared aqueous solutions was examined to find equilibrium surface tension and contact angle, which were used to explain the experimental results. For visualization studies, a camera having a digital resolution of 3264×2448 pixels was utilized at 240 frames/sec to capture images during boiling process.

Raman is one of the vibrational spectroscopy techniques, in particular used for determining fine alterations in the chemical structures of materials owing to its abilities of providing spectral information with high lateral resolution. Raman can identify substances from characteristic spectral patterns (fingerprints), as each chemical bonding in the sample, which has Raman mode, gives a characteristic band in the spectrum. In this study, Raman spectroscopy enabled tracking the changes in the chemical stability of aqueous Xanthan gum solutions with different solid contents, before and after

performing heat transfer experiments. For the measurements, a Raman Renishaw InVia Microscope and Spectroscope with 532 nm green laser, 2400 lines/mm and 50x objective were used.

6.4 Results and Discussion

Non-Newtonian fluids are prepared by adding polymeric additives or surfactants to a base fluid (e.g. water). As a result, viscosity of the fluid becomes shear-dependent, and interfacial fluid properties such as dynamic and equilibrium surface tension and contact angle change. The variation in liquid properties such as surface tension, rheology (i.e. viscosity) and wettability (related to contact angle) strongly affect bubble dynamics and nucleation. For polymeric solutions, the surface wettability is influential in controlling the nucleation sites, and bubble dynamics is dominated by the variations in the equilibrium and dynamic surface tension and shear rate-dependent viscosity [122,148–150].

The viscosities of polymeric solutions compared to the solvent (i.e. water) are shear rate-dependent behavior, which show non-Newtonian behavior. Figure 6.2 exhibits the variations of the viscosity as a function of shear rate at different concentrations. As seen, the viscosity of the solution decreases with shear rate and converges to infinite shear viscosity, which is represented by Carreau model [151] as

$$\mu_{eff}\left(\dot{\gamma}\right) = \mu_{inf} + \left(\mu_0 - \mu_{inf}\right)\left(1 + \left(\lambda\dot{\gamma}\right)^2\right)^{\frac{n-1}{2}} \tag{6.4}$$

where μ_0 is zero shear rate viscosity, μ_{inf} is infinite shear rate viscosity, relaxation time and n is power index. The viscosities of the solutions are higher than that of the solvent, and the increase in concentration results in higher the viscosities.

Figure 6.3 and 6.4 display the equilibrium liquid-vapor interfacial tension and contact angle. It can be observed that the equilibrium surface tension decreases with the addition of polymeric additives into solvent and the increase in concentration, which

was also reported in the literature [118,122,148]. Surface tension values are close to that of water at low concentrations, whereas surface tension dramatically drops beyond concentrations higher than 1000 mg/L. Contrarily, the contact angle exhibits an increasing trend from $44.9°$ (for pure water) up to around $74.4°$ for the solution with concentration of 1000 mg/L. Beyond this concentration, contact angle remains almost constant. From this trend, it is clear that the wettability is less of prepared polymeric solutions than that of water.
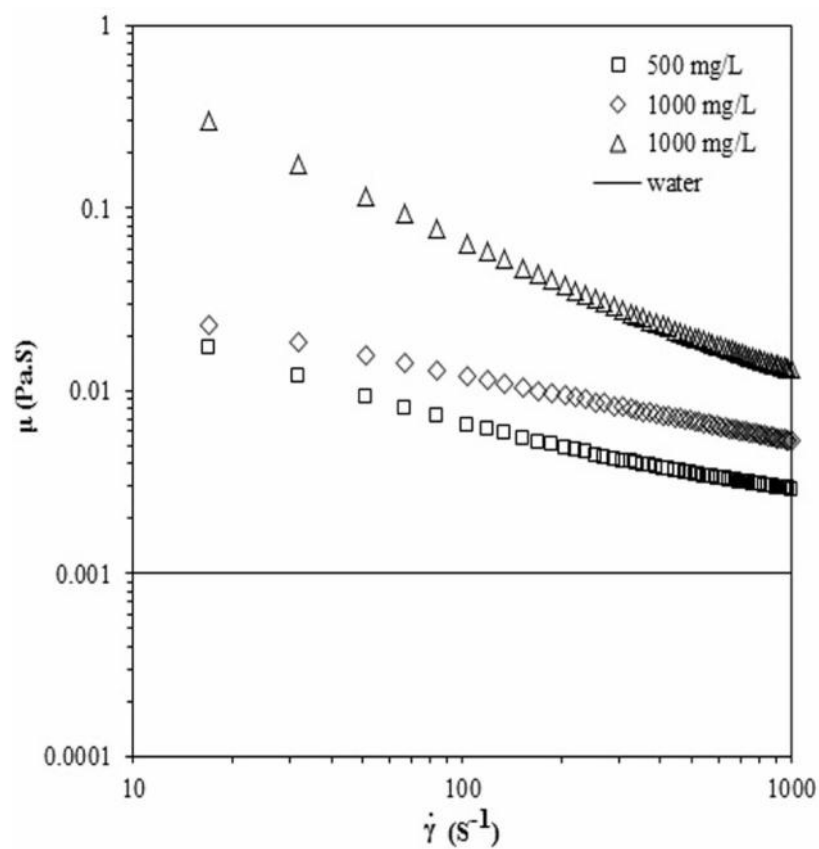
Fig. 6.2 The viscosity as a function of shear rate for Xanthan gum solutions with different concentrations
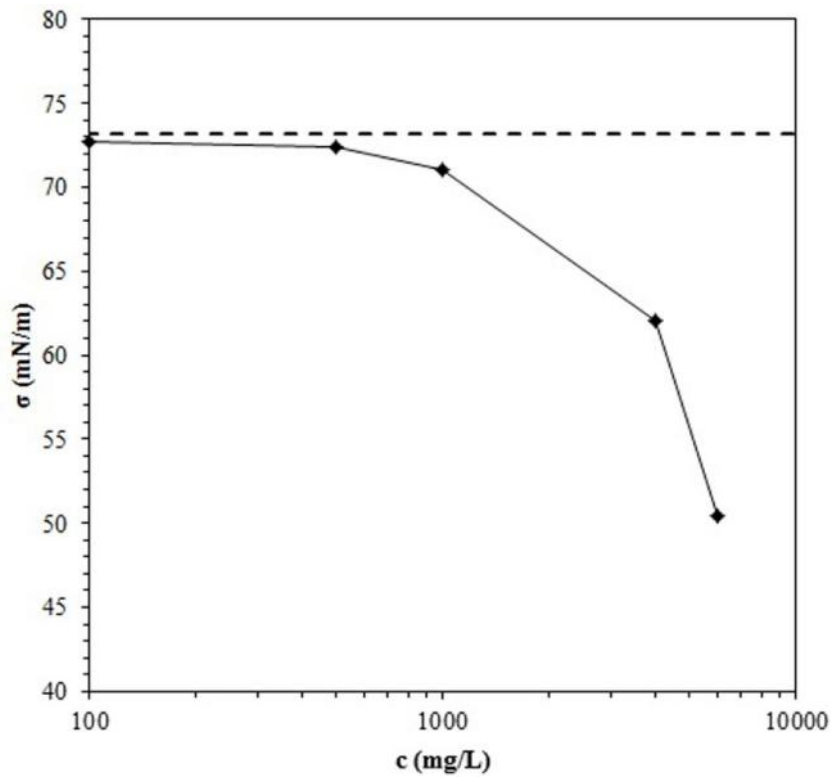
Fig. 6.3 The equilibrium surface tension as a function of solution concentration
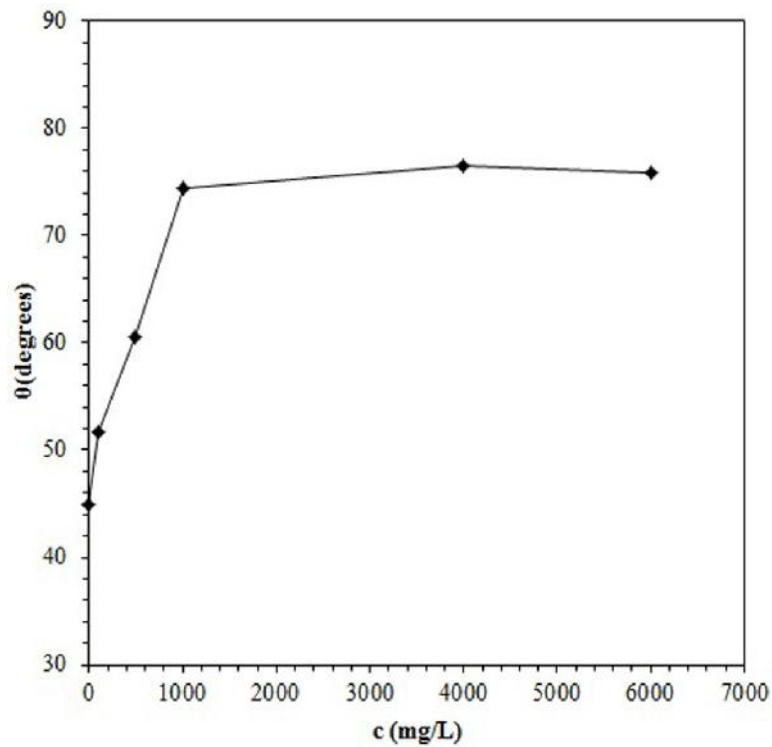
Fig. 6.4 The contact angle as a function of solution concentration

The initial boiling heat transfer tests were done with distilled water to provide validation for the experimental setup via comparisons with available nucleate pool boiling correlations, such as Rohsenow [152], Mostinski [153], and Gorenflo [154]. The

experimental data corresponding to pure water offer a base for comparison with boiling heat transfer performance of prepared polymeric solutions. Fig. 6.5 displays the data of pure water as a function of wall superheat along with the predictions of widely used Rohsenow [152], Mostinski [153], and Gorenflo [154] correlations. As seen, the results are in good agreement with predictions of Mostinski and Gorenflo correlations. At lower heat flux, Gorenflo correlation's prediction is better, while Mostinski correlation provides a better prediction for high heat flux.
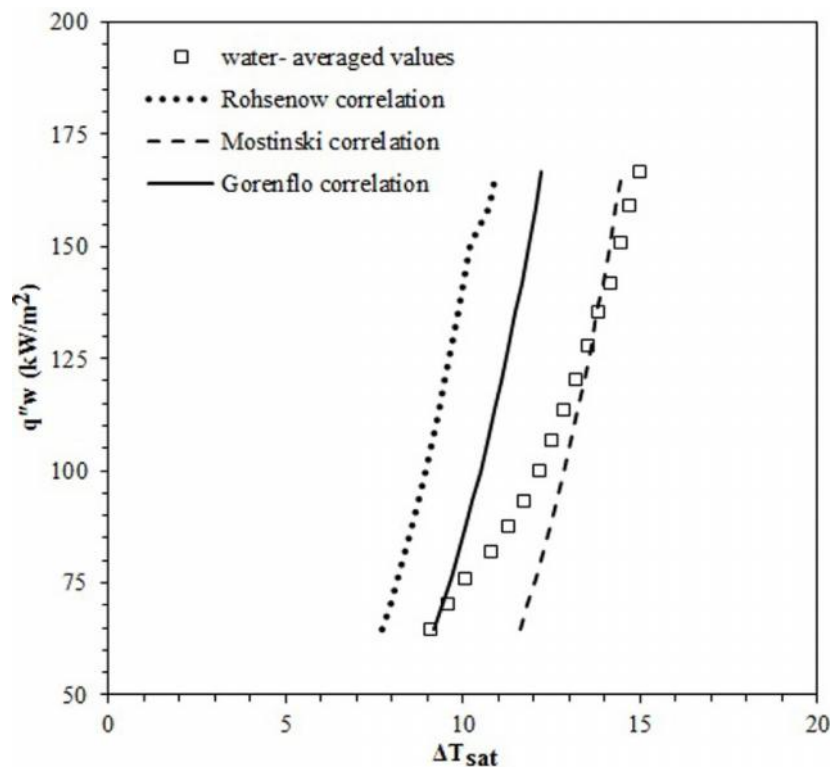
Fig. 6.5 Boiling curve of pure water data along with the predictions of correlations

Boiling curves for Xanthan gum polymeric solutions are shown in Fig. 6.6 at different concentrations along with that of water. As can be seen, the boiling curve shifts to the right hand side with the increase in concentration, which indicates deterioration in the heat transfer performance. The properties of working fluid change when the polymeric additives are introduced, which is reflected in its heat transfer performance relative to the pure fluid. For a fixed heat flux, as the concentration of the solution increases up to 500 mg/L, the wall superheat increase rises up to 27%. When the concentration is raised from 500 to 1000 mg/L, there is an only slight change in the wall superheat. However, for high concentrations (i.e. 4000 and 6000 mg/L), a different trend is apparent. For this

case, a nearly linear relationship with a relatively small slope exists between heat flux and wall superheat, implying a large rise in wall superheat with a moderate increase in heat flux. In contrast, the boiling curves corresponding to water and polymeric solutions with c 1000 mg/L are steep, in particular at the upper range of the heat fluxes. The change in heat flux different aqueous polymeric solutions is accompanied with different wall superheats. For instance, as the heat flux is changed about from 70 to114 kW/m^2, the wall superheat increase is 34.5 % for the solution with a concentration of 100 mg/L, while it is about 177.5 % for the solution with a concentration of 6000 mg/L.
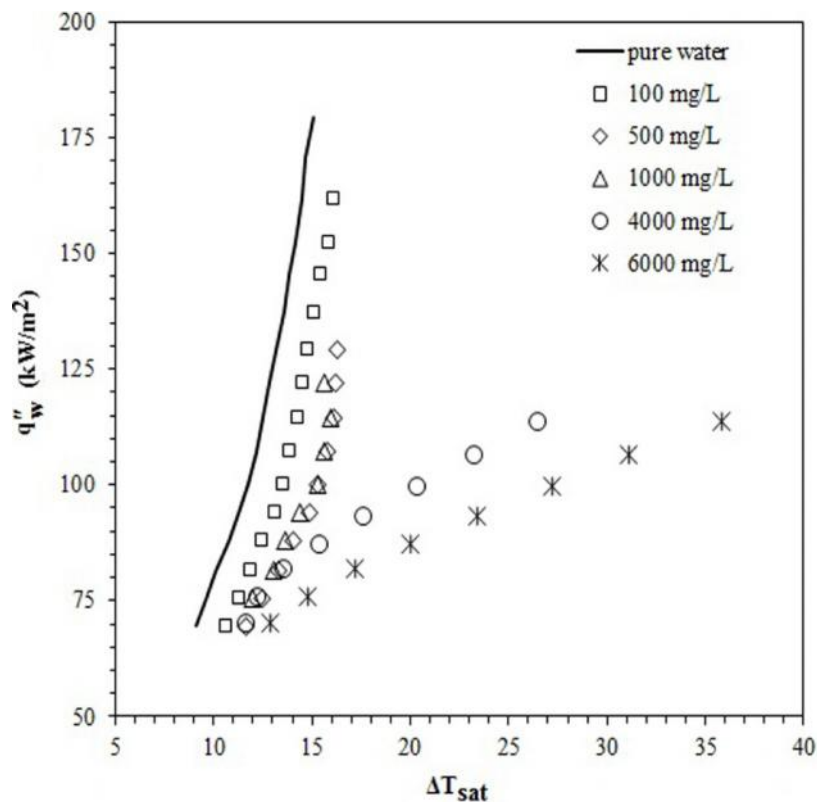
Fig. 6.6 Boiling curves Xanthan gum polymeric solutions
at different concentrations

Boiling heat transfer coefficients of the polymeric solutions with different concentrations are depicted in Fig. 6.7. The variation of the heat transfer coefficients (defined as h=q ∕ T$_{sat}$) as a function of the heat flux, presented in the figure, illustrates that HTC increases with heat flux except for the solution with concentrations of 4000 and 6000 mg/L, for which a monotonically decreasing trend in the heat transfer coefficient with the heat flux is present. Furthermore, the heat transfer deteriorates with the increase in concentration until a specific value of c=500 mg/L. Worsening in boiling heat transfer was already reported in the previous studies such as the study of Zhang

and Manglik [122] on Carbopol solutions, the study of Wang and Hartnett [124] and the study of Paul and Abdel-Khalik [127], who considered on aqueous polyacrylamide solutions. A further increase in concentration (by up to 1000 mg/L) does not result in any significant change in heat transfer performance. However, a different trend is observed for highly viscous aqueous Xanthan gum solutions with high concentrations (e.g. 4000 and 6000 mg/L). In the study of Bakhru and Lienhard [155] on the boiling heat transfer of water and four organic liquids on small horizontal wires, patchy boiling to full blanketing (film boiling) patterns were recorded for most of the experimental data, and the slope of boiling curve was small at high wall superheats. A similar trend exists for the concentration of 4000 and 6000 mg/L in this study, at lower wall superheats. This could be due to bubble crowding, which occurs just after the onset of nucleate boiling. As a result, the nucleate region for these concentrations is rather short, and a shift to patchy boiling pattern occurs. Suppression of micro-convection within the boundary layer as a consequence of high viscosities at high concentrations could be another reason [122]. The concentration of polymeric solutions might be higher than that of the critical polymer concentration or overlap concentration. As known, as concentration of a polymeric solution goes beyond these concentrations, polymer chains agglomerate and coil entanglements would eventually start forming in solution so that a transition happens from dilute to semi dilute regime [156].
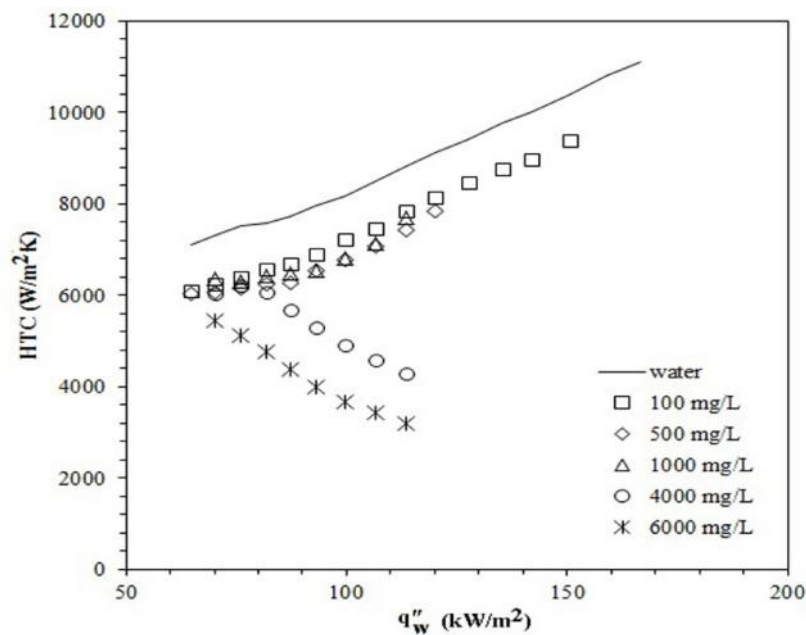
Fig. 6.7 Heat transfer coefficient of Xanthan gum solutions
at different concentrations

Fig. 6.8 exhibits the decrease in heat transfer coefficient in prepared solutions relative to the case of pure water at different concentrations. The dependence profiles on heat flux and thus the relative decrease in heat transfer coefficient remains almost the same for concentrations less than 4000 mg/L. Even though smaller surface tension and larger contact angle promote emergence of smaller and more bubbles from the surface, the effect of increasing viscosity (with concentration) plays an important role. This effect suppresses bulk fluid motion during nucleation and relative motion of emerging bubbles thereby limiting convective heat transfer. For the solutions with concentrations of 4000 and 6000 mg/L, the profiles are monotonically decreasing, and the deterioration in heat transfer reaches more than 65%.
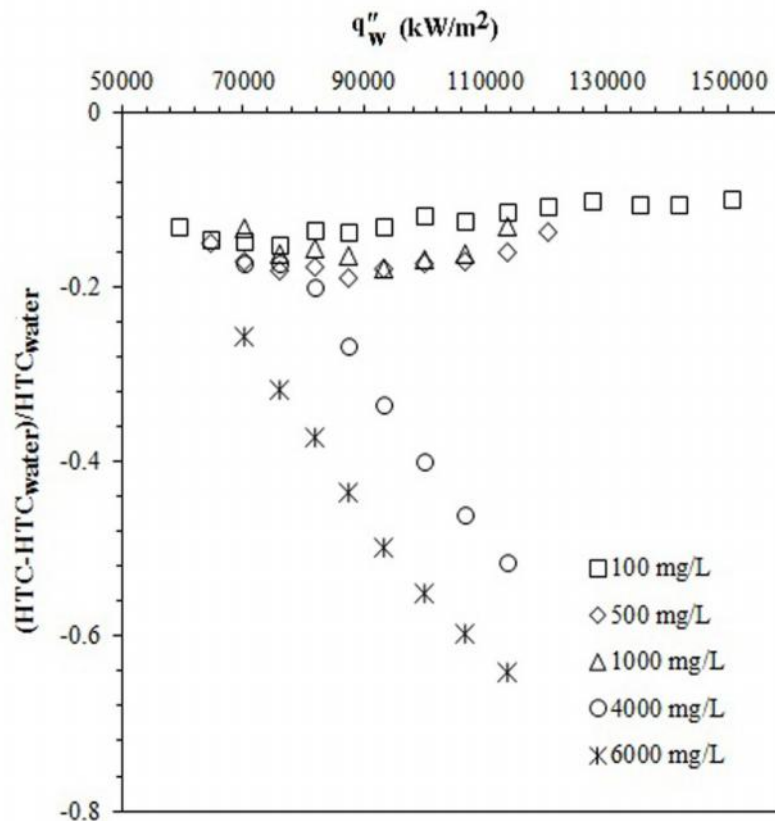
Fig. 6.8 The variation in the heat transfer coefficient deterioration for the Xanthan gum solutions of different concentrations versus heat flux

Pool boiling heat transfer performance is dependent on the bubble formation, bubble distribution on the surface and bubble dynamics (shape, size, frequency, coalescence). Ebullient activity of the polymeric solutions assists shedding light to boiling characteristics. To have more insight to pool boiling of the polymeric solutions, images

of pool boiling are recorded for different concentrations at heat fluxes of 46.5, 55.7, 70.1, 106.5 kW/m^2 (Fig. 6.9).

As can be seen from the images, patterns pertinent to the solutions are clearly different from those of water. This is attributed to the change in the rheological and interfacial properties of the polymeric solutions, whose concentration is a significant parameter.

From the images of pool boiling of water, it can be seen that few nucleation sites (isolated bubbles) exist at low heat flux. With the increase in heat flux, more bubbles form on the surface. At higher heat fluxes, bubbles emerging from the surface coalesce and generate slugs, mushroom shapes and columns. All these patterns are consistent with the literature on pool boiling of water [157]. On the contrary, images of polymeric solutions show different features. Due to smaller surface tension and larger contact angle, the size of emerging bubbles becomes smaller with concentration, and more bubbles are generated on the surface. It is also a result of molecular physisorption (or adsorption of macromolecules) of the polymeric solutions on the heating surface [122,128]. The higher heat fluxes, more bubbles form on the surfaces similar to the case of water. However, the bubbles do not show much tendency to coalesce. Their shapes are more regular, and bubble crowding on the surface is visible for high concentrations, which makes liquid replenishment to the surface more difficult. This effect is further amplified with higher viscosities at high concentrations so that bulk fluid motion and relative bubble motion are hindered. As a result, dry spots on the surface start to form even at small wall heat fluxes for high concentrations, which lead to a decreasing trend in heat transfer coefficient with heat flux.

Two different heat transfer coefficient correlations for low (c 1000mg/L) and high concentrations (c 4000mg/L) are developed using the Least Squares Method [158] to represent the experimental data:

$$h = 23.21 q''^{0.5} \exp\left(-5.28 \times 10^{-5} c\right) \qquad \text{for c } 1000\text{mg/L} \qquad (6.5)$$

$$h = 1.56 \times 10^9 q''^{-1.06} \exp\left(-1.23 \times 10^{-4} c\right) \qquad \text{for c } 4000\text{mg/L}$$

The units of q'' and c in these correlations are W/m^2 and mg/L, respectively. Both of them are based on a typical nucleate boiling heat transfer correlation ($h \sim q''^n$). The exponential function for the concentration accounts for the asymptotic behavior at low concentrations and successfully captures the trends in the experimental data.
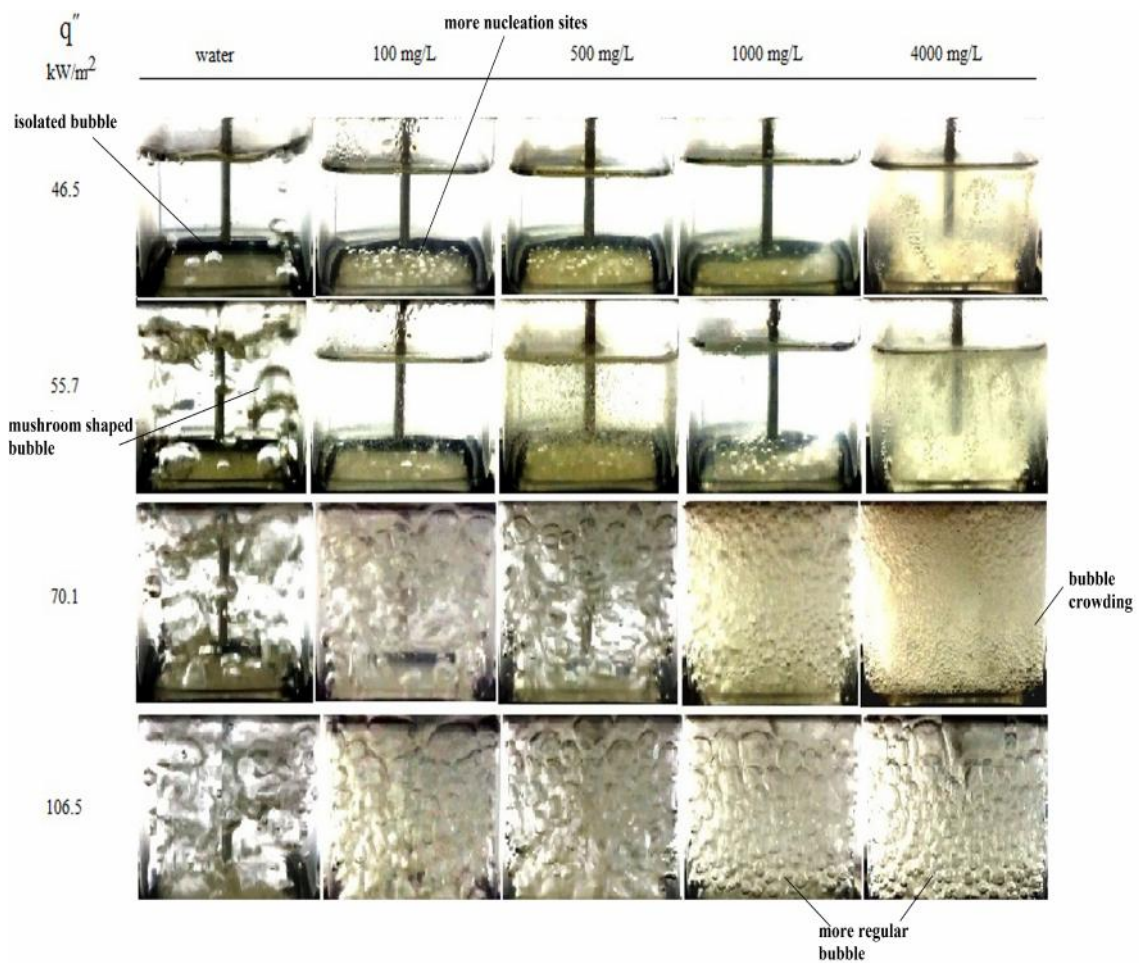
Fig. 6.9 Images of pool boiling over heated plate for pure water and Xanthan gum solutions at different concentrations and heat fluxes

The heat transfer correlations provide an excellent prediction of the experimental data as shown in Fig. 10, and the resulting Mean Absolute Errors (MAE) for experimental data corresponding to the data of low (c 1000mg/L) and high concentrations (c 4000mg/L) are 2.7% and 3%, respectively.

Raman spectra allowed for tracking the alterations in the chemical stability of aqueous Xanthan gum solutions with different solid contents, before and after performing heat transfer experiments (Figs. 11a-d). Raman band observed around 2330 cm^{-1} can be attributed to hydrated hydronium (H$_3$O+) cluster ions, which is due to aqueous solution. Hydronium is the hydrogen ion bonded to a molecule of water, the form in which hydrogen ions are found in aqueous solution. As the intensity of this band decreases in

the solution after heating experiments, it can be suggested that the amount of water decreased due to evaporation of water.
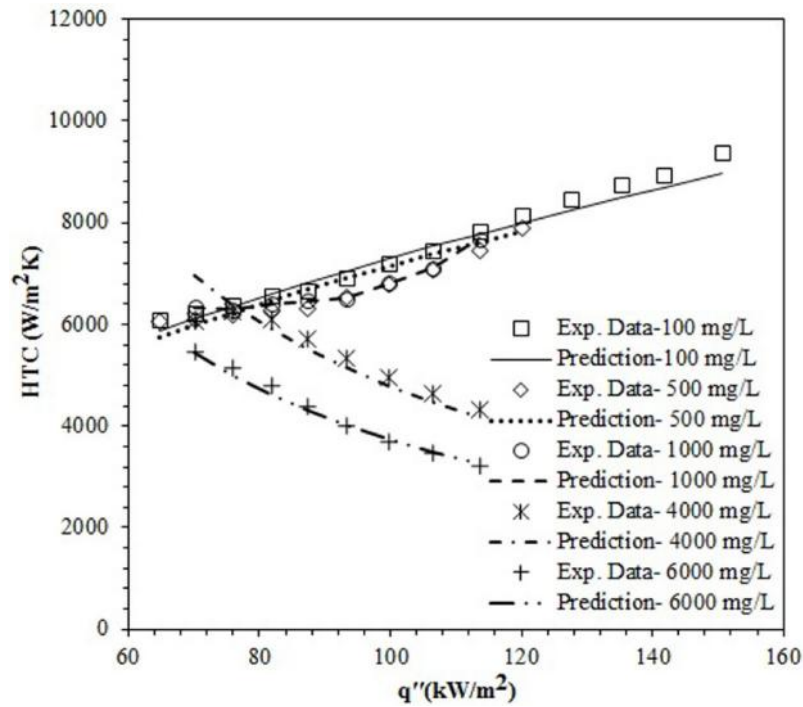
Fig. 6.10 The comparison between the experimental data and predictions of the proposed correlations

Another band observed for the samples before heating experiments is at 1557 cm^{-1} which is correlated to (C=O)bonding in glucose, since one of the main monosaccharides present in Xanthan gum is beta-D-glucose. The decrease in the intensity of this band after heat transfer experiments might be explained by the partial chemical decomposition of the polymeric material in the solution. Also, the band at 1080 cm^{-1} belonging to C-O stretching mode (C-O) vibrations in glucose loses intensity after heating due to partial chemical decomposition of Xanthan gum. As the concentration of the solution becomes more, the chemical stability of the suspension increases with its viscosity. Hence, it can be tracked from the Raman spectra that of the solution with the highest concentration after heat transfer experiments, the corresponding bands lose less intensity than the others. This is also in good correlation with other measurements when the behavior of samples with a concentration of 4000 mg/L is considered.

97

(a)

(b)

98
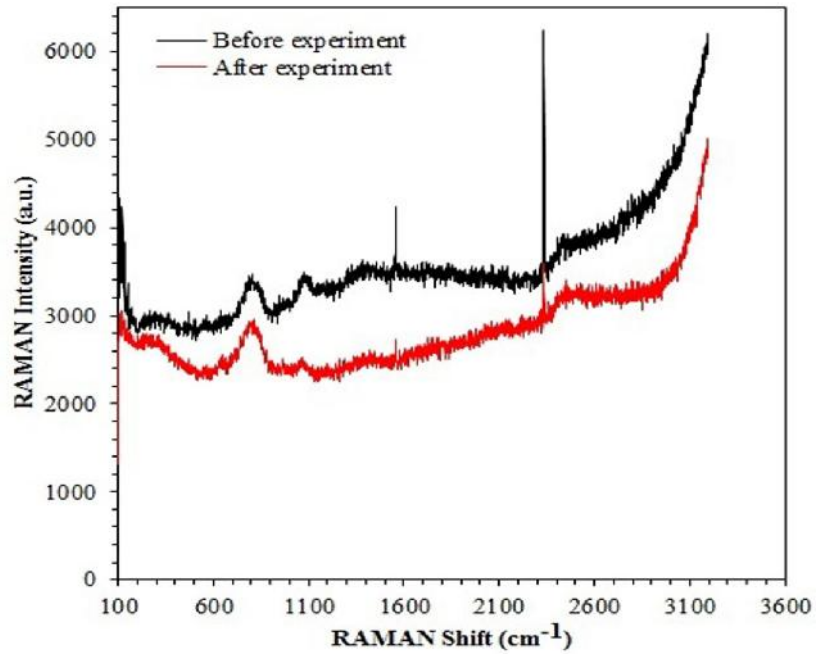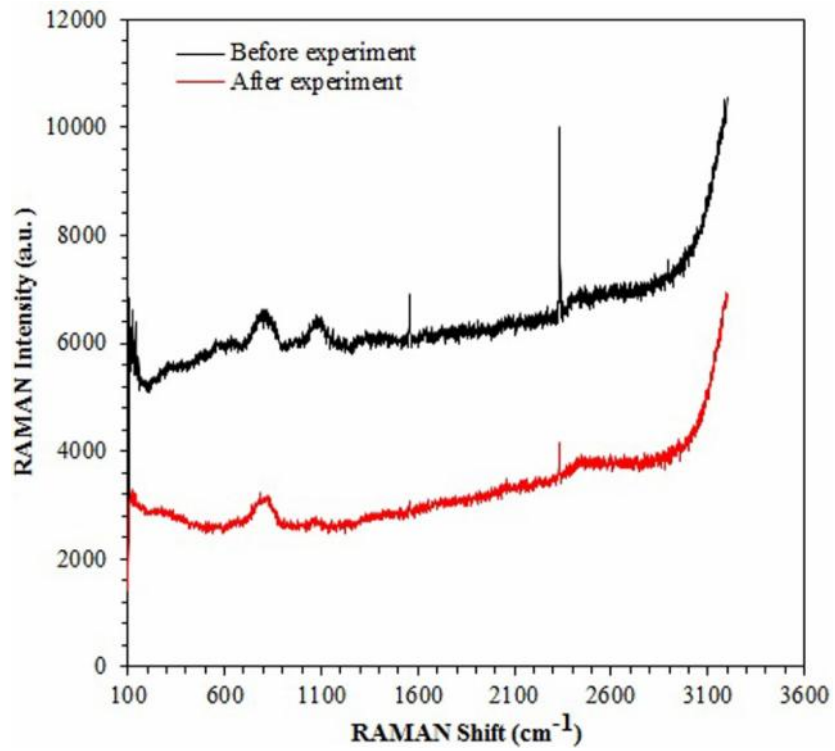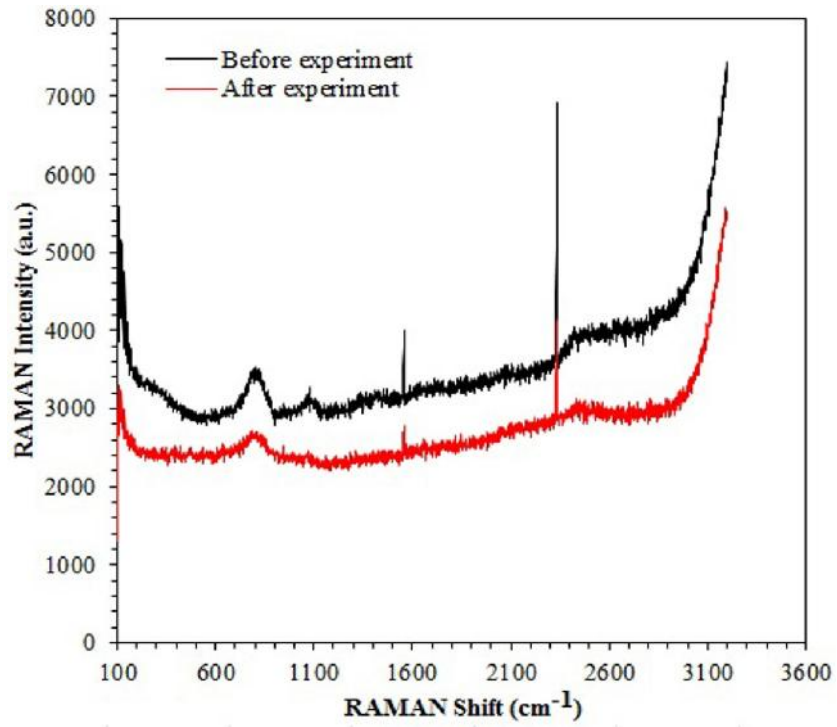
(c)
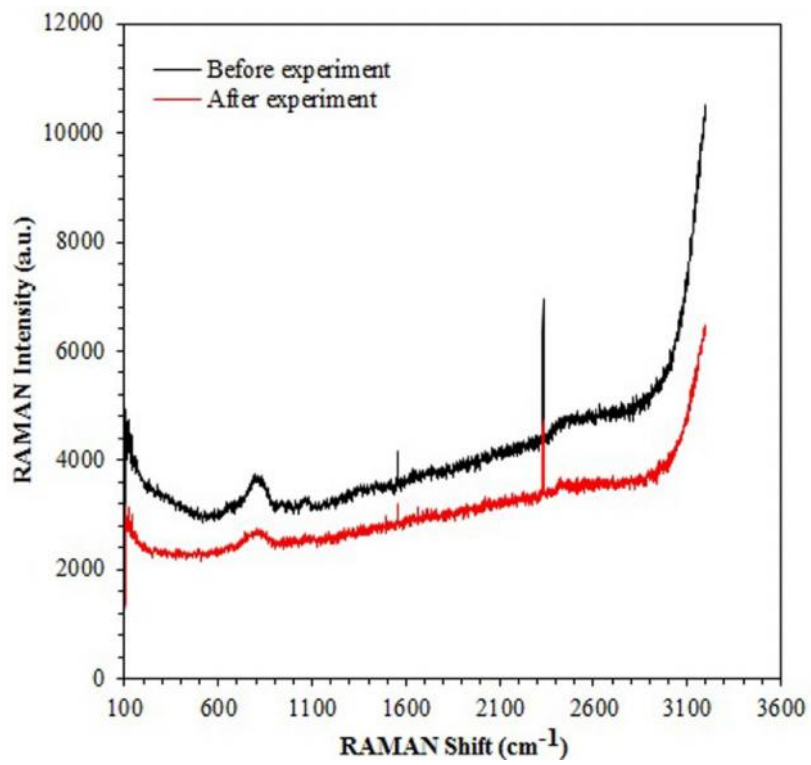
(d)

Fig. 6.11 The Raman spectrum taken from samples
a) 100 mg/L b) 500 mg/L c) 1000 mg/L d) 4000 mg/L

6.5 Conclusion

The different amounts of Xanthan gum were dissolved into deionized water to produce the polymeric solutions. The measurements of the viscosity, contact angle and equilibrium surface tension showed that the rheology and the interfacial properties of the solution would differ from the solvent, affecting on the formation of the behavior of bubbles in terms of their size, number and shape. The stability of the solutions was also examined by doing RAMAN tests. The nucleate boiling heat transfer performance of polymeric solutions over a flat plate was experimentally investigated to give more insight how effective they are for cooling application. The major conclusions from measurements, experimental results, and photographs can be summarized as follows

- The viscosity corresponding to the solutions displays a shear rate-dependency for which the larger values are related to higher concentrations. The measurements illustrate that the contact angle increases with concentration up to 1000 mg/L and after it, the contact angle remain nearly constant. The equilibrium surface tension remains roughly constant until 1000 mg/L and thereafter it starts decreasing.

- The addition of Xanthan gum powder into DI water generally deteriorates the performance of the heat transfer. The increment of concentration first reduces the heat transfer coefficient up to the solution with the concentration of 500 mg/L. A more increase in concentration by up to 1000 mg/L does not further degrade the HTC. At high concentrations (4000 and 6000 mg/L), it was realized that the heat transfer coefficient was decreased with heat flux, which was in opposite trend of those in pure water and other lower concentrations.

- The photographic images demonstrates that as compared to solvent (i.e. water) the number of bubbles increases while they are in more regular shaped with smaller sizes and in less tendency to coalescence.

7. FUTURE WORK AND CONTRIBUTIONS

In this thesis, the non-Newtonian fluids flow and heat transfer characteristics were investigated. Non-Newtonian fluids constitute a prominent research area in engineering science and relevant subjects. In order to assess the heat transfer performance of non-Newtonian fluids, it is essential to consider them in different aspects such as analytical, numerical and experimental approaches. In this regard, heat transfer to non-Newtonian fluids was studied both experimentally and analytically.

In pool boiling experiments, polymeric solutions as a subcategory of them, which were prepared from dissolution of Xanthan gum powder at different amounts into de-ionized water, were examined in terms of their heat transfer performance. It was found that the type of liquid has a profound role in convective heat transfer. In the future, different types of fluids will be studied for improvement of heat transfer performance. Moreover, a second law analysis on pool boiling of such fluids will be performed. Thus, a connection between analytical and experimental approaches will be made, and design guidelines for thermal-fluid systems involving non-Newtonian fluids will be proposed.

In an analytical point of view, internal flows of non-Newtonian fluids in both micro-and macro scale were investigated, where the power-law model was taken into consideration due to its viability and simplicity. The effects of slip, viscous dissipation and temperature-dependent thermophysical properties were included, and some closed form expressions were obtained for velocity, temperature, Nusselt number and entropy generation rate. In future, the heat transfer performance of polymeric solutions in microchannels will be assessed both analytically and experimentally under single-phase and two-phase conditions in order to provide more understanding in convective heat transfer of non-Newtonian fluid flows.

8. REFERENCES

[1] M.M. Denn, Issues in Viscoelastic Fluid Mechanics, Annu. Rev. Fluid Mech. 22 (1990) 13–32.

[2] Y. Cohen, Apparent Slip Flow of Polymer Solutions, J. Rheol. (N. Y. N. Y). 29 (1985) 67.

[3] A. Demsis, B. Verma, S. V. Prabhu, A. Agrawal, Experimental determination of heat transfer coefficient in the slip regime and its anomalously low value, Phys. Rev. E. 80 (2009) 016311.

[4] T. Ewart, P. Perrier, I. Graur, J. Gilbert Méolans, Mass flow rate measurements in gas micro flows, Exp. Fluids. 41 (2006) 487–498.

[5] J. Pitakarnnop, S. Varoutis, D. Valougeorgis, S. Geoffroy, L. Baldas, S. Colin, A novel experimental setup for gas microflows, Microfluid. Nanofluidics. 8 (2009) 57–72. d

[6] L. Szalmas, J. Pitakarnnop, S. Geoffroy, S. Colin, D. Valougeorgis, Comparative study between computational and experimental results for binary rarefied gas flows through long microchannels, Microfluid. Nanofluidics. 9 (2010) 1103–1114.

[7] O. Aydın, M. Avcı, Heat and fluid flow characteristics of gases in micropipes, Int. J. Heat Mass Transf. 49 (2006) 1723–1730.

[8] B. Cao, G.W. Chen, Q. Yuan, Fully developed laminar flow and heat transfer in smooth trapezoidal microchannel, Int. Commun. Heat Mass Transf. 32 (2005) 1211–1220.

[9] M. Renksizbulut, H. Niazmand, G. Tercan, Slip-flow and heat transfer in rectangular microchannels with constant wall temperature, Int. J. Therm. Sci. 45 (2006) 870–881.

[10] K. Hooman, A superposition approach to study slip-flow forced convection in straight microchannels of uniform but arbitrary cross-section, Int. J. Heat Mass Transf. 51 (2008) 3753–3762.

[11] L. Kuddusi, E. Çetegen, Thermal and hydrodynamic analysis of gaseous flow in trapezoidal silicon microchannels, Int. J. Therm. Sci. 48 (2009) 353–362.

[12] K. Hooman, Entropy generation for microscale forced convection: Effects of different thermal boundary conditions, velocity slip, temperature jump, viscous dissipation, and duct geometry, Int. Commun. Heat Mass Transf. 34 (2007) 945–957.

[13] M. Shams, M. Shojaeian, C. Aghanajafi, S.A.R. Dibaji, Numerical simulation of slip flow through rhombus microchannels, Int. Commun. Heat Mass Transf. 36 (2009) 1075–1081.

[14] M. Shojaeian, S.A.R. Dibaji, Three-dimensional numerical simulation of the slip flow through triangular microchannels, Int. Commun. Heat Mass Transf. 37 (2010) 324–329.

[15] S. Shahsavari, A. Tamayol, E. Kjeang, M. Bahrami, Convective Heat Transfer in Microchannels of Noncircular Cross Sections: An Analytical Approach, J. Heat Transfer. 134 (2012) 091701.

[16] D. Byun, J. Kim, H.S. Ko, H.C. Park, Direct measurement of slip flows in superhydrophobic microchannels with transverse grooves, Phys. Fluids. 20 (2008) 113601.

[17] D.C. Tretheway, C.D. Meinhart, A generating mechanism for apparent fluid slip in hydrophobic microchannels, Phys. Fluids. 16 (2004) 1509.

[18] M.-S. Chun, S. Lee, Flow imaging of dilute colloidal suspension in PDMS-based microfluidic chip using fluorescence microscopy, Colloids Surfaces A Physicochem. Eng. Asp. 267 (2005) 86–94.

[19] T.A. Ho, D. V Papavassiliou, L.L. Lee, A. Striolo, Liquid water can slip on a hydrophilic surface., Proc. Natl. Acad. Sci. U. S. A. 108 (2011) 16170–5.

[20] J. Ou, B. Perot, J.P. Rothstein, Laminar drag reduction in microchannels using ultrahydrophobic surfaces, Phys. Fluids. 16 (2004) 4635.

[21] P. Joseph, P. Tabeling, Direct measurement of the apparent slip length, Phys. Rev. E. 71 (2005) 035303.

[22] M.S. El-Genk, I.-H. Yang, Friction Numbers and Viscous Dissipation Heating for Laminar Flows of Water in Microtubes, J. Heat Transfer. 130 (2008) 082405.

[23] G.P. Celata, M. Cumo, S. McPhail, G. Zummo, Characterization of fluid dynamic behaviour and channel wall effects in microtube, Int. J. Heat Fluid Flow. 27 (2006) 135–143.

[24] C. Rands, B.W. Webb, D. Maynes, Characterization of transition to turbulence in microchannels, Int. J. Heat Mass Transf. 49 (2006) 2924–2930.

[25] D.C. Tretheway, C.D. Meinhart, Apparent fluid slip at hydrophobic microchannel walls, Phys. Fluids. 14 (2002) L9.

[26] G.D. Ngoma, F. Erchiqui, Heat flux and slip effects on liquid flow in a microchannel, Int. J. Therm. Sci. 46 (2007) 1076–1083.

[27] G. Rosengarten, J. Cooper-White, G. Metcalfe, Experimental and analytical study of the effect of contact angle on liquid convective heat transfer in microchannels, Int. J. Heat Mass Transf. 49 (2006) 4161–4170.

[28] M. Kundu, K. Vamsee, D. Maiti, Simulation and analysis of flow through microchannel, Asia-Pacific J. Chem. Eng. 4 (2009) 450–461.

[29] W. Qu, I. Mudawar, Experimental and numerical study of pressure drop and heat transfer in a single-phase micro-channel heat sink, Int. J. Heat Mass Transf. 45 (2002) 2549–2565.

[30] G.L. Morini, Viscous heating in liquid flows in micro-channels, Int. J. Heat Mass Transf. 48 (2005) 3637–3647.

[31] K.. Toh, X.. Chen, J.. Chai, Numerical computation of fluid flow and heat transfer in microchannels, Int. J. Heat Mass Transf. 45 (2002) 5133–5141.

[32] M.M. Denn, Extrusion instabilities and wall slip, Annu. Rev. Fluid Mech. 33 (2001) 265–287.

[33] F. Brochard, P.G. De Gennes, Shear-dependent slippage at a polymer/solid interface, Langmuir. 8 (1992) 3033–3037.

[34] D.A. Hill, Wall slip in polymer melts: A pseudo-chemical model, J. Rheol. (N. Y. N. Y). 42 (1998) 581.

[35] N. Bhagavatula, J.M. Castro, Modelling and experimental verification of pressure prediction in the in-mould coating (IMC) process for injection moulded parts, Model. Simul. Mater. Sci. Eng. 15 (2007) 171–189.

[36] M. Akçay, M.A. Yükselen, Drag reduction of a nonnewtonian fluid by fluid injection on a moving wall, Arch. Appl. Mech. (Ingenieur Arch. 69 (1999) 215–225.

[37] C.-H. Chen, Effect of viscous dissipation on heat transfer in a non-Newtonian liquid film over an unsteady stretching sheet, J. Nonnewton. Fluid Mech. 135 (2006) 128–135.

[38] A. Pinarbasi, M. Imal, Viscous heating effects on the linear stability of Poiseuille flow of an inelastic fluid, J. Nonnewton. Fluid Mech. 127 (2005) 67–71.

[39] A. Acrivos, M.J. Shah, E.E. Petersen, Momentum and heat transfer in laminar boundary-layer flows of non-Newtonian fluids past external surfaces, AIChE J. 6 (1960) 312–317.

[40] S.S. Pawar, V.K. Sunnapwar, Experimental studies on heat transfer to Newtonian and non-Newtonian fluids in helical coils with laminar and turbulent flow, Exp. Therm. Fluid Sci. 44 (2013) 792–804.

[41] S.D. Joshi, A.E. Bergles, Experimental Study of Laminar Heat Transfer to In-Tube Flow of Non-Newtonian Fluids, J. Heat Transfer. 102 (1980) 397.

[42] S.G. Etemad, A.S. Mujumdar, R. Nassef, Viscous non-newtonian forced convection heat transfer in semi-circular and equilateral triangular ducts: an experimental study, Int. Commun. Heat Mass Transf. 24 (1997) 609–620.

[43] I. Filkova, A. Lawal, B. Koziskova, A.S. Mujumdar, Heat transfer to a power-law fluid in tube flow: Numerical and experimental studies, J. Food Eng. 6 (1987) 143–151.

[44] D. Béreiziat, R. Devienne, Experimental characterization of Newtonian and non-Newtonian fluid flows in corrugated channels, Int. J. Eng. Sci. 37 (1999) 1461–1479.

[45] M. Gradeck, B.F.Z. Fagla, C. Baravian, M. Lebouché, Experimental thermomechanic study of Newtonian and non-Newtonian suspension flows, Int. J. Heat Mass Transf. 48 (2005) 3469–3477.

[46] H. Ragueb, K. Mansouri, A numerical study of viscous dissipation effect on non-Newtonian fluid flow inside elliptical duct, Energy Convers. Manag. 68 (2013) 124–132.

[47] A. Filali, L. Khezzar, D. Siginer, Z. Nemouchi, Graetz problem with non-linear viscoelastic fluids in non-circular tubes, Int. J. Therm. Sci. 61 (2012) 50–60.

[48] P.S.B. Zdanski, M. Vaz, A.P.C. Dias, Forced convection heat transfer of polymer melt flow inside channels with contraction/expansion sections, Int. Commun. Heat Mass Transf. 38 (2011) 1335–1339.

[49] S. Poncet, S. Haddadi, S. Viazzo, Numerical modeling of fluid flow and heat transfer in a narrow Taylor–Couette–Poiseuille system, Int. J. Heat Fluid Flow. 32 (2011) 128–144.

[50] M. Capobianchi, D. Wagner, Heat transfer in laminar flows of extended modified power law fluids in rectangular ducts, Int. J. Heat Mass Transf. 53 (2010) 558–563.

[51] M.H. Matin, W.A. Khan, Laminar natural convection of non-Newtonian power-law fluids between concentric circular cylinders, Int. Commun. Heat Mass Transf. 43 (2013) 112–121.

[52] R.Y. Jumah, A.S. Mujumdar, Free convection heat and mass transfer of non-newtonian power law fluids with yield stress from a vertical flat plate in saturated porous media, Int. Commun. Heat Mass Transf. 27 (2000) 485–494.

[53] M. Lamsaadi, M. Nami, M. Hasnaoui, Natural convection of non-Newtonian power law fluids in a shallow horizontal rectangular cavity uniformly heated from below, Heat Mass Transf. (2004).

[54] A. Guha, K. Pradhan, Natural convection of non-Newtonian power-law fluids on a horizontal plate, Int. J. Heat Mass Transf. 70 (2014) 930–938.

[55] N.T.M. Eldabe, M.F. El-Sayed, A.Y. Ghaly, H.M. Sayed, Mixed convective heat and mass transfer in a non-Newtonian fluid at a peristaltic surface with temperature-dependent viscosity, Arch. Appl. Mech. 78 (2007) 599–624.

[56] T.-Y. Wang, Mixed convection from a vertical plate to non-Newtonian fluids with uniform surface heat flux, Int. Commun. Heat Mass Transf. 22 (1995) 369–380.

[57] M. Amoura, N. Zeraibi, A. Smati, M. Gareche, Finite element study of mixed convection for non-Newtonian fluid between two coaxial rotating cylinders, Int. Commun. Heat Mass Transf. 33 (2006) 780–789.

[58] C.-C. Wang, C.-K. Chen, Mixed convection boundary layer flow of non-Newtonian fluids along vertical wavy plates, Int. J. Heat Fluid Flow. 23 (2002) 831–839.

[59] C.-H. Chen, Effects of magnetic field and suction/injection on convection heat transfer of non-Newtonian power-law fluids past a power-law stretched sheet with surface heat flux, Int. J. Therm. Sci. 47 (2008) 954–961.

[60] E.M. Abo-Eldahab, A.M. Salem, MHD Flow and heat transfer of non-Newtonian power-law fluid with diffusion and chemical reaction on a moving cylinder, Heat Mass Transf. 41 (2005) 703–708.

[61] K.V. Prasad, D. Pal, V. Umesh, N.S.P. Rao, The effect of variable viscosity on MHD viscoelastic fluid flow and heat transfer over a stretching sheet, Commun. Nonlinear Sci. Numer. Simul. 15 (2010) 331–344.

[62] A. Babaie, M.H. Saidi, A. Sadeghi, Heat transfer characteristics of mixed electroosmotic and pressure driven flow of power-law fluids in a slit microchannel, Int. J. Therm. Sci. 53 (2012) 71–79.

[63] C. Zhao, C. Yang, Joule heating induced heat transfer for electroosmotic flow of power-law fluids in a microcapillary, Int. J. Heat Mass Transf. 55 (2012) 2044–2051.

[64] S. Sánchez, J. Arcos, O. Bautista, F. Méndez, Joule heating effect on a purely electroosmotic flow of non-Newtonian fluids in a slit microchannel, J. Nonnewton. Fluid Mech. 192 (2013) 1–9.

[65] Y.-M. Hung, Viscous dissipation effect on entropy generation for non-Newtonian fluids in microchannels, Int. Commun. Heat Mass Transf. 35 (2008) 1125–1129.

[66] C.H. Chen, Y.L. Hwang, S.J. Hwang, Non-Newtonian Fluid Flow and Heat Transfer in Microchannels, in: Appl. Mech. Mater., 2013: pp. 462–465.

[67] A. Sunarso, T. Yamamoto, N. Mori, Numerical Analysis of Wall Slip Effects on Flow of Newtonian and Non-Newtonian Fluids in Macro and Micro Contraction Channels, J. Fluids Eng. 129 (2007) 23.

[68] M. Barkhordari, S.G. Etemad, Numerical study of slip flow heat transfer of non-Newtonian fluids in circular microchannels, Int. J. Heat Fluid Flow. 28 (2007) 1027–1033.

[69] R. Chiba, M. Izumi, Y. Sugano, An analytical solution to non-axisymmetric heat transfer with viscous dissipation for non-Newtonian fluids in laminar forced flow, Arch. Appl. Mech. 78 (2007) 61–74.

[70] F.T. Pinho, P.M. Coelho, Fully-developed heat transfer in annuli for viscoelastic fluids with viscous dissipation, J. Nonnewton. Fluid Mech. 138 (2006) 7–21.

[71] R.M. Manglik, J. Ding, Laminar flow heat transfer to viscous powerlaw fluids in double-sine ducts, Int. J. Heat Mass Transf. 40 (1997) 1379–1390.

[72] N. Thayalan, Y.M. Hung, Momentum integral method for forced convection in thermal nonequilibrium power-law fluid-saturated porous media, Chem. Eng. Commun. 200 (2013) 269–288.

[73] C.-H. Chen, Electro-Osmotic Heat Transfer of Non-Newtonian Fluid Flow in Microchannels, J. Heat Transfer. 133 (2011) 071705.

[74] A.J. Moghadam, Electrokinetic-Driven Flow and Heat Transfer of a Non-Newtonian Fluid in a Circular Microchannel, J. Heat Transfer. 135 (2013) 021705.

[75] A. Sadeghi, M.H. Saidi, A.A. Mozafari, Heat transfer due to electroosmotic flow of viscoelastic fluids in a slit microchannel, Int. J. Heat Mass Transf. 54 (2011) 4069–4077.

[76] C.P. Tso, J. Sheela-Francisca, Y.-M. Hung, Viscous dissipation effects of power-law fluid flow within parallel plates with constant heat fluxes, J. Nonnewton. Fluid Mech. 165 (2010) 625–630.

[77] J. Sheela-Francisca, C.P. Tso, Y.M. Hung, D. Rilling, Heat transfer on asymmetric thermal viscous dissipative Couette–Poiseuille flow of pseudo-plastic fluids, J. Nonnewton. Fluid Mech. 169-170 (2012) 42–53.

[78] E.R. Monteiro, E.N. Macêdo, J.N.N. Quaresma, R.M. Cotta, Laminar flow and convective heat transfer of non-Newtonian fluids in doubly connected ducts, Int. J. Heat Mass Transf. 53 (2010) 2434–2448.

[79] D.A. Siginer, M.F. Letelier, Heat transfer asymptote in laminar flow of non-linear viscoelastic fluids in straight non-circular tubes, Int. J. Eng. Sci. 48 (2010) 1544–1562.

[80] S. Mahmud, R.A. Fraser, Asymptotic Nusselt and entropy generation numbers for non-Newtonian fluid flow, Heat Mass Transf. 41 (2005) 999–1003.

[81] S. Mahmud, R. Fraser, Second law analysis of forced convection in a circular duct for non-Newtonian fluids, Energy. 31 (2006) 2226–2244.

[82] J.M. Nóbrega, F.T. Pinho, P.J. Oliveira, O.S. Carneiro, Accounting for temperature-dependent properties in viscoelastic duct flows, Int. J. Heat Mass Transf. 47 (2004) 1141–1158.

[83] M.E. Sayed-Ahmed, The effect of variable properties on the helical flow and heat transfer of power law fluids, Acta Mech. 181 (2006) 185–197.

[84] Z. Lian-Cun, Z. Xin-Xin, M. Lian-Xi, Fully Developed Convective Heat Transfer of Power Law Fluids in a Circular Tube, Chinese Phys. Lett. 25 (2008) 195–197.

[85] M. Shojaeian, M. Yildiz, A. Ko ar, Convective heat transfer and second law analysis of non-Newtonian fluid flows with variable thermophysical properties in circular channels, Int. Commun. Heat Mass Transf. 60 (2015) 21–31.

[86] G. V. Vinogradov, L.I. Ivanova, Wall slippage and elastic turbulence of polymers in the rubbery state, Rheol. Acta. 7 (1968) 243–254.

[87] S. Luk, R. Mutharasan, D. Apelian, Experimental observations of wall slip: tube and packed bed flow, Ind. Eng. Chem. Res. 26 (1987) 1609–1616.

[88] J.L. White, The influence of materials of construction on biconical rotor and capillary measurements of shear viscosity of rubber and its compounds and considerations of slippage, J. Rheol. (N. Y. N. Y). 35 (1991) 167.

[89] S.G. Hatzikiriakos, J.M. Dealy, Wall slip of molten high density polyethylenes. II. Capillary rheometer studies, J. Rheol. (N. Y. N. Y). 36 (1992) 703.

[90] K. Migler, H. Hervet, L. Leger, Slip transition of a polymer melt under shear stress, Phys. Rev. Lett. 70 (1993) 287–290.

[91] J.M. Piau, N. El Kissi, Measurement and modelling of friction in polymer melts during macroscopic slip at the wall, J. Nonnewton. Fluid Mech. 54 (1994) 121–142.

[92] Y.-P. Shih, C.-C. Huang, S.-Y. Tsay, Extended Leveque solution for laminar heat transfer to power-law fluids in pipes with wall slip, Int. J. Heat Mass Transf. 38 (1995) 403–408.

[93] R. Ellahi, E. Shivanian, S. Abbasbandy, S.U. Rahman, T. Hayat, Analysis of steady flows in viscous fluid with heat/mass transfer and slip effects, Int. J. Heat Mass Transf. 55 (2012) 6384–6390.

[94] J. Niu, C. Fu, W. Tan, Slip-flow and heat transfer of a non-newtonian nanofluid in a microtube., PLoS One. 7 (2012) e37274.

[95] V. Anand, Slip law effects on heat transfer and entropy generation of pressure driven flow of a power law fluid in a microchannel under uniform heat flux boundary condition, Energy. 76 (2014) 716–732.

[96] A.M. Dehkordi, M. Memari, Transient and steady-state forced convection to power-law fluids in the thermal entrance region of circular ducts: Effects of viscous dissipation, variable viscosity, and axial conduction, Energy Convers. Manag. 51 (2010) 1065–1074.

[97] V.P. Carey, Liquid-vapor phase-change phenomena, (1992).

[98] W.M. Rohsenow, J.P. Hartnett, E.N. Ganic, Handbook of heat transfer fundamentals (2nd edition), (1985).

[99] S.G. Kandlikar, M. Shoji, V.K. Dhir, Handbook of Phase Change: Boiling and Condensation, CRC Press, 1999.

[100] V.K. Dhir, Boiling heat transfer, Annu. Rev. Fluid Mech. 30 (1998) 365–401.

[101] J. Kim, Review of nucleate pool boiling bubble heat transfer mechanisms, Int. J. Multiph. Flow. 35 (2009) 1067–1076.

[102] V.K. Dhir, G.R. Warrier, E. Aktinol, Numerical Simulation of Pool Boiling: A Review, J. Heat Transfer. 135 (2013) 061502.

[103] M. Shojaeian, A. Ko ar, Pool boiling and flow boiling on micro- and nanostructured surfaces, Exp. Therm. Fluid Sci. (2015).

[104] Y.-W. Lu, S.G. Kandlikar, Nanoscale Surface Modification Techniques for Pool Boiling Enhancement—A Critical Review and Future Directions, Heat Transf. Eng. 32 (2011) 827–842.

[105] M. e en, W. Khudhayer, T. Karabacak, A. Ko ar, Compact nanostructure integrated pool boiler for microscale cooling applications, Micro Nano Lett. 5 (2010) 203.

[106] E. Demir, T. Izci, A.S. Alagoz, T. Karabacak, A. Ko ar, Effect of silicon nanorod length on horizontal nanostructured plates in pool boiling heat transfer with water, Int. J. Therm. Sci. 82 (2014) 111–121.

[107] S.U.S. Choi, J.A. Eastman, Enhancing thermal conductivity of fluids with nanoparticles, in: D.A. Siginer, H.P. Wang (Eds.), Developments Applications of Non-Newtonian Flows, Proc. ASME Int. Mech. Eng. Congr. FED-Vol. 231/MD-Vol. 66, ASME, New York, USA. (1995) 99–105.

[108] M. Karimzadehkhouei, S.E. Yalcin, K. endur, M. Pınar Mengüç, A. Ko ar, Pressure drop and heat transfer characteristics of nanofluids in horizontal microtubes under thermally developing flow conditions, Exp. Therm. Fluid Sci. (2014).

[109] C.J. Ho, L.C. Wei, Z.W. Li, An experimental investigation of forced convective cooling performance of a microchannel heat sink with Al2O3/water nanofluid, Appl. Therm. Eng. 30 (2010) 96–103.

[110] S. Soltani, S.G. Etemad, J. Thibault, Pool boiling heat transfer performance of Newtonian nanofluids, Heat Mass Transf. 45 (2009) 1555–1560.

[111] M. Sheikhbahai, M. Nasr Esfahany, N. Etesami, Experimental investigation of pool boiling of Fe3O4/ethylene glycol–water nanofluid in electric field, Int. J. Therm. Sci. 62 (2012) 149–153.

[112] S. Soltani, S.G. Etemad, J. Thibault, Pool boiling heat transfer of non-Newtonian nanofluids, Int. Commun. Heat Mass Transf. 37 (2010) 29–33.

[113] Y. He, Y. Jin, H. Chen, Y. Ding, D. Cang, H. Lu, Heat transfer and flow behaviour of aqueous suspensions of TiO2 nanoparticles (nanofluids) flowing upward through a vertical pipe, Int. J. Heat Mass Transf. 50 (2007) 2272–2281.

[114] H. Chen, W. Yang, Y. He, Y. Ding, L. Zhang, C. Tan, et al., Heat transfer and flow behaviour of aqueous suspensions of titanate nanotubes (nanofluids), Powder Technol. 183 (2008) 63–72.

[115] P. Garg, J.L. Alvarado, C. Marsh, T.A. Carlson, D.A. Kessler, K. Annamalai, An experimental study on the effect of ultrasonication on viscosity and heat transfer performance of multi-wall carbon nanotube-based aqueous nanofluids, Int. J. Heat Mass Transf. 52 (2009) 5090–5101.

[116] V.M. Wasekar, R.M. Manglik, A Review of Enhanced Heat Transfer in Nucleate Pool Boiling of Aqueous Surfactant and Polymeric Solutions, J. Enhanc. Heat Transf. 6 (1999) 135–150.

[117] P. Kotchaphakdee, M.C. Williams, Enhancement of nucleate pool boiling with polymeric additives, Int. J. Heat Mass Transf. 13 (1970) 835–848.

[118] R.M. Manglik, V.M. Wasekar, J. Zhang, Dynamic and equilibrium surface tension of aqueous surfactant and polymeric solutions, Exp. Therm. Fluid Sci. 25 (2001) 55–64.

[119] L. Cheng, D. Mewes, A. Luke, Boiling phenomena with surfactants and polymeric additives: A state-of-the-art review, Int. J. Heat Mass Transf. 50 (2007) 2744–2771.

[120] H.J. Gannett, M.C. Williams, Pool boiling in dilute non-aqueous polymer solutions, Int. J. Heat Mass Transf. 14 (1971) 1001–1005.

[121] D.D. Paul, S.I. Abdel-Khalik, Saturated nucleate pool boiling bubble dynamics in aqueous drag-reducing polymer solutions, Int. J. Heat Mass Transf. 27 (1984) 2426–2428.

[122] J. Zhang, R.M. Manglik, Nucleate pool boiling of aqueous polymer solutions on a cylindrical heater, J. Nonnewton. Fluid Mech. 125 (2005) 185–196.

[123] B.J. Zhang, J. Park, K.J. Kim, Augmented boiling heat transfer on the wetting-modified three dimensionally-interconnected alumina nano porous surfaces in aqueous polymeric surfactants, Int. J. Heat Mass Transf. 63 (2013) 224–232.

[124] A.T.A. Wang, J.P. Hartnett, Influence of surfactants on pool boiling of aqueous polyacrylamide solutions, Wärme- Und Stoffübertragung. 27 (1992) 245–248.

[125] R.Y.Z. Hu, Nucleate pool boiling from a horizontal wire in viscoelastic fluids, Ph.D. Thesis, Univ. Illinois Chicago, Chicago,. (1989).

[126] Y.M. Yang, J.R. Maa, Effects of polymer additives on pool boiling phenomena, Lett. Heat Mass Transf. 9 (1982) 237–244.

[127] D.D. Paul, S.I. Abdel-Khalik, Nucleate boiling in drag-reducing polymer solutions, J. Rheol. (N. Y. N. Y). 27 (1983) 59–76.

[128] S.P. Levitskiy, B.M. Khusid, Z.P. Shulman, Growth of vapour bubbles in boiling polymer solutions—II. Nucleate boiling heat transfer, Int. J. Heat Mass Transf. 39 (1996) 639–644.

[129] K.. Bang, M.. Kim, G.. Jeun, Boiling characteristics of dilute polymer solutions and implications for the suppression of vapor explosions, Nucl. Eng. Des. 177 (1997) 255–264.

[130] L.L. Ferrás, J.M. Nóbrega, F.T. Pinho, Analytical solutions for channel flows of Phan-Thien–Tanner and Giesekus fluids under slip, J. Nonnewton. Fluid Mech. 171-172 (2012) 97–105.

[131] G.G. Pereira, Effect of variable slip boundary conditions on flows of pressure driven non-Newtonian fluids, J. Nonnewton. Fluid Mech. 157 (2009) 197–206.

[132] A. Bejan, Entropy Generation Minimization: The Method of Thermodynamic Optimization of Finite-Size Systems and Finite-Time Processes, CRC Press, 1995.

[133] A. Bejan, Entropy generation through heat and fluid flow, (1982).

[134] G. Tunc, Y. Bayazitoglu, Heat transfer in rectangular microchannels, Int. J. Heat Mass Transf. 45 (2002) 765–773.

[135] O. Reynolds, On the theory of lubrication and its application to beauchamp tower's experiments, Philos. Trans. R. Soc. Lond. (1886) 157–234.

[136] K. Hooman, a. Ejlali, Effects of viscous heating, fluid property variation, velocity slip, and temperature jump on convection through parallel plate and circular microchannels, Int. Commun. Heat Mass Transf. 37 (2010) 34–38.

[137] M. Shojaeian, S.M.N. Shojaee, Viscous dissipation effect on heat transfer characteristics of mixed electromagnetic/pressure driven liquid flows inside micropumps, Korean J. Chem. Eng. 30 (2013) 823–830.

[138] T. Al-Shemmeri, Engineering Fluid Mechanics, Bookboon, 2012.

[139] S.G. Hatzikiriakos, K. Migler, Polymer Processing Instabilities: Control and Understanding - CRC Press Book, Eds., Marcel Dekker, New York. (2004).

[140] A. V. Ramamurthy, Wall Slip in Viscous Fluids and Influence of Materials of Construction, J. Rheol. (N. Y. N. Y). 30 (1986) 337.

[141] P.D. Patil, J.J. Feng, S.G. Hatzikiriakos, Constitutive modeling and flow simulation of polytetrafluoroethylene (PTFE) paste extrusion, J. Nonnewton. Fluid Mech. 139 (2006) 44–53.

[142] M. Shojaeian, A. Ko ar, Convective heat transfer and entropy generation analysis on Newtonian and non-Newtonian fluid flows between parallel-plates under slip boundary conditions, Int. J. Heat Mass Transf. 70 (2014) 664–673.

[143] M. Shojaeian, M. Yildiz, A. Ko ar, Heat transfer characteristics of plug flows with temperature-jump boundary conditions in parallel-plate channels and concentric annuli, Int. J. Therm. Sci. 84 (2014) 252–259.

[144] M.L. V. Ramires, C.A. Nieto de Castro, Y. Nagasaka, A. Nagashima, M.J. Assael, W.A. Wakeham, Standard Reference Data for the Thermal Conductivity of Water, J. Phys. Chem. Ref. Data. 24 (1995) 1377.

[145] M. Shojaeian, M. Shojaeian, Analytical solution of mixed electromagnetic/pressure driven gaseous flows in microchannels, Microfluid. Nanofluidics. 12 (2011) 553–564.

[146] M. Shojaeian, A. Kosar, Numerical Investigation of Fully Developed Fluid Flow and Heat Transfer in Double-Trapezoidal Microchannels, in: Vol. 10 Micro-Nano-Systems Eng. Packag., ASME, 2013: p. V010T11A029.

[147] R.J. Moffat, Describing the uncertainties in experimental results, Exp. Therm. Fluid Sci. 1 (1988) 3–17. doi:10.1016/0894-1777(88)90043-X.

[148] A.D. Athavale, R.M. Manglik, M.A. Jog, An experimental investigation of nucleate pool boiling in aqueous solutions of a polymer, AIChE J. 58 (2012) 668–677.

[149] J. Zhang, R.M. Manglik, Additive Adsorption and Interfacial Characteristics of Nucleate Pool Boiling in Aqueous Surfactant Solutions, J. Heat Transfer. 127 (2005) 684.

[150] R.M. Manglik, M. a. Jog, Molecular-to-Large-Scale Heat Transfer With Multiphase Interfaces: Current Status and New Directions, J. Heat Transfer. 131 (2009) 121001.

[151] C.L. Tucker, Computer Modeling for Polymer Processing (Computer Aided Engineering for Polymer Processing), Hanser Publ. (1989) 23.

[152] W.M. Rohsenow, J.P. Hartnett, Y.I. Cho, Handbook of heat transfer, McGraw-Hill New York. (1998).

[153] I. Mostinski, Application of the rule of corresponding states for calculation of heat transfer and critical heat flux, Teploenergetika. (1963).

[154] D. Gorenflo, Pool Boiling in VDI-Heat Atlas (English Version), VDI-Verlag, Dusseldorf, Ger. (1993).

[155] N. Bakhru, J.H. Lienhard, Boiling from small cylinders, Int. J. Heat Mass Transf. 15 (1972) 2011–2025.

[156] R.P. Wool, Polymer entanglements, Macromolecules. 26 (1993) 1564–1569.

[157] R.F. Gaertner, Photographic Study of Nucleate Pool Boiling on a Horizontal Surface, J. Heat Transfer. 87 (1965) 17.

[158] J.H. Mathews, Numerical Methods for Mathematics, Science, and Engineering, Prentice Hall, New Jersey, 1992.